VYSOKÉ UČENÍ TECHNICKÉ V BRNĚ
BRNO UNIVERSITY OF TECHNOLOGY

FAKULTA STROJNÍHO INŽENÝRSTVÍ
FACULTY OF MECHANICAL ENGINEERING

LETECKÝ ÚSTAV
INSTITUTE OF AEROSPACE ENGINEERING

METODIKA ANALÝZ DAMAGE TOLERANCE LETECKÉ KONSTRUKCE S VYUŽITÍM PROGRAMU AFGROW
AIRCRAFT STRUCTURE DAMAGE TOLERANCE ANALYSIS METHOD AIDED BY AFGROW SOFTWARE

DIPLOMOVÁ PRÁCE
MASTER'S THESIS

AUTOR PRÁCE   Bc. Kristián Rakovský
AUTHOR

VEDOUCÍ PRÁCE   Ing. Martin Nágeľ
SUPERVISOR

BRNO 2016

Master's Thesis Assignment

Institut:	Institute of Aerospace Engineering
Student:	**Bc. Kristián Rakovský**
Degree programm:	Mechanical Engineering
Branch:	Aircraft Design
Supervisor:	**Ing. Martin Nágel'**
Academic year:	2015/16

As provided for by the Act No. 111/98 Coll. on higher education institutions and the BUT Study and Examination Regulations, the director of the Institute hereby assigns the following topic of Master's Thesis:

Aircraft structure Damage Tolerance analysis method aided by AFGROW software

Brief description:

Meeting the goals of damage tolerance structure analysis problematic is crucial for the airplane certification in category FAR 25 and Commuter category according to FAR 23.

The major part of the damage tolerance structure calculations deals with the determination of crack growth curves of simultaneously growing cracks in a statically indeterminate structure. The task is relatively difficult to deal with and requires either a detailed analysis, i.e. using finite element method, or establishment of simplified assumptions, which may lead to overly conservative results.

Master's Thesis goals:

The goal of the diploma thesis is to propose the calculation of dependent crack growth in several structure elements aided by AFGROW software. AFGROW software offers a relatively wide calculation automation by means of the COM (Component Object Model) interface.

In the first part, the author will break down the requirements concerning the size and location of initial flaws in the analysed structure. The main part of the diploma thesis will be the proposal of method for computing crack growth curves of simultaneously propagating cracks in several structural elements in the AFGROW software. The method will also include a determination of residual strength of the evaluated structure. Part of the diploma thesis will be an example of a specific structure joint solving.

The diploma thesis shall be directly usable by the company Aircraft Industries, a.s. for development of new computational methods within the scope of fatigue and damage tolerance analyses of the L 410 NG airplane.

Bibliography:

Vlček, D. (2015): Fatigue and Damage Tolerance Guidelines. MOSTA.0463.A.U.MD, TDC-150-E20-0103-MD-14, IR.

Vlček, D. (2014): Crack Growth Analysis. Residual Strength Analysis. MOSTA.0464.A.U.MD, TDC-150-E20-0103-MD-09, IR.

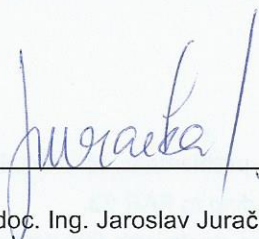Skinn, D. A., Gallagher, J. P. (1994): Damage Tolerant Design Handbook. WL-TR-94-4052.

Harter, J. (2010): AFGROW User's Guide and Technical Manual. Dayton, OH, USA.
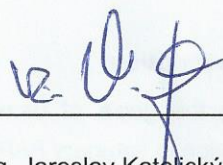
Harter, J., Litvinov, A. (2008): Development of structural integrity analysis methods for aircraft structures: AFGROW Component Object Model (COM). Server interface manual, Release 15.

Students are required to submit the thesis within the deadlines stated in the schedule of the academic year 2015/16.

In Brno, 1. 12. 2015

L. S.

doc. Ing. Jaroslav Juračka, Ph.D.
Director of the Institute

doc. Ing. Jaroslav Katolický, Ph.D.
FME Dean

ABSTRACT

Master's thesis deals with a methodology proposal for the calculation of the dependent growth of cracks in multiple structural components using AFGROW software. The presented methodology, which also includes the residual strength analysis, has been practically applied in the damage tolerance analysis of the selected locations of the L 410 NG wing structure.

KEYWORDS

Damage tolerance analysis, dependent crack growth, residual strength analysis

ABSTRAKT

Diplomová práce se zabývá návrhem metodiky výpočtu závislého šíření trhlin ve více konstrukčních částech s využitím programu AFGROW. Prezentována metodika, která také zahrnuje stanovení zbytkové pevnosti, byla aplikována v damage tolerance analýzách vybraných míst na konstrukci křídla L 410 NG.

KLÍČOVÁ SLOVA

Damage tolerance analýza, závislé šíření trhlin, analýza zbytkové pevnosti

BIBLIOGRAPHIC CITATION

RAKOVSKÝ, K. *Aircraft structure Damage Tolerance analysis method aided by AFGROW software.* Brno: Brno University of Technology, Faculty of Mechanical Engineering, 2016. 101 p. Master's thesis supervisor Ing. Martin Nágel'.

BIBLIOGRAFICKÁ CITACE

RAKOVSKÝ, K. *Metodika analýz Damage Tolerance letecké konstrukce s využitím programu AFGROW.* Brno: Vysoké učení technické v Brně, Fakulta strojního inženýrství, 2016. 101 s. Vedoucí diplomové práce Ing. Martin Nágel'.

AFFIDAVIT

I declare that I developed my master's thesis *"Aircraft structure Damage Tolerance analysis method aided by AFGROW software"* on my own under the supervision of the master's thesis supervisor and with usage of the literature and additional information sources that are all cited in the thesis and stated in a list at the end of the thesis.

In Brno on 20.5.2016

....
Kristián Rakovský

ČESTNÉ PROHLÁŠENÍ

Prohlašuji, že svou diplomovou práci na téma „Metodika analýz Damage Tolerance letecké konstrukce s využitím programu AFGROW" jsem vypracoval samostatně pod vedením vedoucího diplomové práce a s použitím odborné literatury a dalších informačních zdrojů, které jsou všechny citovány v práci a uvedeny v seznamu literatury na konci práce.

V Brně dne 20.5.2016

....
Kristián Rakovský

ACKNOWLEDGEMENT

POĎEKOVÁNÍ

CONTENTS

1   INTRODUCTION

This master's thesis is based on author's work on the development of the L 410 NG commuter aeroplane performed at Aircraft Industries. The main objective of the thesis is to propose a viable methodology of analysing the fatigue crack growth of simultaneously propagating cracks in several structural elements. The need for such methodology arose during the process of fatigue and damage tolerance evaluation of the L 410 NG wing structure.

The first part of the thesis defines the problem and introduces relevant basic terms related to damage tolerance. Subsequently, the problem is described in greater detail, mainly in terms of the regulatory background.

The third part of the thesis briefly presents the theoretical instruments of fracture mechanics commonly used throughout the industry in damage tolerance analyses.

The next chapter states the major assumptions made during the development of the proposed methodology. The use of software is also discussed within this chapter, especially the utilization of AFGROW crack propagation software in the calculation process, which was also one of the objectives of this thesis.

The fifth chapter is dedicated to detailed description of the proposed methodology. Great concern is given to determination of the stress intensity factor of interfering cracks and dependent crack growth calculation procedure. The previously named aspects are the keystone of this thesis.

Practical application of the developed methodology in damage tolerance evaluation of the selected locations on the L 410 NG wing structure is presented in the sixth chapter. Last but not least, the benefits of the proposed methodology application are reviewed in the final chapter.

1.1 Problem definition

The solved problem comprises calculating the fatigue growth curves of multiple cracks in a statically indeterminate structure. A frequently encountered task within damage tolerance evaluation is to analyse the propagation of cracks initiated in commonly drilled holes of a riveted connection of adjacent structural element, as depicted in Figure 1.1. The regulatory basis of such task is interpreted in Subchapter 2.1.
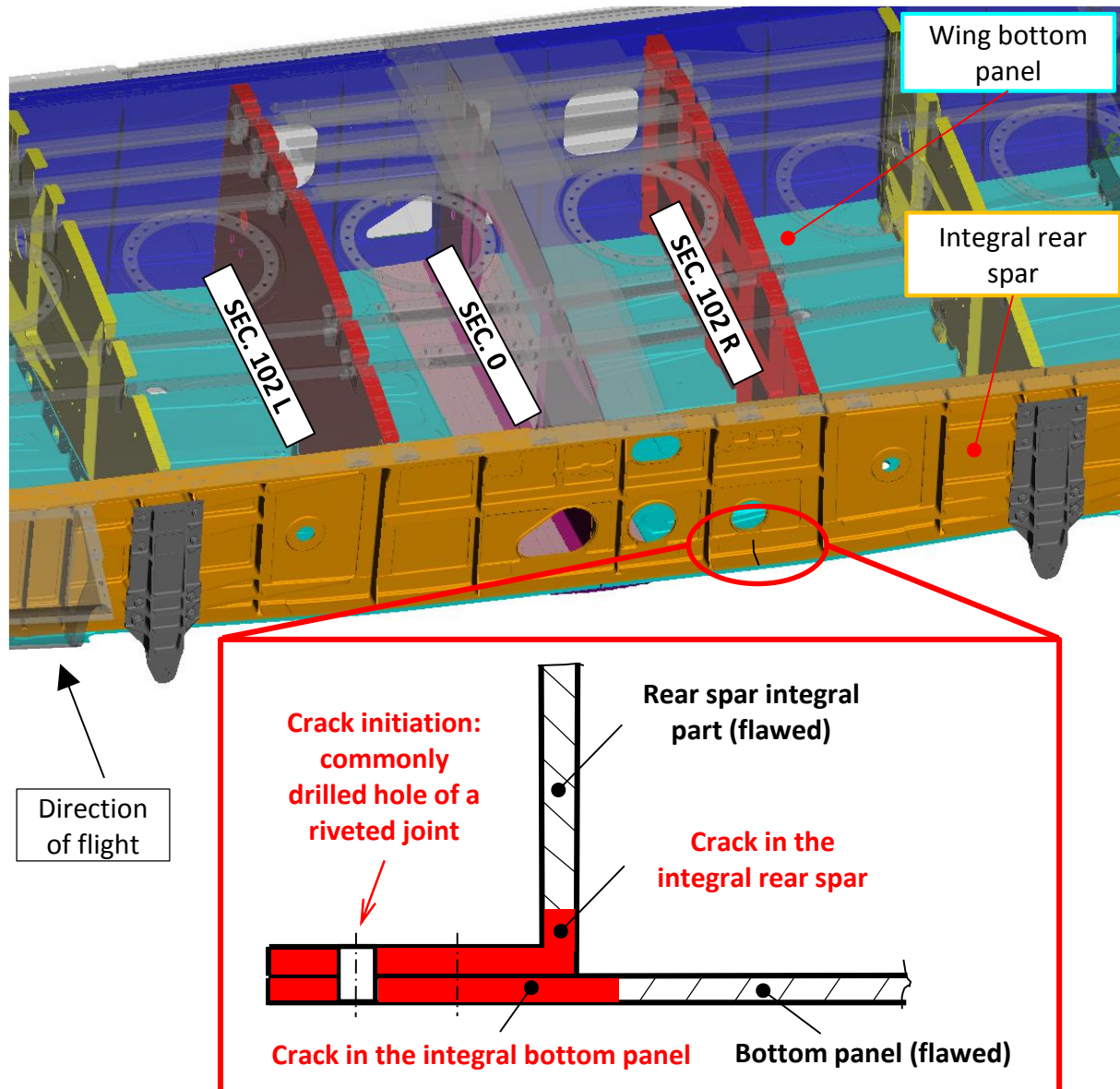
Figure 1.1 An example of a scenario in damage tolerance analysis of the L 410 NG wing. Cracks are initiated in rivet holes, both in the integral rear spar and bottom panel between section 0 and 102 R.

From the nature of a statically indeterminate structure it is clear, that the larger the crack in a given structural element, the more load is being redistributed onto the surrounding structure. This effect causes the fatigue growth of one crack to be significantly influenced by the growth of the other crack and vice versa. It is obvious, that a thorough analysis leads to a complex iterative step-by-step calculation. A solution with simplifying assumptions on the other hand can yield overly conservative results. The path of an

elaborate approach was selected for investigation in this master's thesis and it is described altogether with the assumptions made in the following chapters. Chapter 6 presents the confrontation of the results with simplified techniques.

1.2 Relevant major terms in fatigue and damage tolerance

Following is a list of relevant term definitions related to fatigue evaluation of an airframe. These terms are also used in Advisory Circulars [2] and [3].

Fatigue evaluation approaches

- **Safe-life** – one of the two major approaches of treating an airframe in terms of fatigue damage. The failure of such structure due to fatigue cracking leading to a catastrophic event is extremely improbable during its service life. The aeroplane is withdrawn from use (or the critical part is changed) after reaching the end of its safe service life.
- **Damage tolerance** – the other major approach of the aeroplane structure fatigue evaluation. It is an attribute of the structure that permits it to retain its required residual strength for a period of use after the structure has sustained a given level of fatigue, corrosion, accidental or discrete source damage until the damage is discovered by prescribed inspections. This approach applies to L 410 NG commuter aeroplane fatigue evaluation according to appropriate regulations [1].

Structure load distribution classification

- **Single load path** – describes structure, the applied loads of which are eventually distributed through a single structural member, the failure of which would result in the loss of the structural capability to carry the applied loads (see Figure 1.2).
- **Multiple load path** – applies to structure, the applied loads of which are distributed through redundant structural members, so that the failure of a single structural member does not result in the loss of structural capability to carry the applied loads (see Figure 1.2).
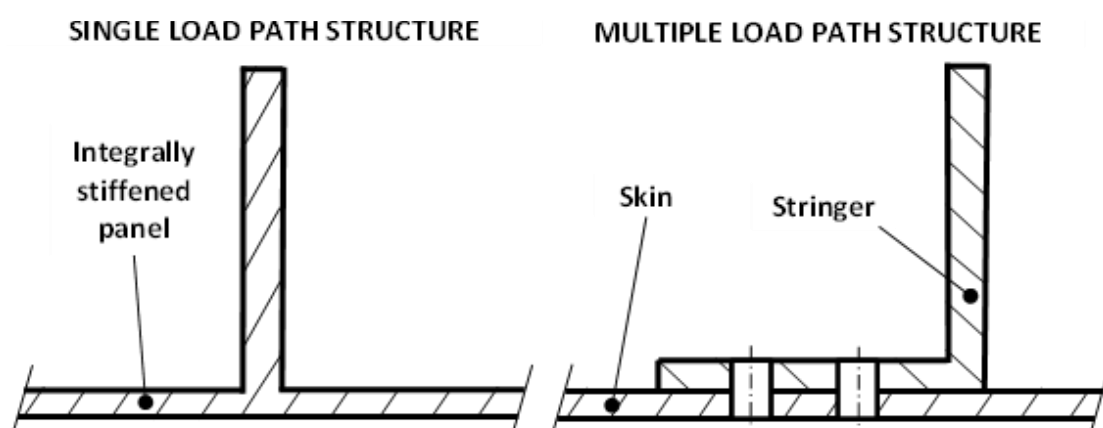

Figure 1.2 Comparison of the single and multiple load path structure.

Other terms and definitions

- **Principal structural element (PSE)** – an element that contributes significantly to the carrying of flight, ground or pressurization loads, and whose integrity is essential in maintaining the overall structural integrity of the aeroplane.

- **Residual strength** – the strength capability of a structure after the structure has been damaged due to fatigue, corrosion or discrete source damage. The residual strength capability includes consideration of static strength and fracture.
- **Fail-safe** – the attribute of structure that permits it to retain required residual strength for a period of unrepaired use after the failure or partial failure of a principal structural element.
- **Widespread fatigue damage (WFD)** – the simultaneous presence of cracks at multiple structural locations that are of sufficient size and density such that the structure will no longer meet the residual strength requirements. There are generally two sources of WFD: multiple site damage (simultaneous presence of fatigue cracks in the same structural element) and multiple element damage (simultaneous presence of fatigue cracks in adjacent structural elements) – see Figure 1.3.
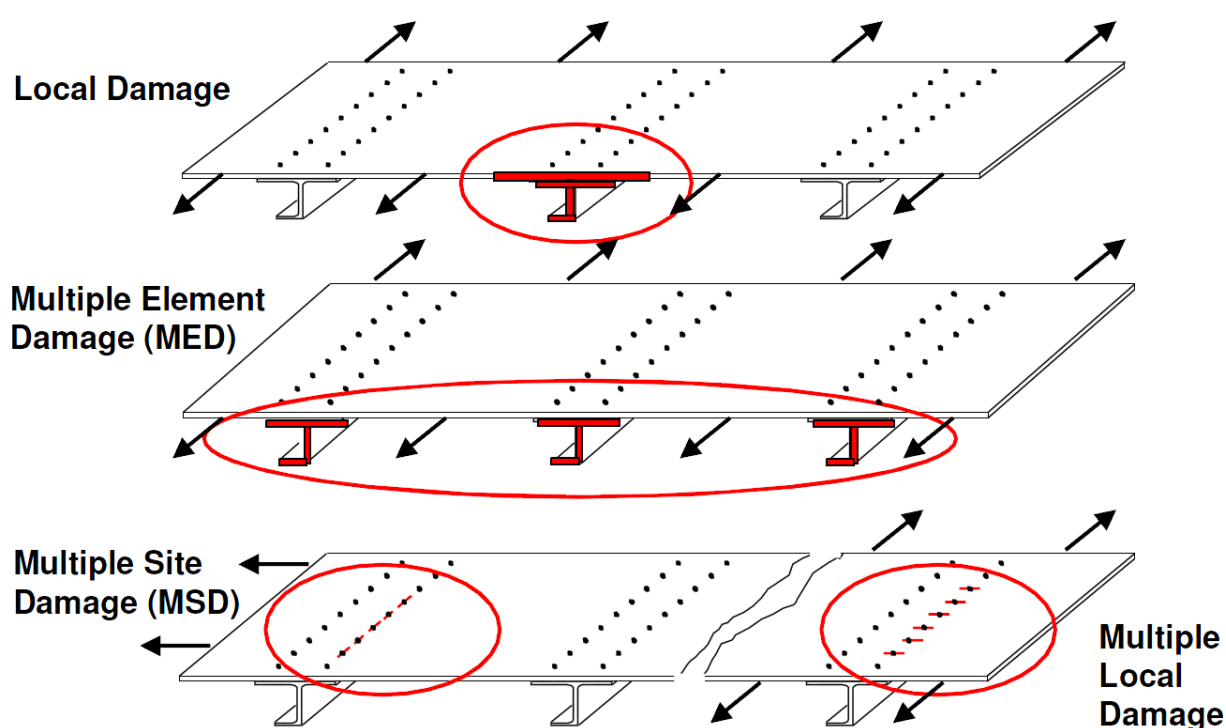
Figure 1.3 Comparison of local damage and widespread fatigue damage [20].

- **Design service goal (DSG)** – the period of time (in flight cycles, flight hours or both) established at design and/or certification during which the aeroplane structure is reasonable free from significant cracking.
- **Limit of validity (LOV)** (of the engineering data that supports the structural maintenance program) – the period of time (in flight cycles, flight hours or both), up to which it has been demonstrated by test evidence, analysis and, if available, service experience and teardown inspection results, that widespread fatigue damage will not occur in the aeroplane structure. The aeroplane cannot be operated after reaching its LOV.
- **Scatter factor** – a life-reduction factor used in interpreting fatigue analysis and test results.

Additional terms, together with an example of analysis and structural maintenance programme of a damage tolerant aeroplane, are presented in Figure 1.4.

18
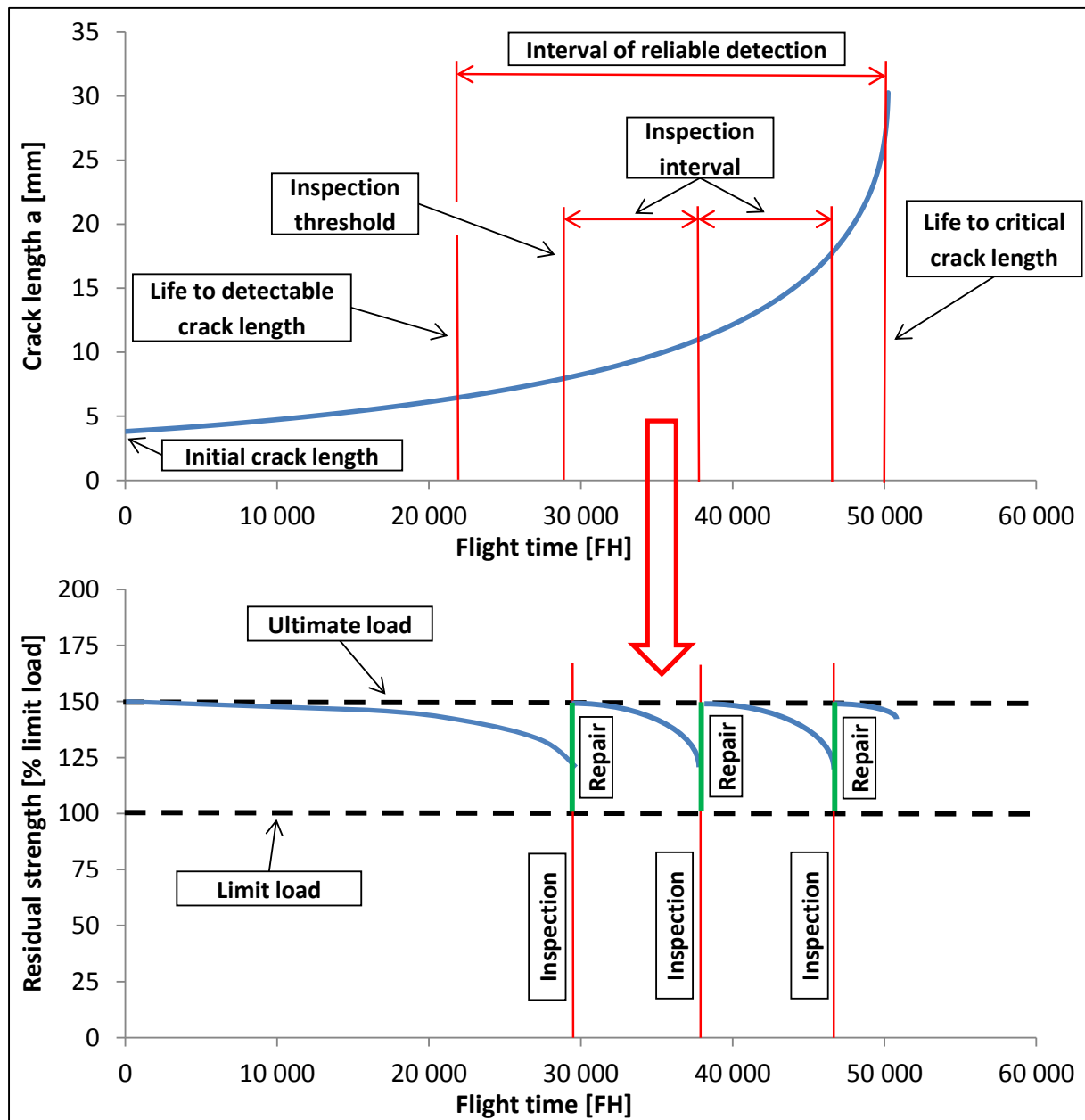
Figure 1.4 A basic example of crack growth analysis and determination of the structural maintenance programme of a damage tolerant aeroplane.

1.3 Brief description of the L 410 NG aeroplane

The L 410 NG is a newly designed derivative of the L 410 all-metal high-wing commuter aeroplane (see Figure 1.5 for three-view drawing), which is able to operate from both paved and unpaved airfields. The aeroplane made its maiden flight in 1969 with many modified versions to follow. The most significant structural changes introduced to the NG version when compared to its predecessors are:

- Built-up wing structure is mostly replaced by integral parts manufactured by high speed machining (e.g. skin stiffened by stringers is replaced by machined integral panels – see Figure 1.2).
- Integral fuel tanks replace the original bladder tanks (which results in a large increase of their capacity).

- The wing structure type is changed from a spar structure (with massive spar caps) to a semi-monocoque structure (cross-section area of the spar caps is reduced, extensive skin stiffening by stringers).
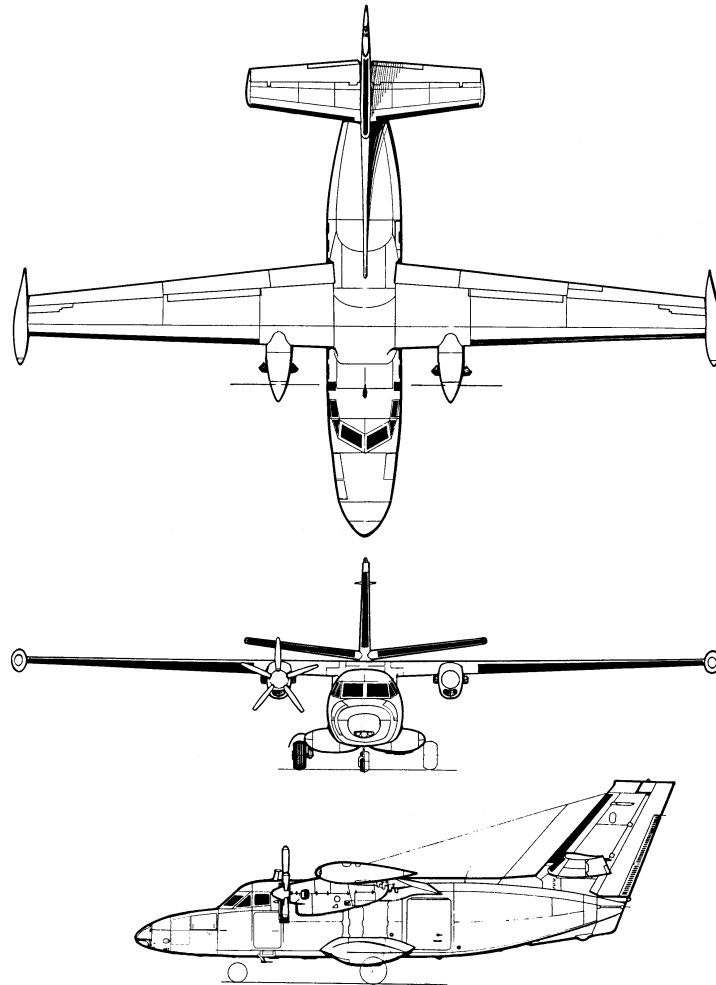
Figure 1.5 L 410 NG three-view drawing [8].

A comparison of the basic parameters of the NG version and the UVP-E20 version (the latest version currently in production) is presented in Table 1.1.

Table 1.1 Comparison of the basic parameters of L 410 NG and L 410 UVP-E20.

Aeroplane	L 410 NG	L 410 UVP-E20
Maximum take-off weight	7 000 kg	6 600 kg
Empty weight	4 200 kg	4 200 kg
Wingspan	19.48 m	19.98 m
Payload	2 200 kg	1 800 kg
Passengers	19	19
Engines	GE H-80-200	GE H-80-200
Propellers	Avia 725 five-blade	Avia 725 five-blade
Maximum speed (TAS)	412 km/h	398 km/h
Maximum range (ISA, 45 min. res.)	2 840 km	1 520 km
Service life	30 000 FH/landings	20 000 FH/landings

2 ANALYSIS OF THE PROBLEM

This chapter presents the scope of requirements imposed on the L 410 NG airframe in terms of fatigue and damage tolerance.

It also illustrates the typically analysed problems concerning multiple crack growth analysis, which arise as consequences of application of these requirements.

Furthermore, approaches of dealing with the specifics of multiple crack growth analysis currently used within L 410 NG damage tolerance evaluation are also stated in this chapter.

2.1 Regulatory basis

The L 410 NG is seeking certification under FAR 23 airworthiness standard. The binding requirements of this standard are introduced in this subchapter.

Since the demands of this standard are very general, detailed documents (FAA Advisory Circulars) describing the acceptable means of compliance are also investigated.

Moreover, additional materials related to damage tolerance analysis methodology and means of inspection are analysed. Joint Service Specification Guide 2006 (JSSG 2006), stipulating the initial flaw sizes and distribution, is of greatest importance for the subject of this thesis.

2.1.1 Airworthiness standard

Chapter "Fatigue Evaluation" of the FAR 23 airworthiness standard summarizes the requirements for fatigue and damage tolerance evaluation of an airframe. The following paragraphs are applicable for commuter category aeroplanes:

- **§ 23.574** – requirements concerning commuter category aeroplanes.
- **§ 23.573** – describes the extent of the damage tolerance evaluation.
- **§ 23.575** – deals with inspection program of the structure.

§ 23.574 Metallic damage tolerance and fatigue evaluation of commuter category aeroplanes

For commuter category aeroplanes:

(a) Metallic damage tolerance. An evaluation of the strength, detail design, and fabrication must show that catastrophic failure due to fatigue, corrosion, defects, or damage will be avoided throughout the operational life of the airplane. This evaluation must be conducted in accordance with the provisions of §23.573, except as specified in paragraph (b) of this section, for each part of the structure that could contribute to a catastrophic failure.

(b) Fatigue (safe-life) evaluation. Compliance with the damage tolerance requirements of paragraph (a) of this section is not required if the applicant establishes that the application of those requirements is impractical for a particular structure. This structure must be shown, by analysis supported by test evidence, to be able to withstand the repeated loads of variable magnitude expected during its service life without detectable cracks. Appropriate safe-life scatter factors must be applied.

§ 23.573   Damage tolerance and fatigue evaluation of structure

(a) **Composite airframe structure.** Not applicable for L 410 NG (all metal commuter).

(b) **Metallic airframe structure.** If the applicant elects to use §23.571(c) or §23.572(a)(3), then the damage tolerance evaluation must include a determination of the probable locations and modes of damage due to fatigue, corrosion, or accidental damage. Damage at multiple sites due to fatigue must be included where the design is such that this type of damage can be expected to occur. The evaluation must incorporate repeated load and static analyses supported by test evidence. The extent of damage for residual strength evaluation at any time within the operational life of the airplane must be consistent with the initial detectability and subsequent growth under repeated loads. The residual strength evaluation must show that the remaining structure is able to withstand critical limit flight loads, considered as ultimate, with the extent of detectable damage consistent with the results of the damage tolerance evaluations.

§ 23.575   Inspections and other procedures

Each inspection or other procedure, based on an evaluation required by §23.571, 23.572, 23.573 or 23.574, must be established to prevent catastrophic failure and must be included in the Limitations Section of the Instructions for Continued Airworthiness required by §23.1529.

2.1.2 Related Advisory circulars

AC 23-13A

This Advisory Circular (AC) sets forth acceptable means (but not the only means) of showing compliance with FAR 23 airworthiness standard. This guidance is applicable to fatigue, fail-safe, and damage tolerance evaluations of metallic structure in normal, utility, acrobatic, and commuter category aeroplanes. Material in this AC is neither mandatory nor regulatory in nature and does not constitute a regulation.

The following topics are dealt with in detailed manner:

- Small aeroplane fatigue regulations (together with basic terms definition).
- Safe-life fatigue evaluation.
- Fail-safe design.
- Damage tolerance evaluation – this part refers the applicant to AC 25.571-1D, since no guidance has been developed unique to FAR 23 damage tolerance evaluation. It also states the only significant regulatory difference between FAR 23 and FAR 25, which is that no discrete source damage capability (except for rotor burst) is required in FAR 23.
- Rotor burst requirements.
- Flights with known cracks.

AC 25.571-1D

This advisory circular (AC) provides guidance for compliance with the provisions of FAR 25 airworthiness standard (and also FAR 23 airworthiness standard in case the damage tolerance approach is opted for), pertaining to the requirements for damage-tolerance and fatigue evaluation of transport category aircraft structure, including evaluation of

widespread fatigue damage (WFD) and establishing a limit of validity of the engineering data that supports the structural-maintenance program (hereinafter referred to as the LOV). This AC also includes guidance pertaining to discrete source damage (not requested for FAR 23, except for rotor burst).

2.1.3 JSSG-2006

This guide establishes the joint structural performance and verification requirements for the airframe.

L 410 NG damage tolerance analyses follow this guides recommendations concerning **initial flaw size and flaw distribution**, which are stated in Part A.3.12.1 "Flaw sizes" of the guide and which are summed up in the following paragraphs.

Initial flaws are assumed to exist from the time of aeroplane manufacture as a result of material and structure manufacturing and processing operations. Each element of the structure should be surveyed to determine the most critical location and orientation (most unfavourable with respect to applied stresses and material properties) for the assumed initial flaws considering such features as edges, fillets, holes, and other potentially highly stressed areas.

Only **one initial flaw in the most critical hole** and **one initial flaw at a location other than a hole** need to be assumed to exist **in any structural element**. Interaction between these assumed initial flaws need not be considered. **Considering multiple and adjacent elements, the initial flaws need not be situated at the same location, except for structural elements where fabrication and assembly operations are conducted in such a way that flaws in two or more elements can exist at the same location.** The most common example of such an operation is the **assembly drilling of attachment holes**. Previous statements are the main causes of the problem of **multiple crack growth analysis** in L 410 NG damage tolerance evaluation, which is dealt with in this thesis.

The initial (primary) flaw sizes for locations with various geometrical configurations are depicted in Figure 2.2.

Secondary flaws, located **opposite the primary flaws**, are assumed to grow independently of the primary flaws up to the point that the primary flaw induces a failure. After the point of the full ligament failure, the continuing damage includes the growth of the secondary crack. The size of the secondary crack is shown in Figure 2.1.
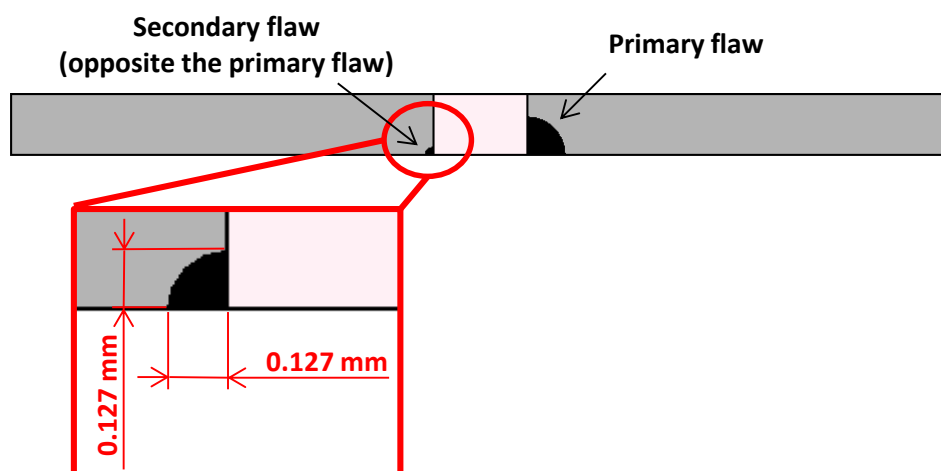
Figure 2.1 Secondary flaw size according to [4].
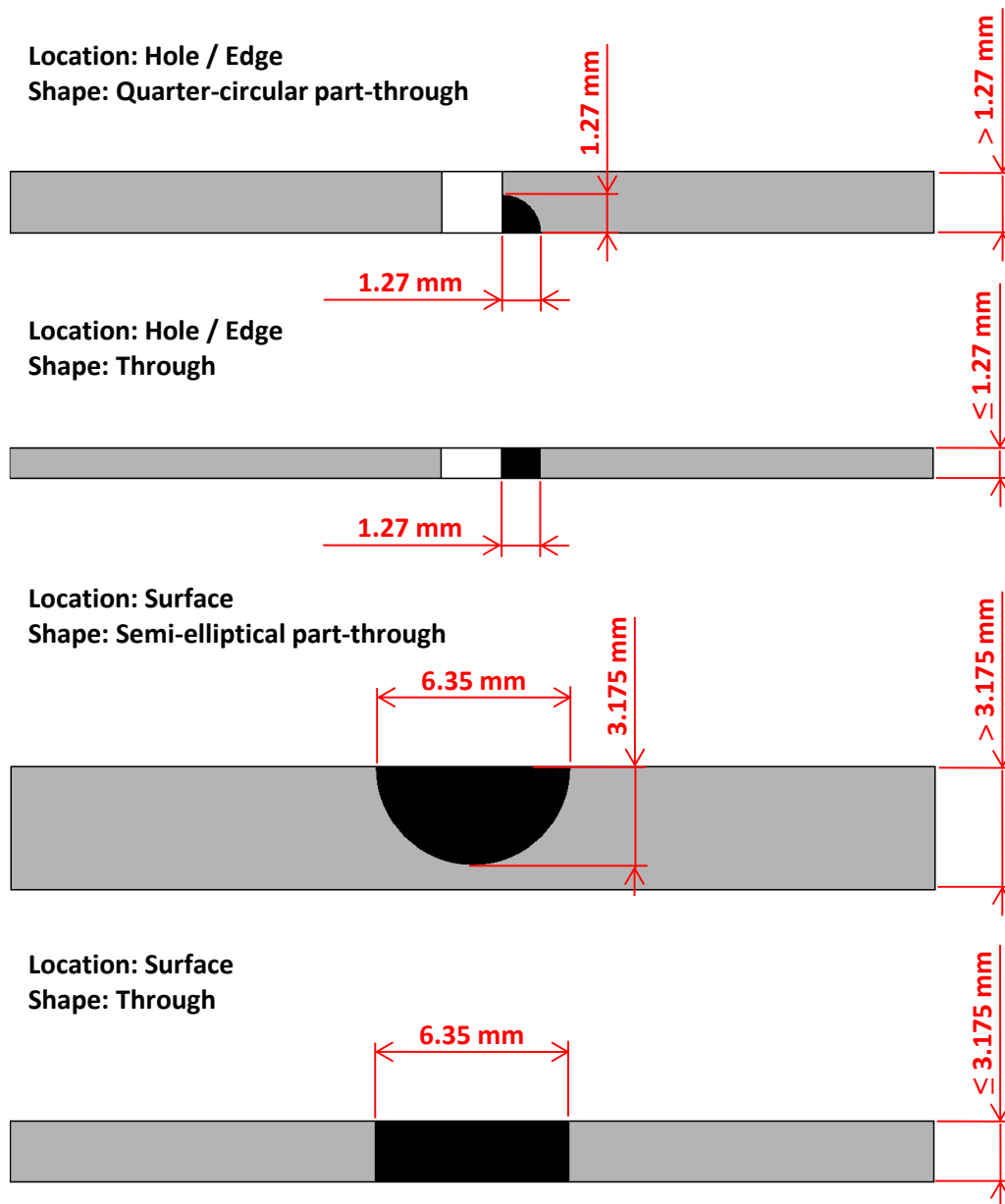
Figure 2.2 Primary flaw sizes according to [4].

2.1.4 MSG-3

Maintenance Steering Group 3 (MSG-3) is a procedure logic for maintenance of aeroplanes developed by Air Transport Association of America (ATA).

MSG-3 also sets a standard for determining detectable flaw sizes in an arbitrary location, which is widely acknowledged throughout the industry. MSG-3 methodology assumes two inspection methods (general visual inspection GVI and detailed visual inspection DET) and takes several factors into considerations (e.g. access to the location, congestion of the area, light conditions, etc.). The full typical MSG-3 logic sheet for detectable crack determination is shown in Figure 2.3.

MSG-3 LOGIC

INSPECTION LEVEL	GENERAL VISUAL INSPECTION (GVI)	DETAILED VISUAL INSPECTION (DET)

VIEWING RATING

CONGESTION RATING	Poor			Moderate			Good		
	Congested	Moderate congestion	Clear	Congested	Moderate congestion	Clear	Congested	Moderate congestion	Clear
	1	2	3	2	3	4	3	4	5
	ACCES RATING								

LIGHTING RATING

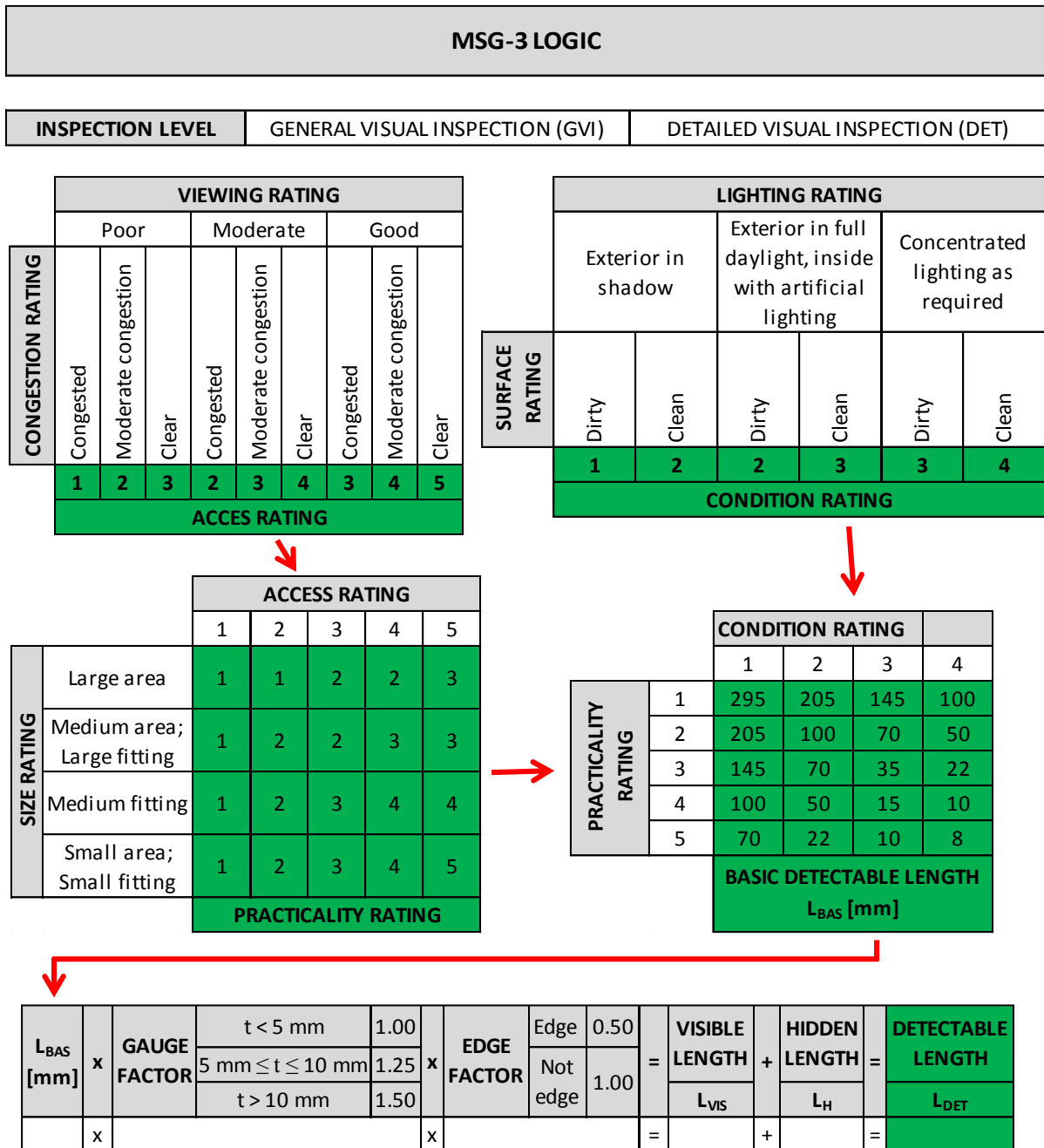| SURFACE RATING	Exterior in shadow		Exterior in full daylight, inside with artificial lighting		Concentrated lighting as required	
	Dirty	Clean	Dirty	Clean	Dirty	Clean
	1	2	2	3	3	4
	CONDITION RATING					

ACCESS RATING

SIZE RATING		1	2	3	4	5
	Large area	1	1	2	2	3
	Medium area; Large fitting	1	2	2	3	3
	Medium fitting	1	2	3	4	4
	Small area; Small fitting	1	2	3	4	5
	PRACTICALITY RATING					

CONDITION RATING

PRACTICALITY RATING		1	2	3	4
	1	295	205	145	100
	2	205	100	70	50
	3	145	70	35	22
	4	100	50	15	10
	5	70	22	10	8

BASIC DETECTABLE LENGTH L_{BAS} [mm]

L_{BAS} [mm]	x	GAUGE FACTOR	t < 5 mm	1.00	x	EDGE FACTOR	Edge	0.50	=	VISIBLE LENGTH L_{VIS}	+	HIDDEN LENGTH L_H	=	DETECTABLE LENGTH L_{DET}
			5 mm ≤ t ≤ 10 mm	1.25			Not edge	1.00						
			t > 10 mm	1.50										
	x				x				=		+		=	

Figure 2.3 MSG-3 logic analysis. Based on [5].

2.2 Typically analysed scenarios

This subchapter states example problems of dependent multiple crack growth, which are consequent to following the requirements and recommendations of the regulations and guidance material introduced in Subchapter 2.1.

The most frequently encountered scenario in L 410 NG damage tolerance analysis is shown in Figure 2.4. It is the case of **crack initiation in a commonly drilled hole of a riveted joint** of two adjacent structural elements (in this case the spar cap and shear web). These flaws can be treated independently (or with simple load redistribution assumptions) when they are of short length. However, at the point of full ligament failure on both flawed elements (see Figure 1.1) the crack interaction is significant and their growth becomes

strongly dependent on one another. L 410 NG damage tolerance analysis has addressed the problem so far by making one of the following simplifying assumptions:

- **Assuming a complete spar cap failure at the point of full spar cap ligament failure** – this approach is possible when the shear web is the structural element of interest. The problem then becomes the analysis of continuing damage growth in the shear web with a completely failed spar cap.
- **Assuming a crack growth ratio in the elements of 1:1 after the full ligament failure on both elements** – this approach accounts for the simultaneous multiple crack growth in a simple way. First, a crack grow ratio of 1:1 is assumed in the stress analyses of the structure for increasing crack lengths. The results of the stress analyses are subsequently used for predicting the growth of the two cracks. The resultant growth curves are derived from the growth curve of the faster growing crack.
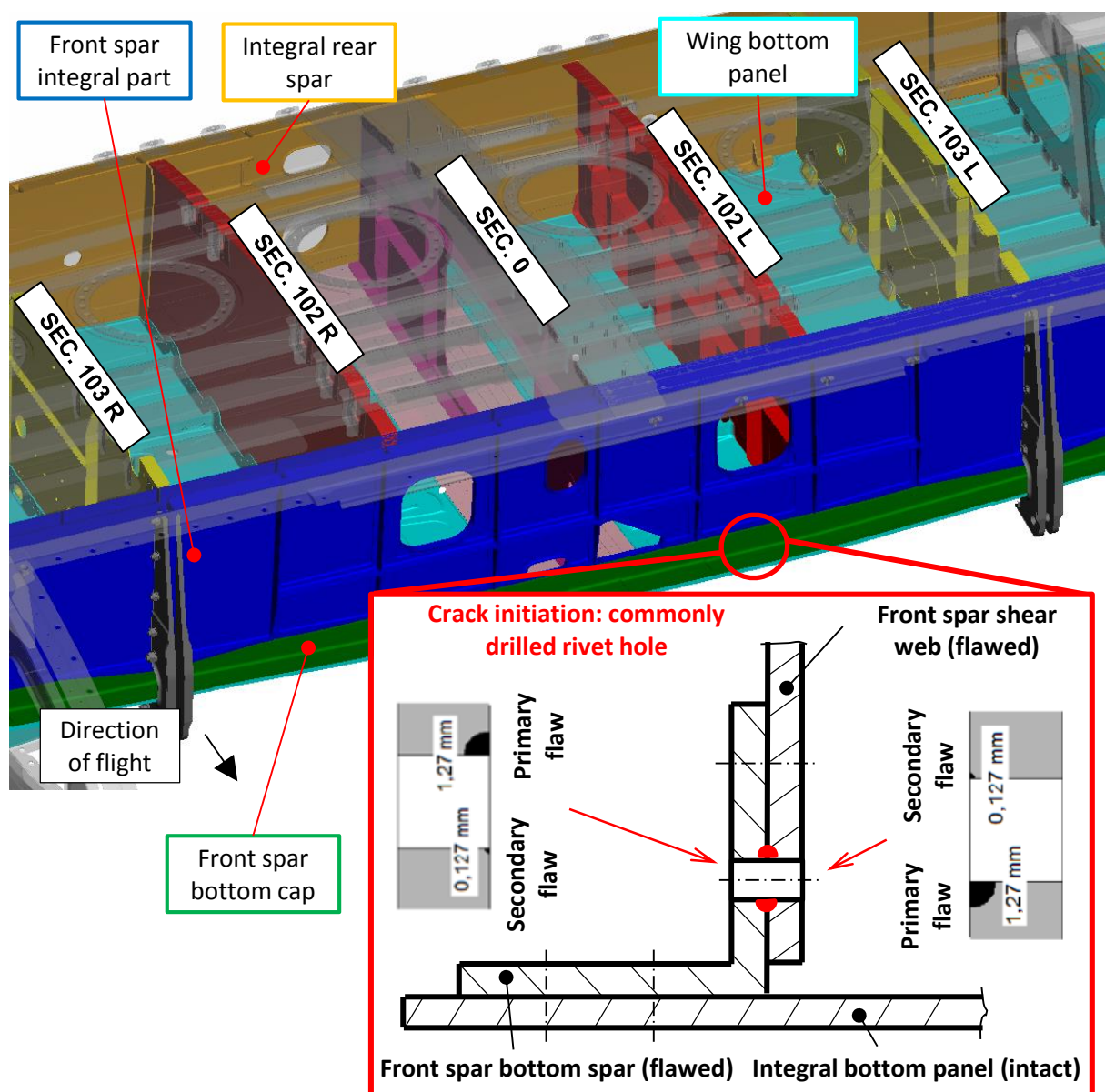

Figure 2.4 Example multiple crack growth problem – crack initiation at a commonly drilled hole of a riveted joint of two adjacent structural members.

Another example of dependent crack growth encountered in L 410 NG damage tolerance evaluation is depicted in Figure 2.5. This may not seem as a dependent crack growth problem, since it is possible to treat the primary and secondary flaws independently up until the point of primary flaw inducing a full ligament failure (according to JSSG-2006 [4]). However, after the continuing damage propagates to the skin of the integral panel, the problem becomes the growth analysis of an **internal through crack under non-symmetrical conditions**. Once again, a simplified approach **assuming symmetrical propagation** has been adopted so far in L 410 NG damage tolerance analysis (see the previous paragraph for closer description).
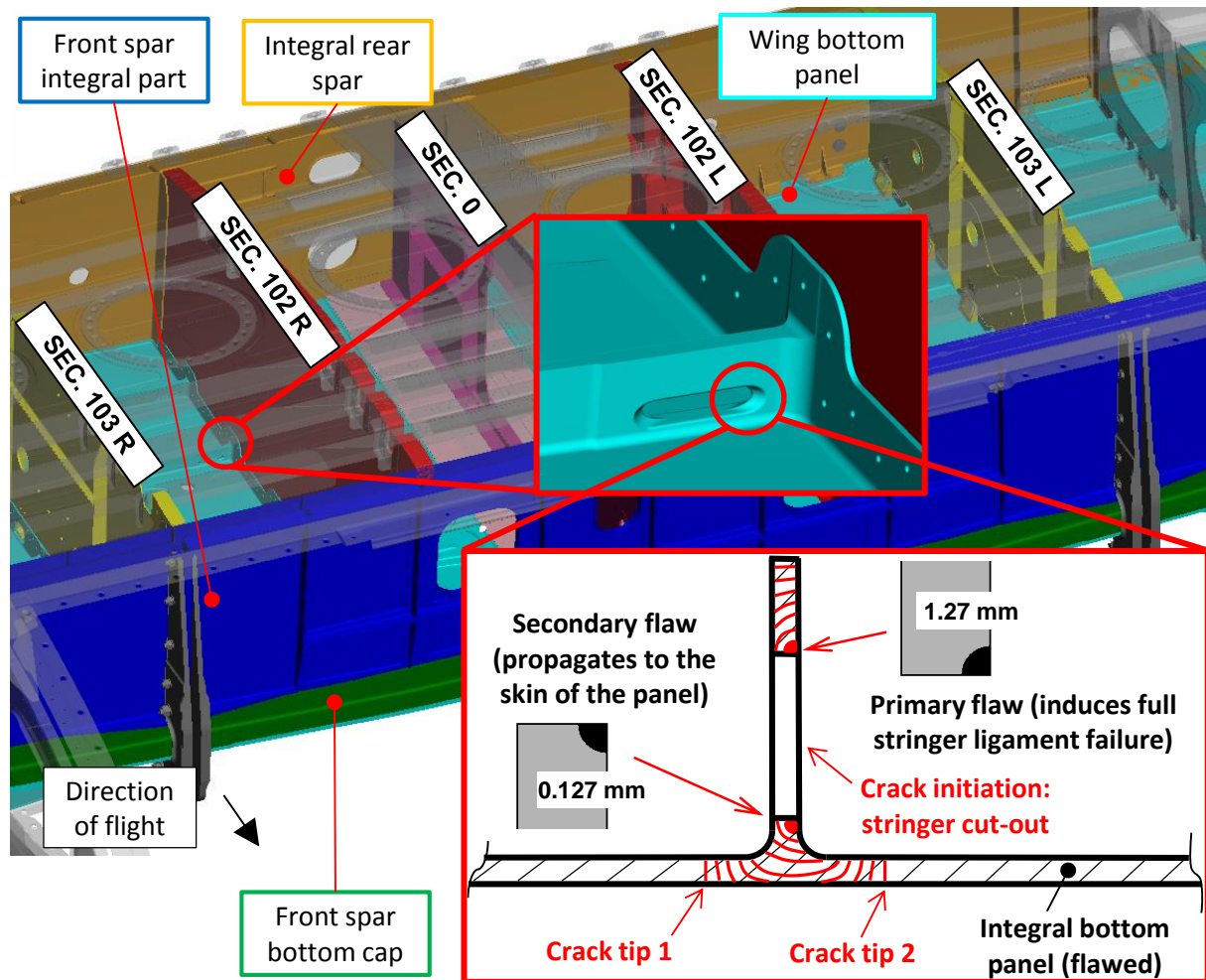

Figure 2.5 Example dependent crack growth problem – unsymmetrical propagation of an internal panel crack (growth of tip 1 is dependent on the growth of tip 2 and vice versa).

Treating the mentioned multiple crack growth problems by simplifying assumptions described in the previous two paragraphs can lead to overly conservative results, especially concerning the inspection interval. The reason for this is that MSG-3 logic (see Subchapter 2.1.4) yields detectable crack lengths, which the flaws usually reach after the point of full ligament failure on both members. The crack interaction plays a vital role in the crack growth beyond this point. The value of **inspection interval**, which is calculated by factoring the difference of life to critical flaw length and life to detectable flaw length (see Figure 1.4), **can be vastly affected by the assumptions made concerning dependent crack growth**. A detailed investigation of the crack interaction phenomenon performed in this thesis is therefore justified.

3 THEORETICAL BACKGROUND

This chapter briefly states the essentials of **linear elastic fracture mechanics (LEFM)**, which is a basic instrument utilized in L 410 NG damage tolerance analyses. For a more thorough description of the tools used in L 410 NG damage tolerance evaluation the reader is referred to literature [10].

3.1 Stress intensity factor

Since a crack is a notch with a zero tip radius, the notch concentration factor is infinite and so is the theoretical value of the stress at the crack tip for any crack length. This is therefore not a meaningful concept of describing the severity of the stress distribution around the crack tip. A **stress intensity factor (SIF, K)** concept, which accounts for the load and geometric properties, was developed for the description of the severity of the stress distribution at the crack tip. The modes of crack tip loading (denoted as I, II and III) are shown in Figure 3.1.
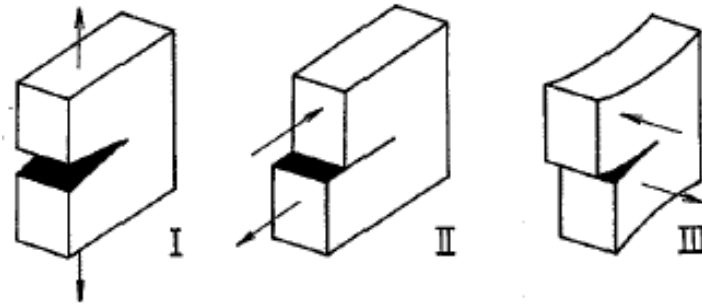

Figure 3.1 Crack opening modes. Mode I – Tensile opening. Mode II – in-plane shear. Mode III – anti-plane shear [12].

The stress intensity factor is usually defined in the following form:

$$K_I = \beta \sigma \sqrt{\pi a} \qquad (3.1)$$

In the equation above, K_I is the stress intensity factor of a crack under "Mode I" load conditions, σ is the remote loading stress and a is the crack length (half crack length in case of an internal crack, full crack length in case of an edge crack). The term $\sigma \sqrt{\pi a}$ represents the stress intensity factor of a crack in an infinitely wide plate and **β is the so-called β-function or shape function**, which accounts for geometric arrangement, type of loading, etc.

As discussed in the first paragraph of this section, a crack can be considered as a notch with zero radius. This implies a stress singularity at the crack tip. This is however not feasible for a real material, which shows yielding. A plastic zone therefore occurs at the crack tip. The size (radius) of the plastic zone can be estimated using a simple one dimensional approach based on reviewing the magnitude of the stress in the y-direction (perpendicular to the crack, see Figure 3.2) along the x-direction (see Figure 3.2), which can be calculated according to Equation (3.2) [13].

$$\sigma_y(r, 0) = \frac{K_I}{\sqrt{2\pi r}} \qquad (3.2)$$

The radius of the plastic zone can be estimated as per Equation (3.3) [13]. Note that the size of the plastic zone under plane stress conditions is three times larger than that under plane strain conditions. This is caused by the fact that the yield strength is larger under plane strain conditions.

$$r_p(plane\ stress) = \frac{1}{2\pi}\left(\frac{K}{R_{p0.2}}\right)^2 \; ; \; r_p(plane\ strain) = \frac{1}{6\pi}\left(\frac{K}{R_{p0.2}}\right)^2 \qquad (3.3)$$
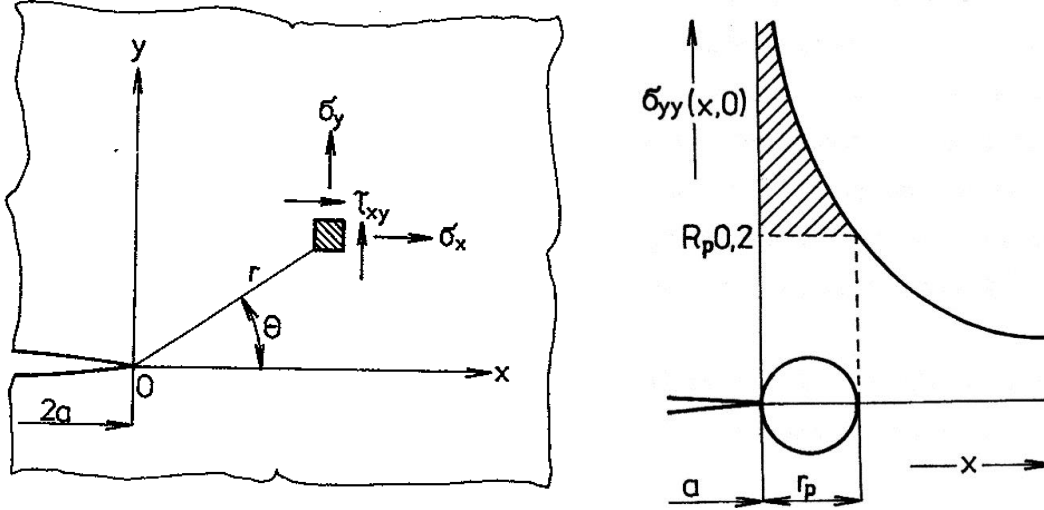

Figure 3.2 On the plastic zone at the crack tip [12].

The accuracy of linear elastic fracture mechanics is deemed to be sufficient if the following condition is satisfied:

$$r_p \ll \alpha \qquad (3.4)$$

A mixed mode I and II loading can be addressed as per Equation (3.5) . This equation is applicable in case that K_{II} is small compared to K_I, which is satisfied in most problems.

$$K = \sqrt{K_I^2 + K_{II}^2} \qquad (3.5)$$

For more details concerning stress intensity factor and other theoretical basis of linear elastic fracture mechanics the reader is referred to literature [12] and [13].

3.1.1 Analytical solution

There are many analytical solutions available. Most of them are for relatively simple geometries, but there are also solutions for aircraft structures, such as stiffened panels. Example can be seen below (Figure 3.3, Equation (3.6) [13]) for a central internal crack in a finite-width plate under uniaxial stress.

$$K_I = \sigma\sqrt{\pi a}\,\beta = \sigma\sqrt{\pi a}\,\sqrt{\frac{1}{\cos\left(\frac{\pi a}{w}\right)}} \qquad (3.6)$$
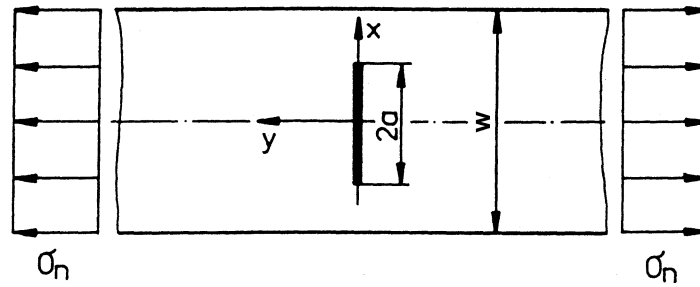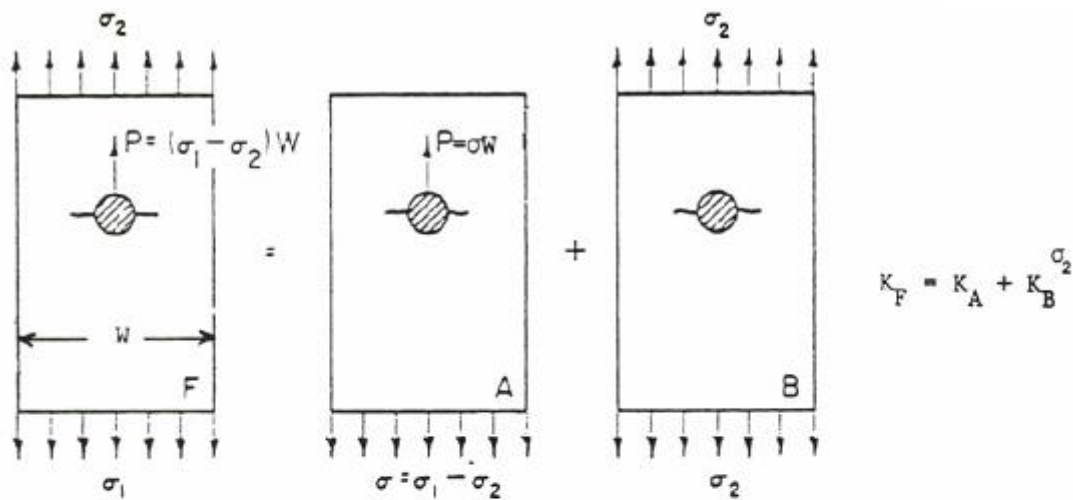
Figure 3.3 Central internal crack in a finite plate under uniaxial stress.

Furthermore, linear elastic fracture mechanics allow for obtaining solutions for complex loading of a given geometry by linear superposition as demonstrated in Figure 3.4.
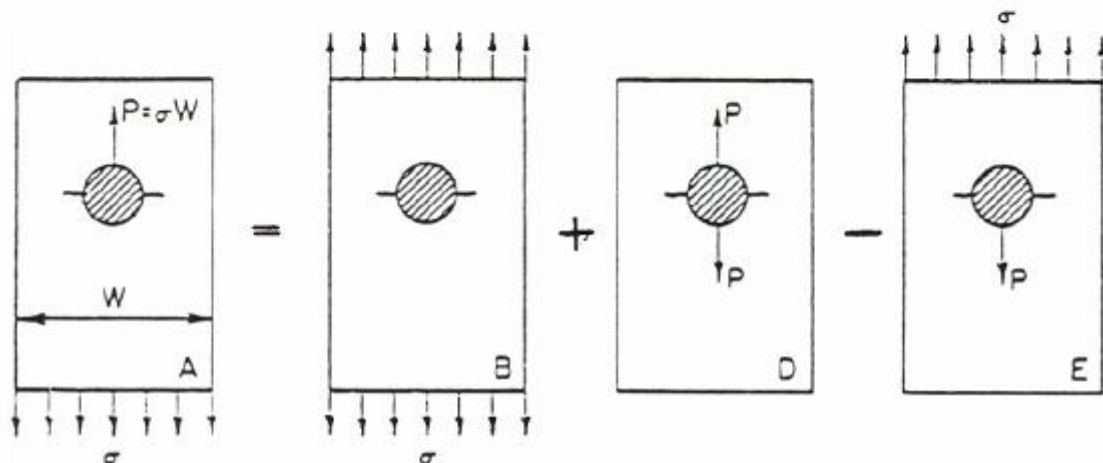

Figure 3.4 Superposition of solutions – pin loaded hole [10].

Analytical stress intensity factor solutions are suitable for relatively short crack lengths (up to 10 mm), since they account for geometrical and loading details, that would be very demanding to include in a finite element model. Many analytical solutions for various geometries and loadings are available in the AFGROW software, which is used for crack

growth calculation. An example frequently used in L 410 NG damage tolerance analyses is the case of the pin loaded hole (Figure 3.4) representing riveted connection, which is usually used up until the point of full ligament failure in the crack growth calculation.

On the other hand, analytical stress intensity factors do not account for load redistribution in a statically indeterminate structure. This effect is very significant for long cracks and analytical SIF solutions tend to be overly conservative for such cracks.

3.1.2 Numerical solution

The numerical solution is obtained by finite element method (FEM) by one of the three following approaches:

- Calculation from the stress field
- Calculation from the displacement field
- Energetic method

Calculation by the **displacement field approach** is included in **MSC NASTRAN** finite element code in the form of special crack tip elements. The calculation utilizing these elements in MSC NASTRAN is used in the L 410 NG damage tolerance methodology [10]. It is therefore shortly described below.

Equation (3.7) [13] presents the known equation for the y-direction displacement (in its modified form) for $\theta = \pi$ (see Figure 3.2) and plane stress conditions.

$$v(r,\pi) = \frac{4K_I}{E}\sqrt{\frac{r}{2\pi}} \tag{3.7}$$

After rearrangement one obtains the following equation, which is then solved numerically:

$$K_I = \lim_{r\to 0}\frac{E}{4}\sqrt{\frac{2\pi}{r}}\ v(r,\pi) \tag{3.8}$$

The influence of element size on the accuracy of the method above in MSC NASTRAN was investigated in [27]. The results are compared to an analytical solution in Figure 3.5.
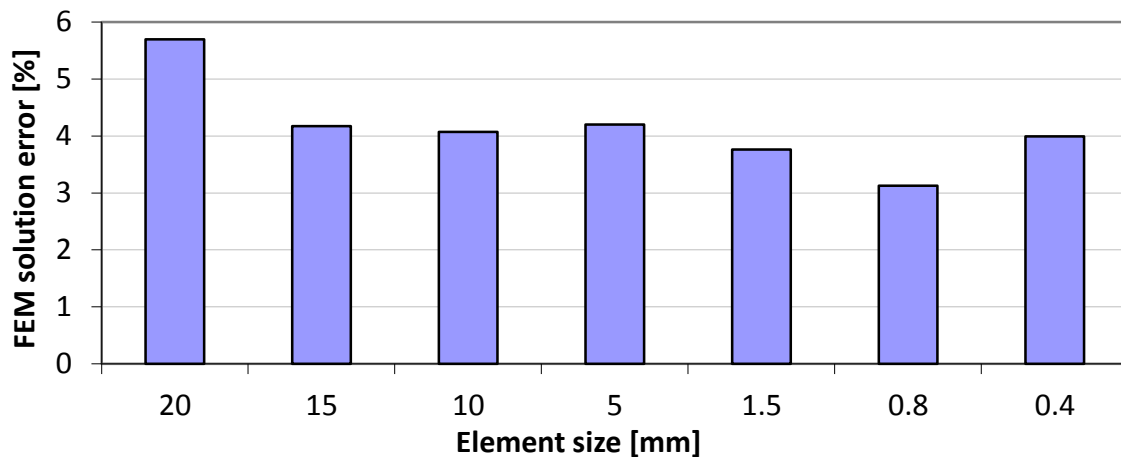

Figure 3.5 Influence of the element size on the accuracy of the FEM solution [27].

31

3.2 Fatigue crack growth prediction

Crack growth prediction is an integral part of the L 410 NG damage tolerance analysis. This subchapter covers the absolute basics of the crack propagation calculation currently used in the L 410 NG damage tolerance methodology [10]. For more details the reader is referred to the methodology [10] and to literature [12], [13] and [16].

3.2.1 Crack propagation under constant amplitude loading

Figure 3.6 presents a typical **da/dN vs. ΔK** curve (crack length increment per cycle vs. stress intensity factor range), which characterises the crack growth under constant amplitude loading. The stress intensity factor range is defined as per Equation (3.9).

$$\Delta K = \beta \Delta \sigma \sqrt{\pi a} \qquad\qquad (3.9)$$
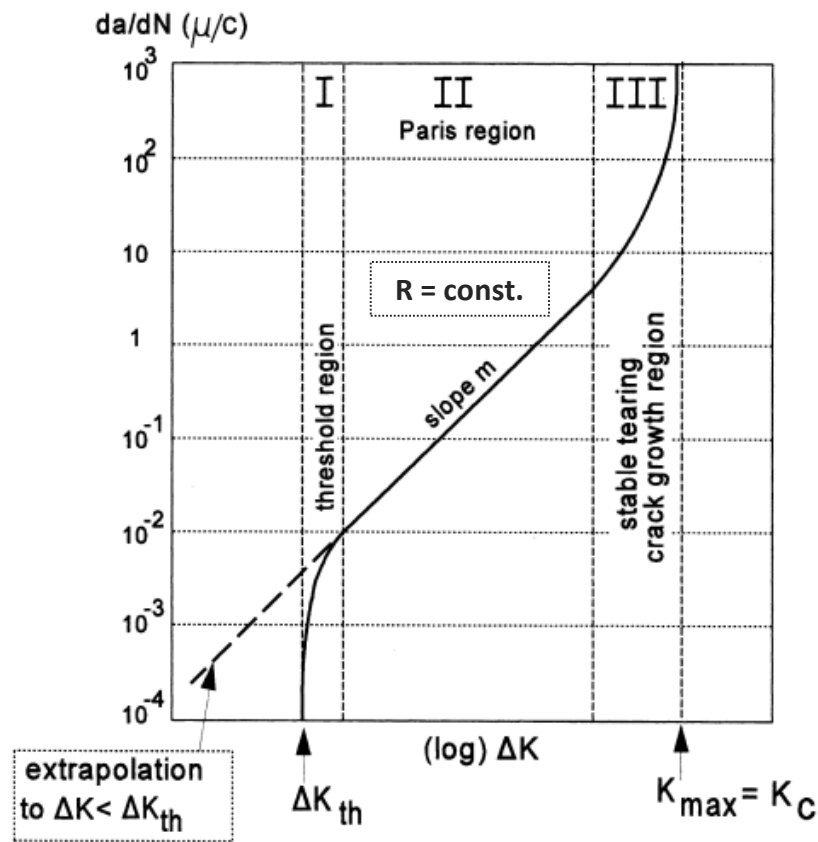

Figure 3.6 Crack propagation under constant amplitude loading [13].

The da/dN vs. ΔK curve in Figure 3.6 is split into the following three regions:

- **Threshold region** (denoted as "I") – crack with a ΔK lower than the threshold value (ΔK_{th}) does not grow. Note that this concept is valid only for macro-cracks. However, Schijve [13] alleges, that the ΔK_{th} concept may not be a safe assumption, especially for variable amplitude loading. It is rather recommended to extrapolate the Paris region backwards as shown in Figure 3.6. This recommendation is implemented in L 410 NG crack growth analyses.
- **Paris region** (denoted as "II") – represents the stable growth of a crack.
- **Stable tearing region** (denoted as "III") – represents the fast crack growth prior to the final failure.

Equations (3.10) through (3.13) introduce three of the many crack growth models that were developed over the years.

- **Paris – Erdogan** law [13] – Describes region "II" and disregards the influence of R-ratio. C and m are material constants.

$$\frac{da}{dN} = C\Delta K^m \tag{3.10}$$

- **Klesnil and Lukáš** equation [15] – Covers regions "I" and "II" and also accounts for the effect of changing R-ratio in the ΔK_{th} determination. A, m and γ are material constants.

$$\frac{da}{dN} = A(\Delta K^m - \Delta K_{th}^m) \tag{3.11}$$

$$\Delta K_{th} = A(1-R)^\gamma \tag{3.12}$$

- **Forman equation** [13] – Includes regions "II" and "III" and also the influence of the changing R-ratio. C, m and K_{cf} are material constants.

$$\frac{da}{dN} = \frac{C\Delta K^m}{(1-R)K_{cf} - \Delta K} \tag{3.13}$$

Subchapter 3.1 discusses the monotonic plastic zone at the crack tip, which occurs during loading of the structure. However, as soon as the structure is unloaded a so called **reverse plastic zone** takes place at the crack tip, which closes the crack tip due to a residual compression stress distribution around the tip – see Figure 3.7.
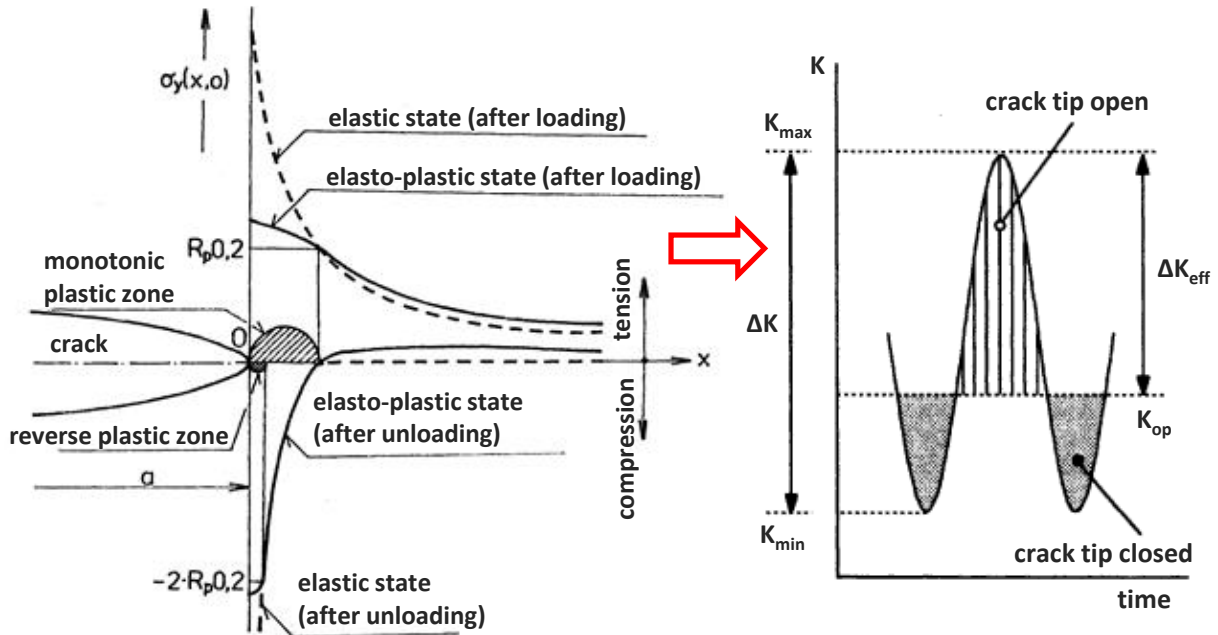

Figure 3.7 Monotonic and reverse plastic zone [12] [13].

The consequence of the occurrence of the reverse plastic zone is that the crack tip is open and the stress singularity exists only during a part of the load cycle, even if the load

cycle is in pure tension – see Figure 3.7. This effect is called **crack closure**. An effective stress intensity factor range, representing the part of the load cycle during which the crack tip is open, can be defined as per Equation (3.14). Its value is usually calculated by a semi-empirical approach.

$$\Delta K_{eff} = K_{max} - K_{op} \qquad (3.14)$$

Expressing the crack growth rate as a function of ΔK_{eff}, rather than ΔK, results in that there is only one curve for all R-ratios, as depicted in Figure 3.8.
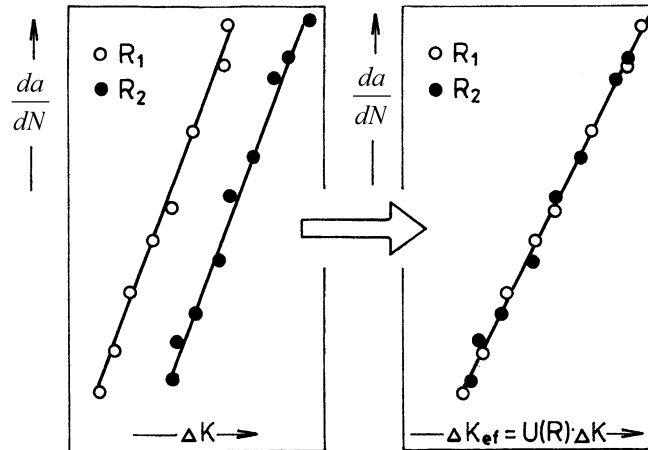

Figure 3.8 Comparison of the crack growth rate expressed as a function of ΔK and ΔK_{eff} [12].

3.2.2 Crack propagation under variable amplitude loading

Crack closure, discussed in the previous subchapter, is a significant factor influencing not only crack growth under constant amplitude loading, but especially crack growth under variable amplitude loading. The reason for this is that when a load peak is encountered during the variable loading, both monotonic and reverse plastic zones are enlarged. This causes the increase of the compression field at the crack tip and ultimately results in decreased crack opening and the subsequent crack growth being slowed down. This phenomenon is called **crack growth retardation** or **load interaction** and is illustrated in Figure 3.9.
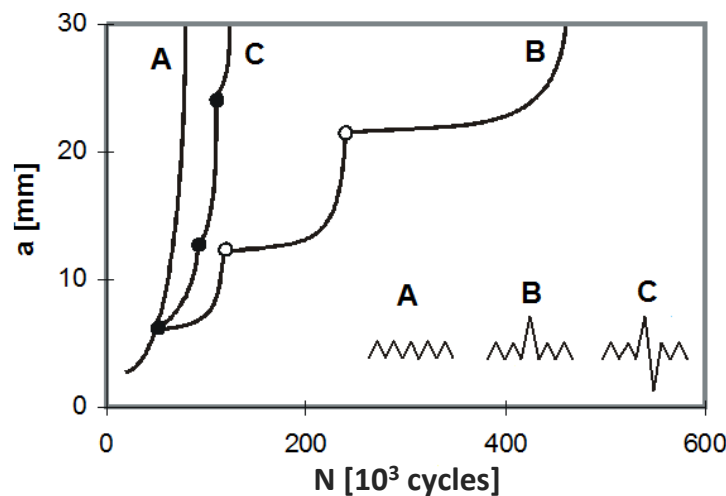

Figure 3.9 Load interaction under variable amplitude loading [13].

34

Figure 3.10 presents the industry renowned procedure of crack growth calculation under variable amplitude loading. It is worth noting, that material data obtained under constant amplitude loading are used for predictions under variable amplitude loading. However, this is a widely accepted practice.
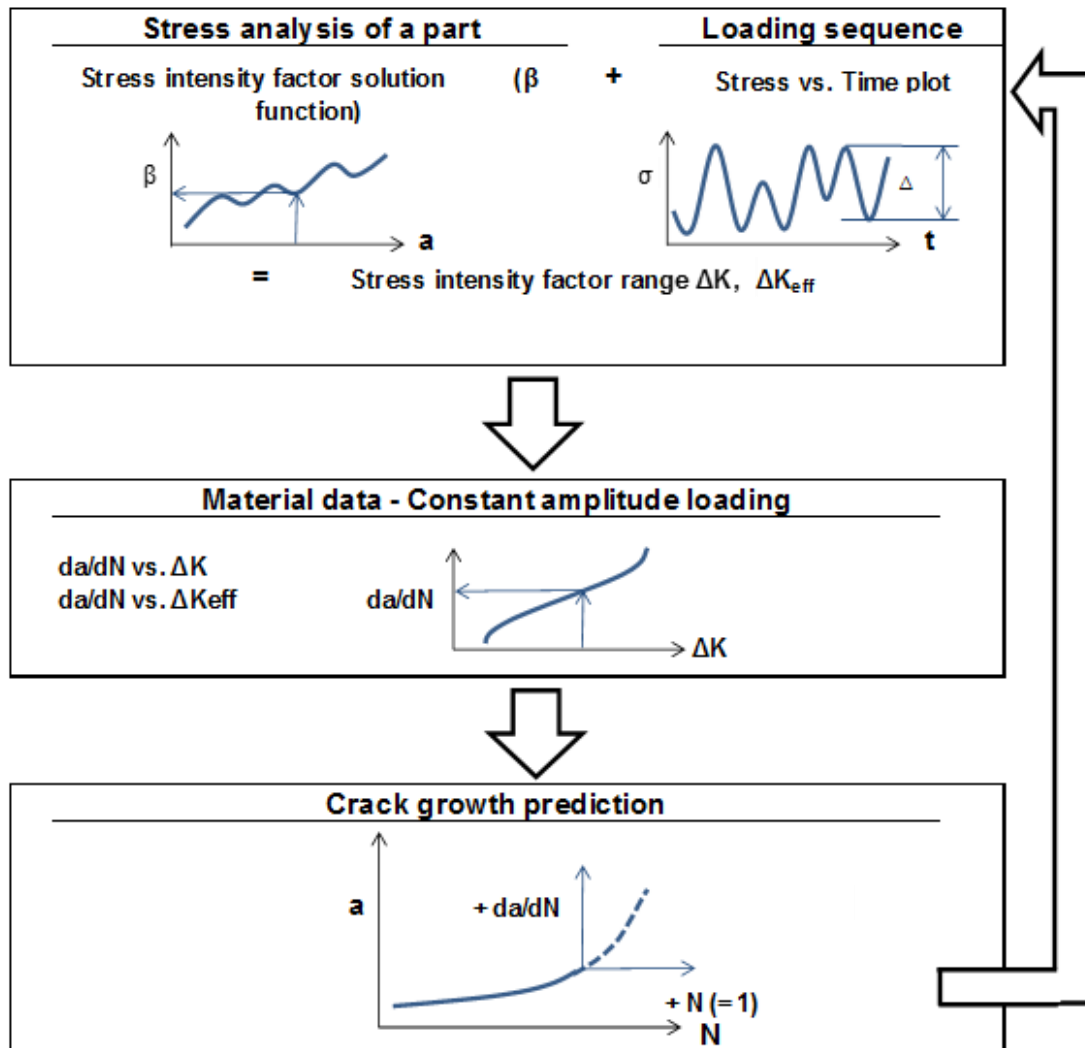

Figure 3.10 Procedure of calculating crack growth under variable amplitude loading [10].

The following two approaches are utilized for the task of crack growth prediction under variable amplitude loading:

- **Calculation without interaction effects** – a simple approach disregarding any load interaction effects. Crack growth is dependent only on the severity of the pertaining load cycle. A **highly conservative solution** is usually obtained. This approach has been **used so far in L 410 NG damage tolerance analyses**, since there is not enough test evidence to support crack retardation at the moment.
- **Calculation with interaction effects** – the complexity of this approach depends on the selected interaction model, from the simplest yield zone models, through crack closure models, to strip yield models, which have the most solid physical background. The overview of load interaction models is shown in Figure 3.11. For a much more detailed theoretical description of the crack retardation models the reader is referred to literature [6] and [13].
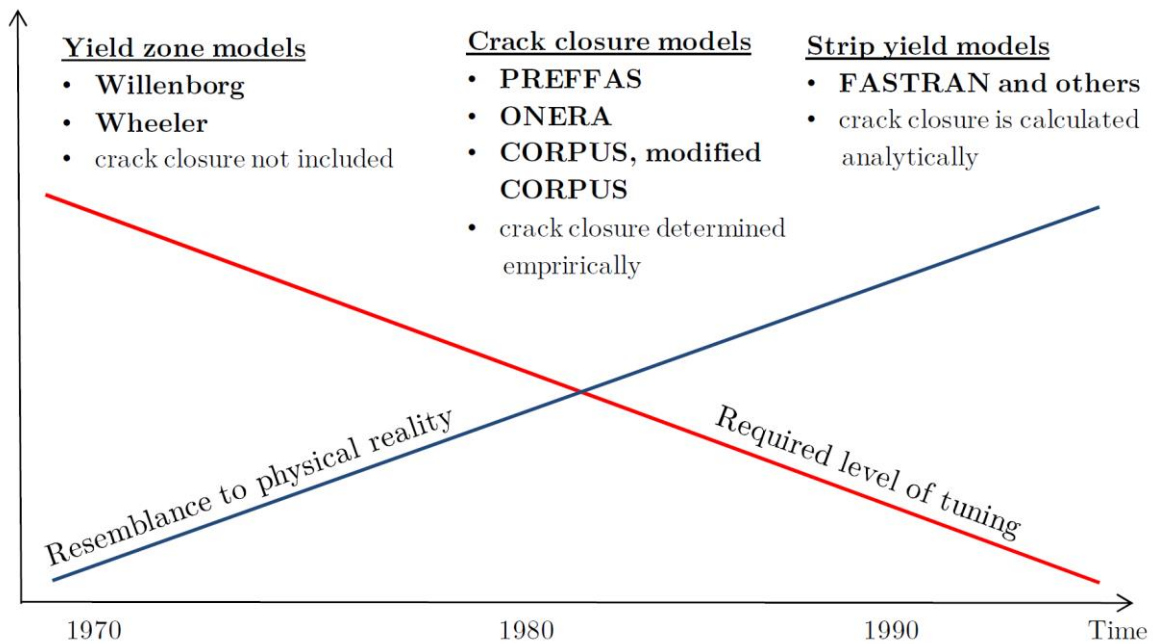
Figure 3.11 Overview of the load interaction models [10].

3.2.3 Loading sequence

A randomized flight-by-flight loading sequence representing 3000 flight hours is used in L 410 NG damage tolerance evaluation. It simulates both airborne and ground loads. An example of one flight within the sequence is depicted in Figure 3.12. The loading sequence generation is closely described in report [11].
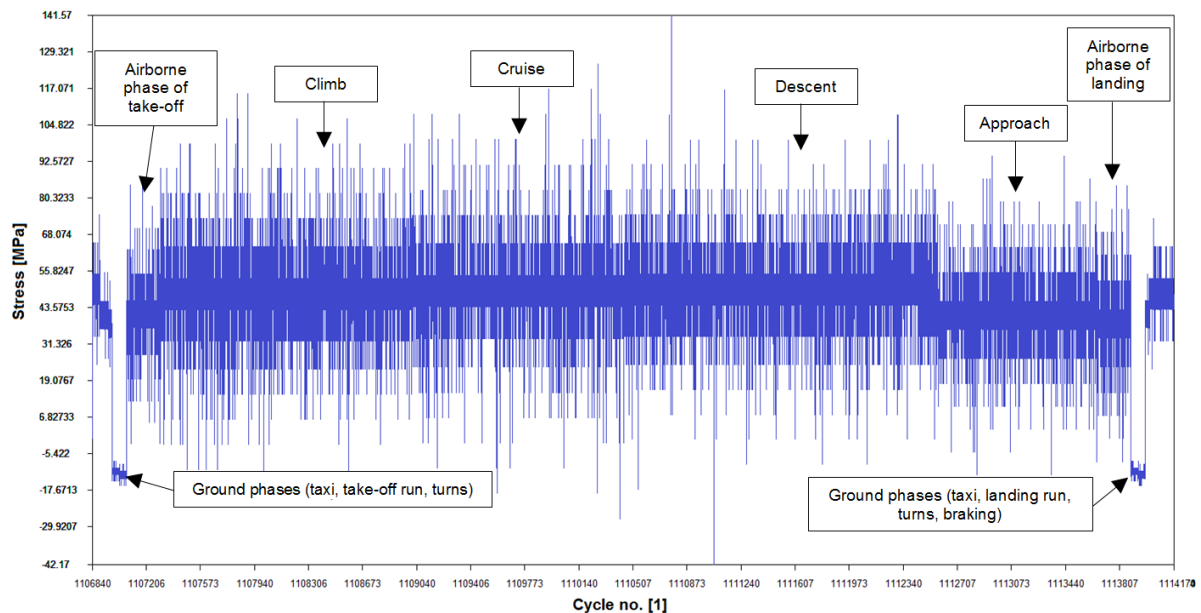

Figure 3.12 An example of one flight within the loading sequence [10].

3.3 Unstable tear

Two cases of analysing the unstable tear are discussed below:

- **Thick structures** – plain strain conditions are assumed to prevail at the crack tip. There is no evident crack extension before the fracture, unstable tear occurs when stress intensity factor is equal or greater than the plain strain **fracture toughness K_{IC}**.
- **Thin structures** – the crack tip is assumed to be under plane stress conditions. There is a significant crack extension prior to failure, which is documented by the so called **resistance curve (R-curve)**. Equations (3.15) and (3.16) state the conditions for the occurrence of unstable tear. A so called **engineering critical crack length** represents the starting crack length of the last half-cycle before final failure. It is of great importance from the engineering point of view and is used for critical flaw length determination. A practical critical length determination is illustrated in Figure 3.13.

$$K = K_R \tag{3.15}$$

$$\frac{\partial K}{\partial a} = \frac{\partial K_R}{\partial a} \tag{3.16}$$
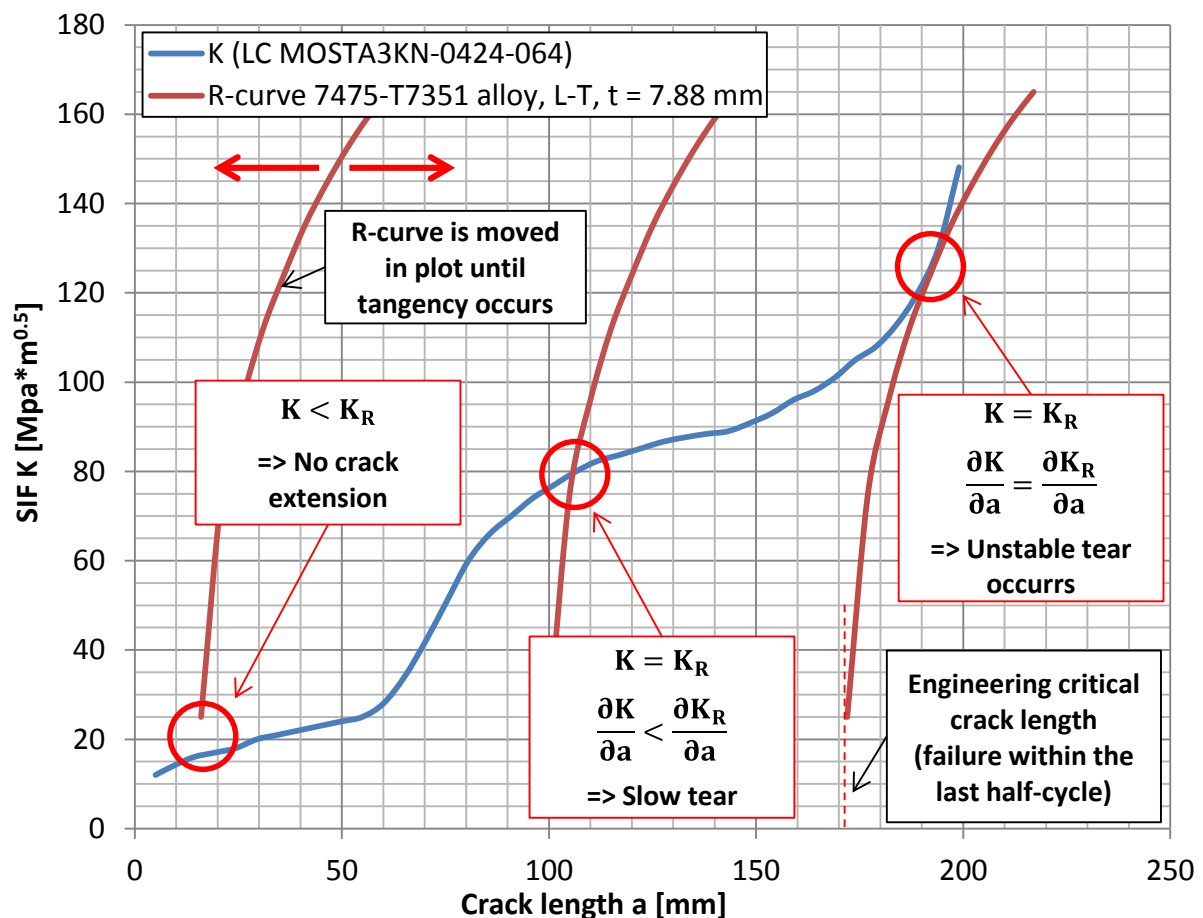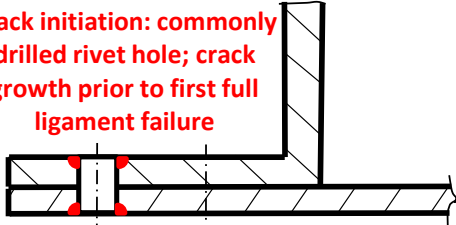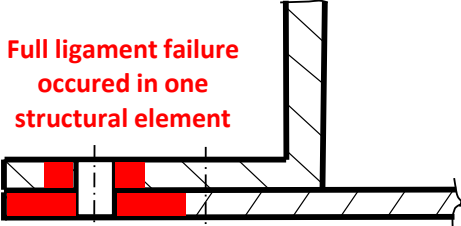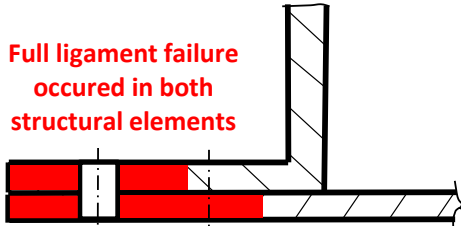

Figure 3.13 Determination of the critical crack length utilizing the R-curve concept.

4   MAJOR ASSUMPTIONS

This chapter states the major assumptions made during the development of the methodology of dependent crack growth analysis. These assumptions are summarized in the following bullet points:

- The proposed methodology is **based on general crack growth and residual strength analysis methodology for the L 410 NG aeroplane** [10]. Modifications are proposed in order to accommodate the special considerations for dependent multiple crack growth.
- **Simultaneous crack growth propagation in no more than two structural elements is assumed**. An analysis of joints of more than two structural members is rather rare and can be converted to a less complex problem by making certain simplifications (e.g. disregarding the structural members which do not significantly contribute to load transfer).
- The **calculation is typically split into three stages** (denoted as "1", "2" and "3") as illustrated in Table 4.1.
  - **Stage 1** includes growth from the initial crack lengths prior to first full ligament failure in one part. The crack interaction is usually disregarded.
  - **Stage 2** includes the continuing growth up to the moment of full ligament failure in the other part. Crack interaction is accounted for by stress level increase, which is obtained by load redistribution analysis.
  - **Stage 3** represents growth after full ligament failure in both structural members. A detailed analysis is used to account for **crack interaction**, which is **considered to play a crucial role** at this stage of the calculation.

Table 4.1 Stages of the crack growth calculation.

Calculation stage	Stage description	Means of accounting for crack interaction
1	**Crack initiation: commonly drilled rivet hole; crack growth prior to first full ligament failure**	Crack interaction disregarded
2	**Full ligament failure occured in one structural element**	Stress level increase (based on load redistribution)
3	**Full ligament failure occured in both structural elements**	Complex approach (crack interaction deemed as significant)

- The **structure is assumed to behave linearly up to the limit load**. This assumption must be later subjected to experimental verification.
- Methodology assumes the **crack growth calculation without load interaction**, although the eventual use of it is reviewed. Furthermore, **da/dN curves are extrapolated backwards from the Paris region** as stated in Subchapter 3.2.
- The **randomized flight-by-flight loading sequence** (as described in Subchapter 3.2.3) includes gusts, manoeuvres, landing impact, take-off and landing run, braking, straight taxi and turns during taxi. All loading sequences are range pair filtered.
- The **critical flaw** is determined for **limit load conditions taken as ultimate.**
- **Scatter factors** for inspection program determination are in compliance with [9].
- **Scenarios** for analysis should be selected based on various aspects of criticality, such as load, fatigue life, detectability, etc.
- The methodology, more specifically the approach of accounting for crack interaction, was developed on the case of crack initiation in bottom panel stringer cut-outs, which is closely described in Subchapters 2.2 and 6.1.
- Fatigue evaluation (i.e., durability analysis) is outside the scope of this methodology.

4.1 Use of software

The most important software tools used for damage tolerance analyses are dealt with within this subchapter.

4.1.1 MSC Nastran FE code

MSC Nastran FE code is used for all **stress analyses** of the structure, including stress intensity factor calculation after the full ligament failure, load redistribution determination and residual strength evaluation.

The **FEM model** comprises a coarse model **of the wing and centre part of the fuselage**, as shown in Figure 4.1.
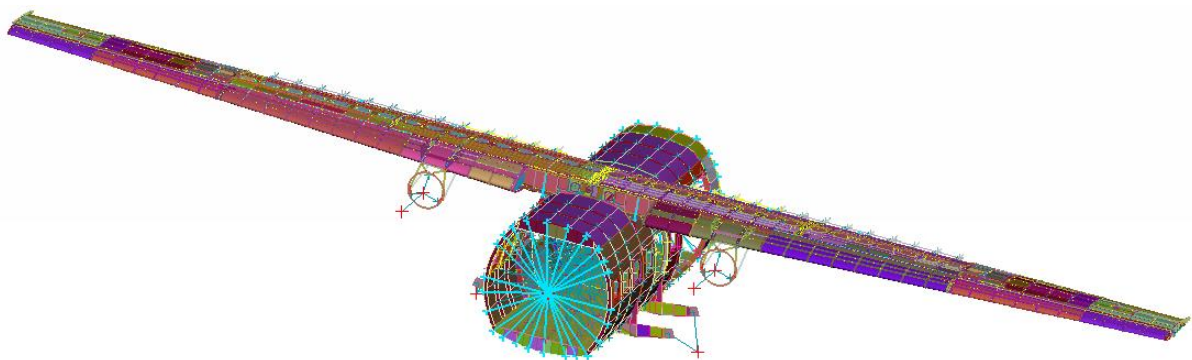

Figure 4.1 FEM model used within the analyses.

Following is a brief description of used modelling techniques, for more detail the reader is referred to literature [10] and [31].

- ANSA pre-processor, version 15.2.4, was used for modifying the model.
- **Shell elements** (CQUAD4, CTRIA3) are used as a predominant element type, beam elements (CBEAM, CROD) are used to simulate stiffness of parts such as engine mounts, flaps and fuselage stiffeners.
- Material property with Young's modulus of **E = 210 000 MPa is used for steel structures** (engine mounts, wing-fuselage attachments), **E = 70 000 MPa is used for the rest of the structure (aluminium alloys).**
- The model is loaded by loads from the SAVLE database, which are transferred to the model by SAVNAS program. **Load cases for residual strength evaluation** are selected based on the report [23].
- A **refinement** of the model to greater detail is carried out **in the area of interest**, including mesh refinement to 5 mm elements.
- Rigid elements (RBE2) are predominantly used for connecting structural parts.
- **Spring elements** (CBUSH) are used for modelling fasteners in the vicinity of a crack, as shown in Figure 4.2. More detailed information about fastener modelling can be found in Subchapter 5.4.3.
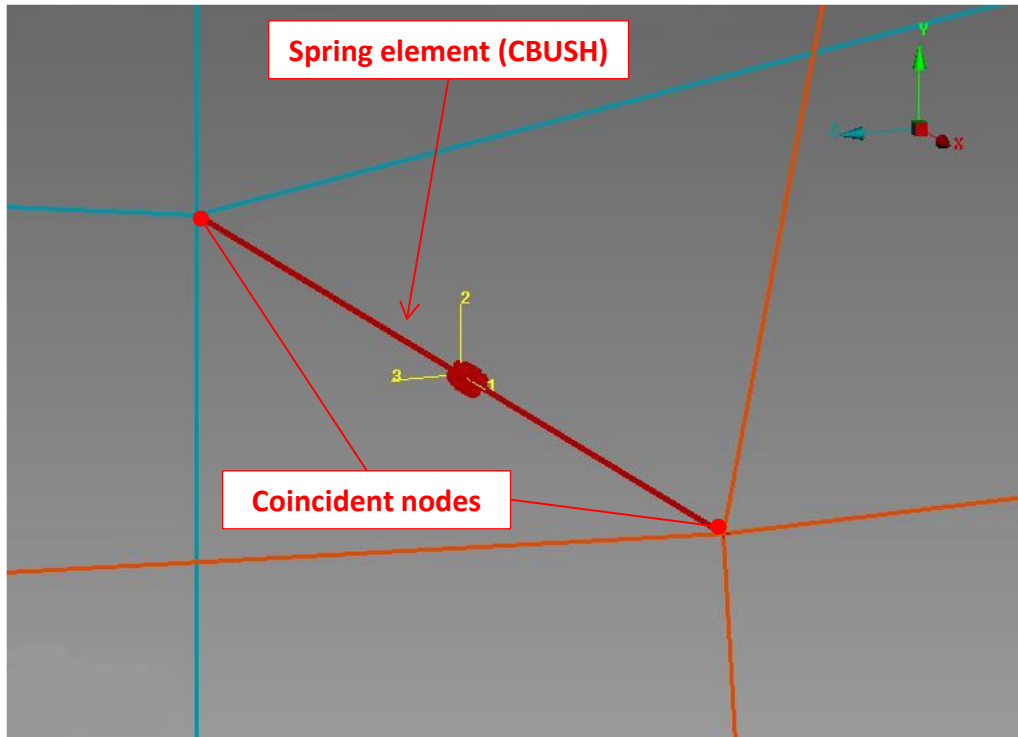

Figure 4.2 Spring elements used as a representation of fastener joints.

- **Crack tip singularity element** (CRAC2D) is used for stress intensity factor calculation by finite element method. Cracks are assumed to propagate perpendicularly to the major principal stress vector, as illustrated in Figure 4.3. Angular deviation from this direction is checked by Equation (4.1) [21] after the calculation and the mesh is subsequently modified accordingly.

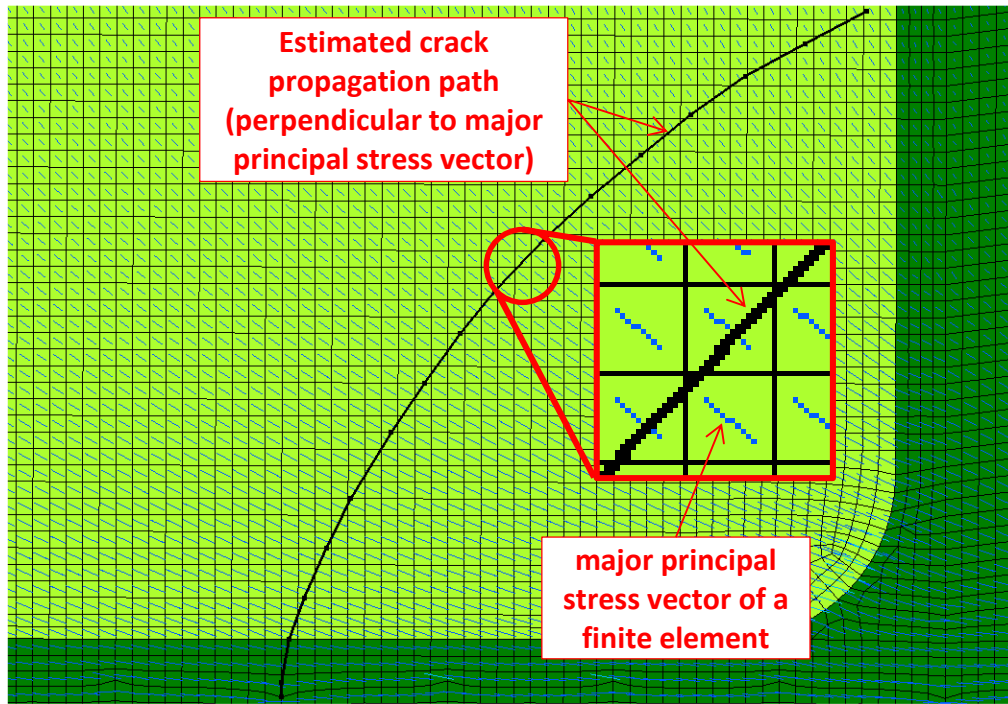$$\theta^\wedge = \arccos\left(\frac{3K_{II}^2 + \sqrt{K_I^4 + 8K_I^2 K_{II}^2}}{K_I^2 + 9K_{II}^2}\right) \tag{4.1}$$

Figure 4.3 Estimated direction of crack growth. Vector plot of major principal stress. Example of a shear web FE model.

4.1.2 AFGROW

Crack growth analysis is conducted in **AFGROW** software, version 5.02.01.18. Appropriate model should be selected, based on the part geometry, loading and flaw distribution – see Figure 4.4 for AFGROW modelling philosophy. AFGROW stress intensity factor solutions are used before the full ligament failure of the part, in order to account for various details, such as pin loading of a rivet hole. More details concerning AFGROW usage can be found in literature [6] and [10].
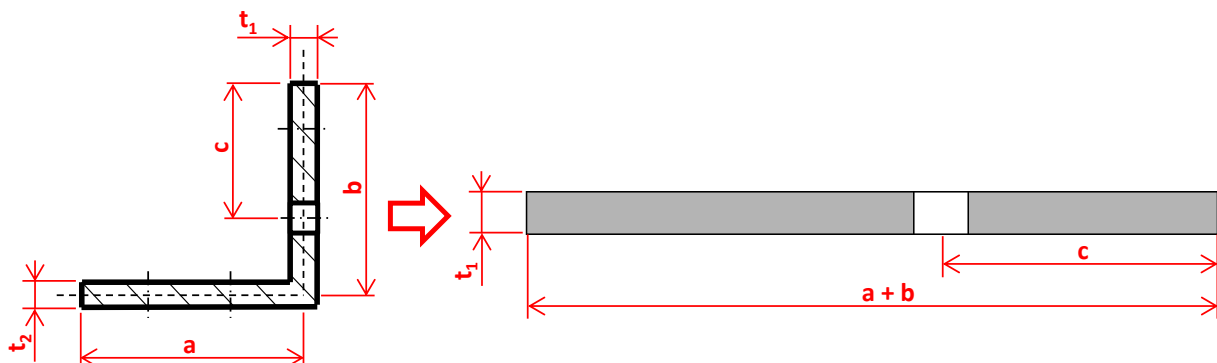
Figure 4.4 An example of AFGROW modelling philosophy.

4.1.3 MS Excel

It is obvious that a detailed analysis of the dependent crack growth would not be viable without some degree of automation. **MS Excel 2010** was used for the development of a macro for a step-by-step stage 3 crack growth calculation (hereinafter referred to as **macro** or **SIMGROW**). This macro was developed in Microsoft Visual Basic for Applications (VBA), which controls AFGROW software through Component Object Model (COM) interface [7]. The macro, together with its technical manual, is present in the appendices to this thesis.

5 DETAILED DESCRIPTION OF THE PROPOSED METHODOLOGY

This chapter applies the theoretical instruments presented in the previous chapters in the development of an effective methodology for dependent crack growth analysis. The proposed methodology is based on the existing L 410 NG crack growth and residual strength analysis [10]. This chapter mainly focuses on the modifications made in order to accommodate the special considerations for dependent multiple crack growth.

The presented methodology proposal consists of the following major damage tolerance aspects:

- **Determination of crack growth scenarios (initial flaw distribution)**
- **Stress intensity factor calculation**
- **Fatigue crack growth prediction**
- **Residual strength analysis**

The last subchapter presents a summary of the developed methodology in the form of a simple flow chart.

Note: The damage tolerance analysis procedure described in this chapter was developed using the case of a crack growth in the bottom panel. The scenario is described in greater detail in Figure 5.1 and Subchapter 6.1. All data presented within this chapter are related to this specified case, if not stated otherwise.

5.1 Determination of initial flaw distribution

Crack growth scenarios, i.e. initial flaw distribution, should be determined in accordance with the requirements of applicable regulations, mainly the Joint Service Specification Guide 2006 (JSSG-2006), which is discussed in Subchapter 2.1.3. The following aspects should be taken into account when deciding the initial damage scenarios:

- Stress level
- Stress concentration
- Bearing load of fastener holes
- Fatigue life (durability)
- Detectability
- Ligament failure
- Holes and cut-outs located in the estimated crack growth path

The most common initial damage scenario is the crack initiation in a commonly drilled fastener hole, as described in Subchapter 2.2. However, the proposed methodology was developed on a case of initiation in a cut-out of the bottom panel stringer. The reasoning for such a scenario is the stress concentration in the cut-out, which is shown in Figure 5.1.
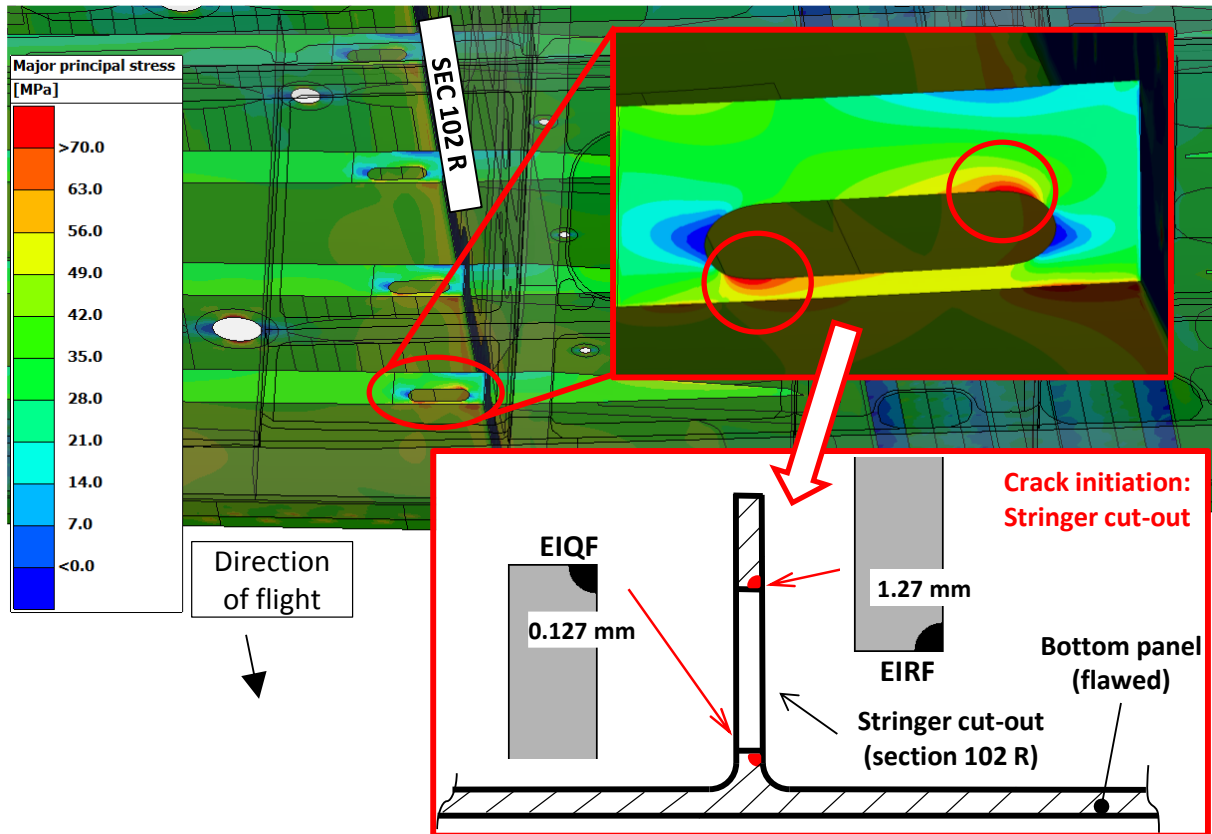
Figure 5.1 Initial flaw distribution used for methodology development. Reasoning: stress concentration on the edges of the cut-out of the most loaded stringer. Contour plot of major principal stress in cruise flight (LC 111) on the bottom panel in section 102 R.

5.2 Stress intensity factor calculation

This subchapter proposes various strategies of stress intensity factor K calculation. Depending on the crack configuration (as per Table 4.1), the K calculation strategies are divided into two major groups:

- **Quasi-independent cracks** – crack interaction is either disregarded or accounted for in a simple manner. These means of calculation are used in **stages 1 and 2** of the crack growth prediction – see Table 4.1.
- **Dependent cracks** – crack interaction is the subject of a detailed analysis. This calculation strategy is utilized in **stage 3** of the crack growth prediction – see Table 4.1.

5.2.1 Quasi-independent cracks

Quasi-independent crack growth is assumed in first two stages of the crack growth prediction:

- **Stage 1** – crack propagation period from the initial lengths up to the moment of full ligament failure occurrence on one structural part.
- **Stage 2** – crack propagation period from the moment of full ligament failure of one part up to the moment of full ligament failure of the other part.

43

Stage 1

As was previously mentioned, stage 1 represents the crack growth period from the initial lengths to the moment of full ligament failure of one structural part.

Analytical solution is used for stress intensity factor calculation in this stage. Suitable AFGROW standard library models, which provide analytical solutions for a wide variety of geometries and types of loading, are used in accordance with literature [6] and [10]. Figure 5.2 illustrates a frequently utilized example of such a model and the resultant analytical β-function solution.
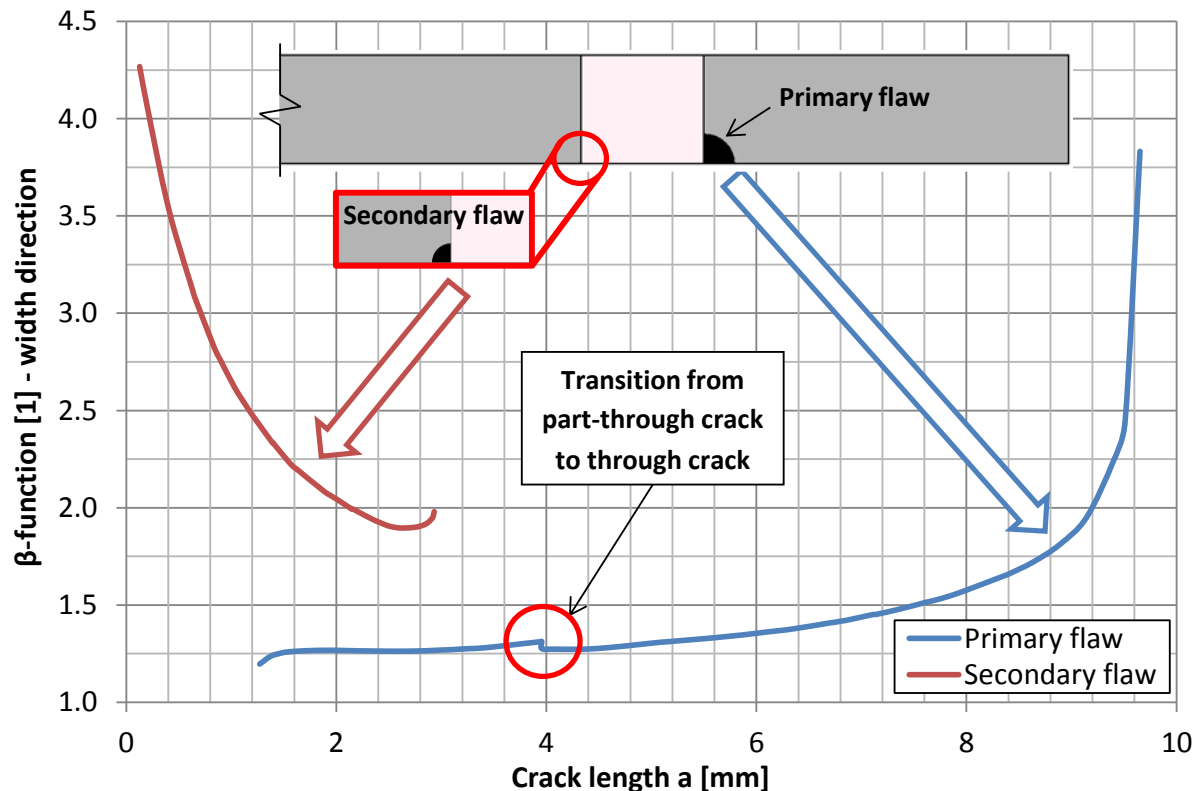

Figure 5.2 A general example of an AFGROW model frequently used in stage 1 of crack growth prediction. Load comprises by-pass stress and bearing stress.

Interaction between the flaws in the analysed structural parts (load paths respectively) in this stage **is usually deemed insignificant, and therefore disregarded**. However, in case large crack lengths are reached in stage 1, or there is a significant crack propagation asymmetry in the two analysed structural members, the crack interaction can be accounted for in a manner, which is described in the next paragraph.

Stage 2

This stage represents the portion of crack growth life after the full ligament failure of one load path but before the full ligament failure on the other load path.

Analytical solution from stage 1 (see previous paragraph) is applied to the part with its ligament still partially intact. However, additionally to stage 1, a **load increase as a result of load redistribution** in the structure is considered, as depicted in Figure 5.3. This load redistribution, which is a result of crack growth in the other structural member, **is obtained by means of FEM** and can be implemented by a one-time increase to a conservatively high value or by further division of the prediction procedure.
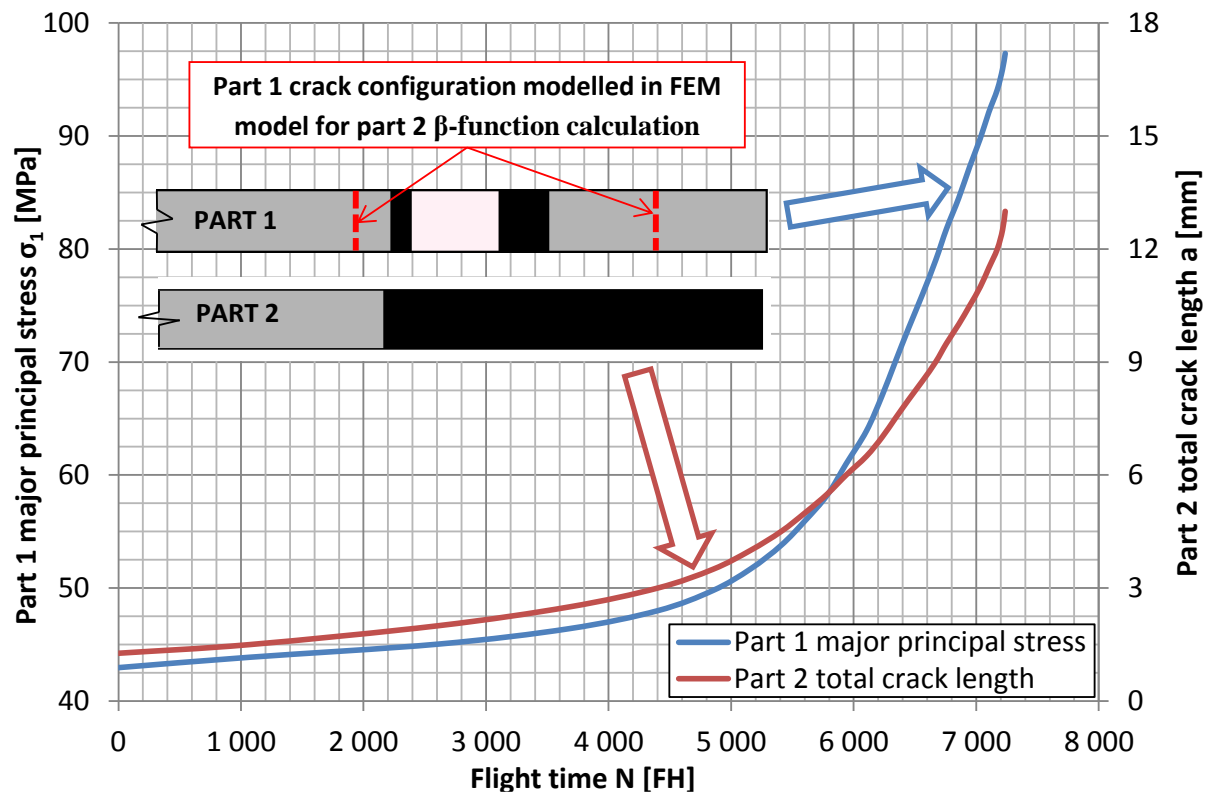
Figure 5.3 A general example of means of accounting for load redistribution in the structure in stage 2 of the crack growth prediction.

Finite element method using CRAC2D element in MSC NASTRAN is employed in obtaining the stress intensity factor solution for the load path with fully failed ligament, as per Subchapter 3.1.2 and 4.1.1. The stress intensity factor is calculated with appropriate crack length increment, usually set to 5 millimeters. For more details on calculating β-function by FEM the reader is referred to literature [10] and [31]. **Crack interaction** is accounted for by a conservatively large **flaw in the structural part with partially intact ligament being included in the finite element model**, as shown in Figure 5.3.

5.2.2 Dependent cracks

Crack interaction is assumed to play a **crucial role in stage 3** of the crack growth prediction procedure, i.e. after the full ligament failure of both flawed structural parts (load paths respectively). Means of accounting for crack interaction in greater detail are investigated within this subchapter.

Analytical solution

Analytical solutions are able to account for **crack interaction only for limited geometries and types of loading**. Moreover, **load redistribution in the whole structure is not included** in the analytical solutions, which can lead to overly conservative results, since this effect is of great significance for large crack lengths achieved in stage 3 of the crack propagation analysis. Analytical stress intensity factor solutions are therefore **generally considered as not suitable for dependent crack growth calculation** in L 410 NG damage tolerance analyses.

An example of an analytical solution for multiple cracks is presented in the following figure and equations, originally postulated by Tada [18]:
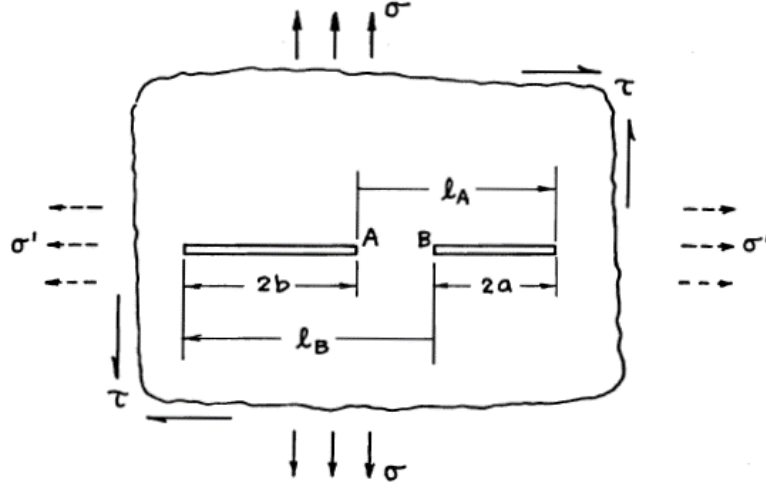
Figure 5.4 Two neighbouring cracks in an infinitely wide plate under biaxial tensile and shear loading [18].

$$\begin{Bmatrix} K_I \\ K_{II} \end{Bmatrix}_A = \begin{Bmatrix} \sigma \\ \tau \end{Bmatrix} \sqrt{\pi b} \; \frac{1}{\sqrt{1-\alpha_A}} \left(1 - \frac{1}{\alpha_B}\left(1 - \frac{E(k)}{K(k)}\right)\right) \qquad (5.1)$$

$$\begin{Bmatrix} K_I \\ K_{II} \end{Bmatrix}_B = \begin{Bmatrix} \sigma \\ \tau \end{Bmatrix} \sqrt{\pi a} \; \frac{1}{\sqrt{1-\alpha_B}} \left(1 - \frac{1}{\alpha_A}\left(1 - \frac{E(k)}{K(k)}\right)\right) \qquad (5.2)$$

Following equations present the definition of terms used in the two equations above.

$$\alpha_A = \frac{2a}{l_A} \qquad (5.3)$$

$$\alpha_B = \frac{2b}{l_B} \qquad (5.4)$$

$$k = \sqrt{\alpha_A \alpha_B} \qquad (5.5)$$

$$K(k) = \int_0^{\pi/2} \frac{d\phi}{\sqrt{1 - k^2 \sin^2(\phi)}} \qquad (5.6)$$

$$E(k) = \int_0^{\frac{\pi}{2}} \sqrt{1 - k^2 \sin^2(\phi)} \, d\phi \qquad (5.7)$$

Dynamic FEM calculation

After ruling out analytical solutions, numerical method of obtaining stress intensity factor was investigated.

In order to calculate the SIF for both crack tips, the crack configuration corresponding to a given point in life of the structure must be known. However, this crack configuration depends on the growth of the cracks. It is therefore obvious, that the **SIF calculation and crack growth prediction are dependent on each other and cannot be separated**, as was the case of the independent crack growth. A detailed analysis clearly requires a complex iterative approach.

46

The most straight-forward approach in principle would be the **dynamic FEM calculation**. The basic idea is the implicit SIF calculation in FEM code during the crack growth prediction, which is illustrated in Figure 5.5.
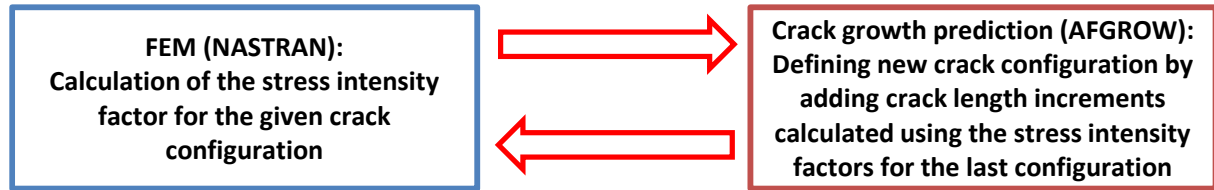
| FEM (NASTRAN): Calculation of the stress intensity factor for the given crack configuration | ⇄ | Crack growth prediction (AFGROW): Defining new crack configuration by adding crack length increments calculated using the stress intensity factors for the last configuration |

Figure 5.5 General principle of the dynamic FEM calculation of the stress intensity factor.

This method is very demanding from the computational time point of view, due to the vast number of FEM calculations needed to be performed. It would be also very hard to create an interface between AFGROW (version 5.02.01.18) and MSC NASTRAN in their forms and versions currently used at Aircraft Industries. This type of SIF determination strategy was therefore considered as unfeasible for L 410 NG damage tolerance analyses.

Note: Next version of AFGROW is expected to be able to effectively interact with STRESS CHECK FE code, making this kind of solution more viable.

Crack interference factor approach

Since the dynamic FEM calculation turned out to be unviable, an **engineering approach** was adopted, in order to define the **two-variable stress intensity factor function**, i.e. define the dependence of SIF on the lengths of both cracks, as per Equation (5.8) and (5.9):

$$K_1 = f(a_1, a_2) \tag{5.8}$$

$$K_2 = f(a_1, a_2) \tag{5.9}$$

Definition of terms related to equations above is stated below.

K_1 – Stress intensity factor of crack 1

K_2 – Stress intensity factor of crack 2

a_1 – Crack 1 length

a_2 – Crack 2 length

It is assumed, that the **enlargement of a crack in one load path** causes a **load increase in the other load path**. The expression for SIF can be therefore rewritten as per Equation (5.10), i.e. the resultant SIF is made of two components. This reasoning is not valid for crack tips in one structural component growing towards each other (e.g. Figure 5.4), due to a vast change in the stress field in the vicinity of the crack tips. However, this case is not encountered within standard L 410 NG analysis of local damage resistance.

$$K_1(a_1, a_2) = \beta(a_1)\left(\sigma + \Delta\sigma(a_2)\right)\sqrt{\pi a_1} = K_1(a_1) + \Delta K_1(a_1, a_2) \tag{5.10}$$

Note: Following calculations are performed for crack 1 only. The procedure for crack 2 is analogical.

Standard FEM analyses are performed to obtain K_1 vs. a_1 curve of crack 1, i.e. FEM calculation is performed for increasing crack 1 (by a specified increment – see Subchapter 5.2.1), while crack 2 remains its initial length. This initial length is the length of crack 2 at the beginning of stage 3 of the crack propagation. The same procedure is subsequently performed for crack 2.

The results are the **standard K vs. a curves for stand-alone propagation** of crack 1 and 2, but also **curves, which indicate the increase of SIF of a given crack caused by the enlargement of the other crack**, as illustrated in Figure 5.6. These curve points represent the first row and column of the stress intensity factor matrices – see Figure 5.7.
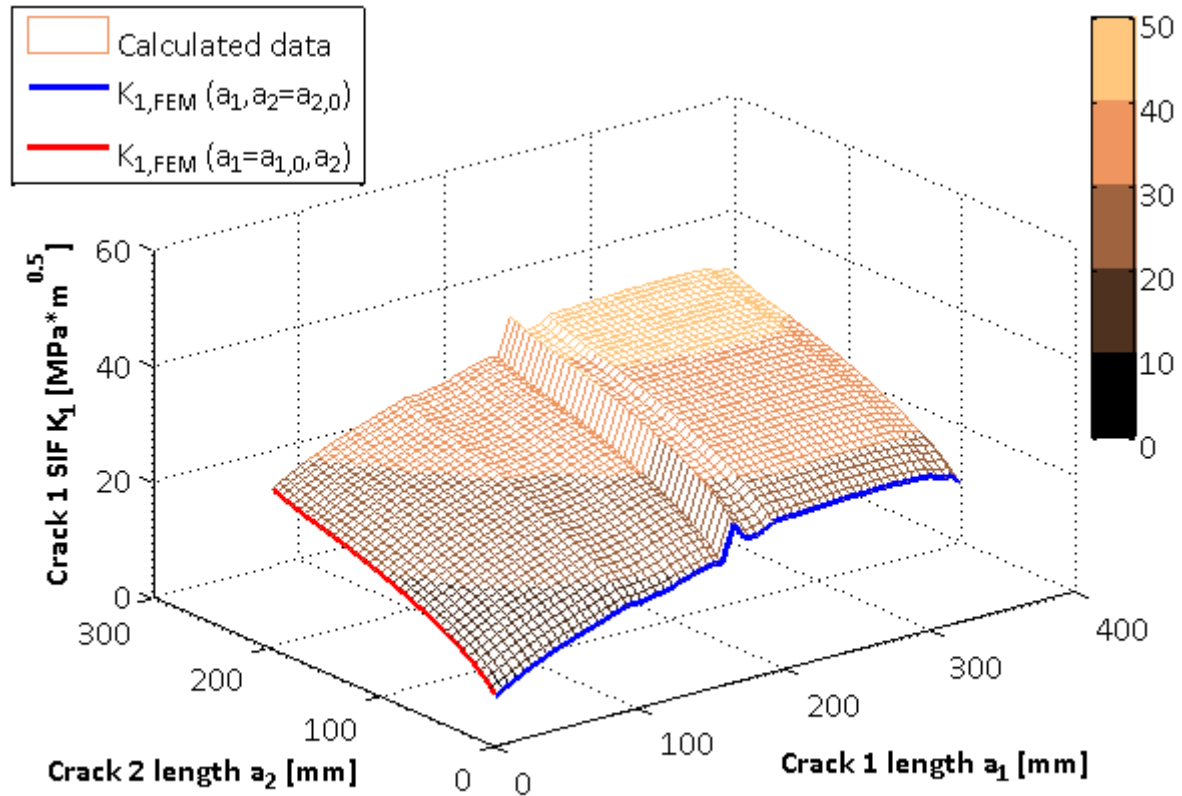

Figure 5.6 Graphical representation of the stress intensity factor function calculated by crack interference factor method. Blue and red lines are obtained by FEM, while the rest is calculated using the crack interference factor method.

A so called **crack interference factor** can be defined according to Equation (5.11). The rest of the SIF matrix in Figure 5.7 can be calculated by Equation (5.12) assuming that the crack interference factor **remains constant for all crack lengths**:

Crack 1 SIF K₁ matrix		Crack 2 length a₂ [mm]													Values obtained by FEM analysis
		$5 = a_{2,0}$	10	15	20	25	30	$35 = a_2^*$	40	45	50	55	60	65	
Crack 1 length a₁ [mm]	$5 = a_{1,0}$	$K_{1,0}$						$K_{1,2}$			●				
	10														
	15														
	20														
	25														
	30														
	$35 = a_1^*$	$K_{1,1}$						K_1^*							Calculated values
	40														
	45										●				
	50														
	55														
	60														
	65														

Figure 5.7 A general example of the SIF matrix calculated by the crack interference factor method.

$$\Delta K\ (a_2^*) = K_{1,2}\ (a_2^*) -\ K_{1,0} \tag{5.11}$$

$$K_1^*\ (a_1^*, a_2^*) = K_{1,1}\ (a_1^*) + \Delta K(a_2^*) \tag{5.12}$$

Following is a list of symbol meanings related to the previous equations.

a_1^* – Given crack 1 length

a_2^* – Given crack 2 length

$a_{1,0}$ – Crack 1 initial length at the beginning of stage 3

$a_{2,0}$ – Crack 2 initial length at the beginning of stage 3

K_1^* – Crack 1 SIF for given crack 1 and crack 2 lengths

$K_{1,2}$ – Crack 1 SIF for crack 1 initial length and a given crack 2 length

$K_{1,1}$ – Crack 1 SIF for a given crack 1 length and the crack 2 initial length

$K_{1,0}$ – Crack 1 SIF in the stage 3 initial configuration

ΔK – Crack interference factor (i.e. the increase of K₁ caused by crack 2 enlargement)

A two-step linear interpolation in the SIF matrix is used to obtain values for an arbitrary crack configuration, as shown in Figure 5.8.

The applicability of the described method is reviewed in the last paragraph of this subchapter.
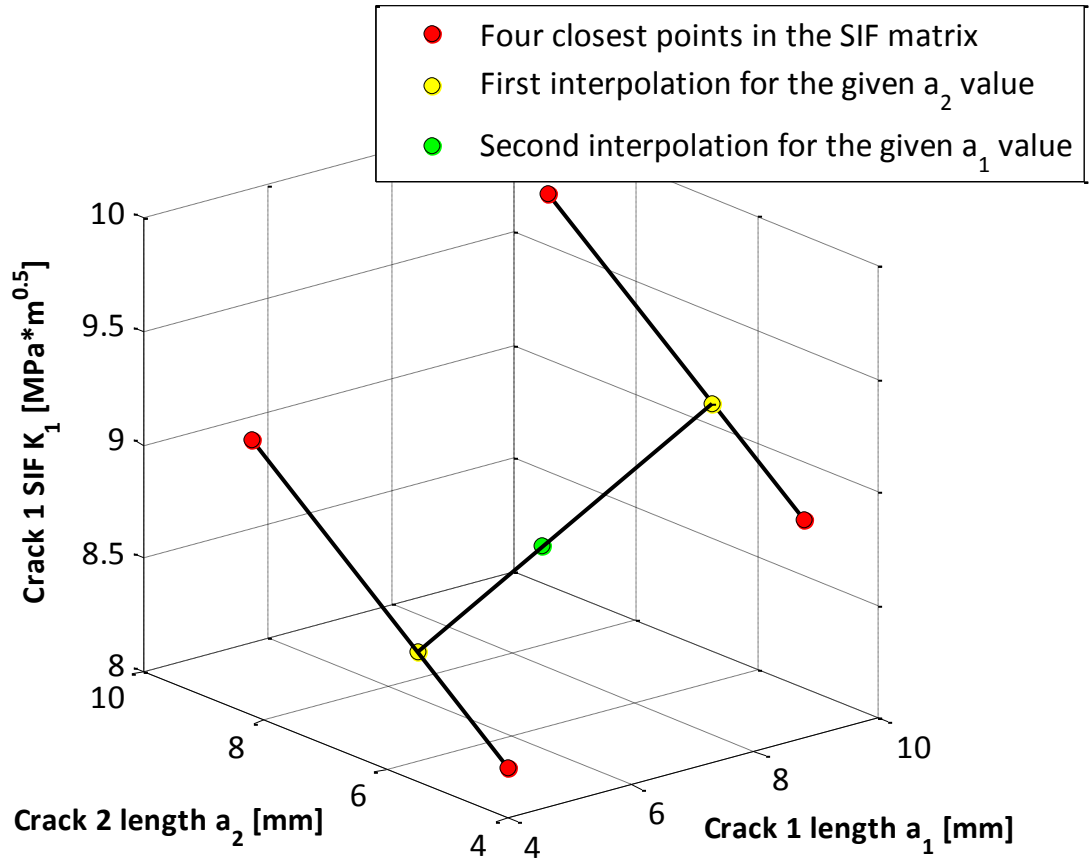
Figure 5.8 Two-step interpolation employed in determining the stress intensity factor for an arbitrary crack configuration.

Modified crack interference factor approach

The crack interference factor approach, described in the previous paragraph, uses finite element method to determine the crack interference factor for the stage 3 initial crack length, which is then assumed to remain constant for all crack lengths. As it turned out, this is not a valid assumption.

A hypothesis of **changing crack interference factor with crack length** was therefore introduced to the Equation (5.12) in the form of a **modification factor C**. This modification factor is **calculated from data obtained by FEM for additional crack configurations**, as depicted in Figure 5.10, while assuming **linear change of the crack interference factor** within a block of the SIF matrix – see Figure 5.9. The calculation of the rest of the SIF matrix elements is done according to Equations (5.13), (5.14) and (5.15).

Final step of determining K for an arbitrary configuration is a two-step interpolation in the SIF matrix, as shown in Figure 5.8.

The described procedure is quite similar to that used by Harter [6] in determining β-functions for multiple cracks that are a part of the AFGROW model library.

$$K_1^* \left(a_1^*, a_2^*\right) = K_{1,1} \left(a_1^*\right) + C(a_1^*) \, \Delta K(a_2^*) \tag{5.13}$$

$$\Delta K \left(a_2^*\right) = K_{1,2} \left(a_2^*\right) - K_{1,a} \tag{5.14}$$

$$C \left(a_1^*\right) = 1 + \frac{\left(K_{1,c} - K_{1,b}\right) - \left(K_{1,d} - K_{1,a}\right)}{a_{1,bc} - a_{1,ad}} \left(a_1^* - a_{1,ad}\right) \tag{5.15}$$

Terms of equations stated on the previous page are described below.

a_1^* – Given crack 1 length

a_2^* – Given crack 2 length

$a_{1,ad}$ – Minimal crack 1 length in the currently calculated block

$a_{1,bc}$ – Maximal crack 1 length in the currently calculated block

$a_{2,ab}$ – Minimal crack 2 length in the currently calculated block

$a_{2,dc}$ – Maximal crack 2 length in the currently calculated block

K_1^* – Crack 1 SIF for given crack 1 and crack 2 lengths

$K_{1,2}$ – Crack 1 SIF for block minimal crack 1 length and a given crack 2 length

$K_{1,1}$ – Crack 1 SIF for a given crack 1 length and the block minimal crack 2 length

$K_{1,a-d}$ – Crack 1 SIF corner values of the currently calculated block (see figure below)

ΔK – Crack interference factor (i.e. the increase of K_1 caused by crack 2 enlargement)

C – Modification factor (i.e. the linear change of the interference factor with crack 1 length)

Figure 5.9 A general example of the SIF matrix calculated block-by-block by the modified crack interference factor method.
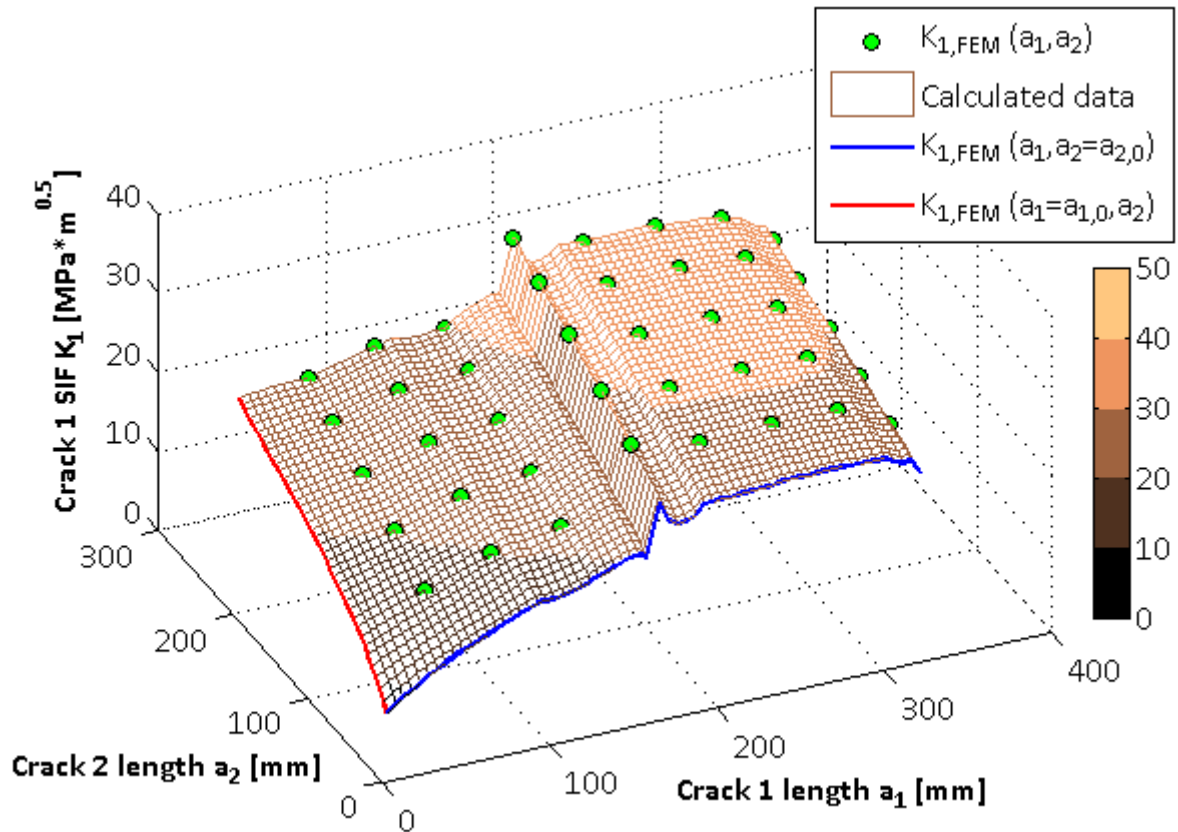
Figure 5.10 Graphical representation of the stress intensity factor function calculated by modified crack interference factor method. Blue and red lines and green points are obtained by FEM, while the rest is calculated using the modified crack interference factor method.

The effect of modification factor on the accuracy, together with the optimal number of additional FEM calculations, is discussed in the next paragraph of this subsection.

Comparison, Recommendations & Remarks

Crack interference factor and modified crack interference factor approach appear to be the most viable solutions for determining stress intensity factors for multiple cracks in L 410 NG DT analyses. Their accuracy is therefore confronted in Figure 5.11, which shows the decreasing trend of relative error in K with increasing number of additional FEM calculations.

It can be seen, that a 5% relative error is achieved with ca. 15 additional FEM calculations, while the number of stand-alone crack propagation calculations was 103 (63 stand-alone propagation data points for crack 1 and 40 for crack 2).

It is therefore recommended to use the modified crack interference factor approach with the number of additional FEM calculation being 15 / 103 ≈ 15 % of the total number of stand-alone crack propagation data points. The data points additionally calculated by FEM should be spread evenly across the SIF matrix. The presented recommendation is assumed to be valid for L 410 NG wing analyses.

The scenario used for error evaluation is depicted in Figure 5.1. The error presented in Figure 5.11 is the absolute value of the maximum of errors relative to a value calculated by FEM in a set of control points, which are shown in Figure 5.12.

Both the crack interference factor approach and its modified version are included in the SIMGROW macro, developed for the purposes of this thesis, which is, together with its technical manual, an appendix to this master's thesis.
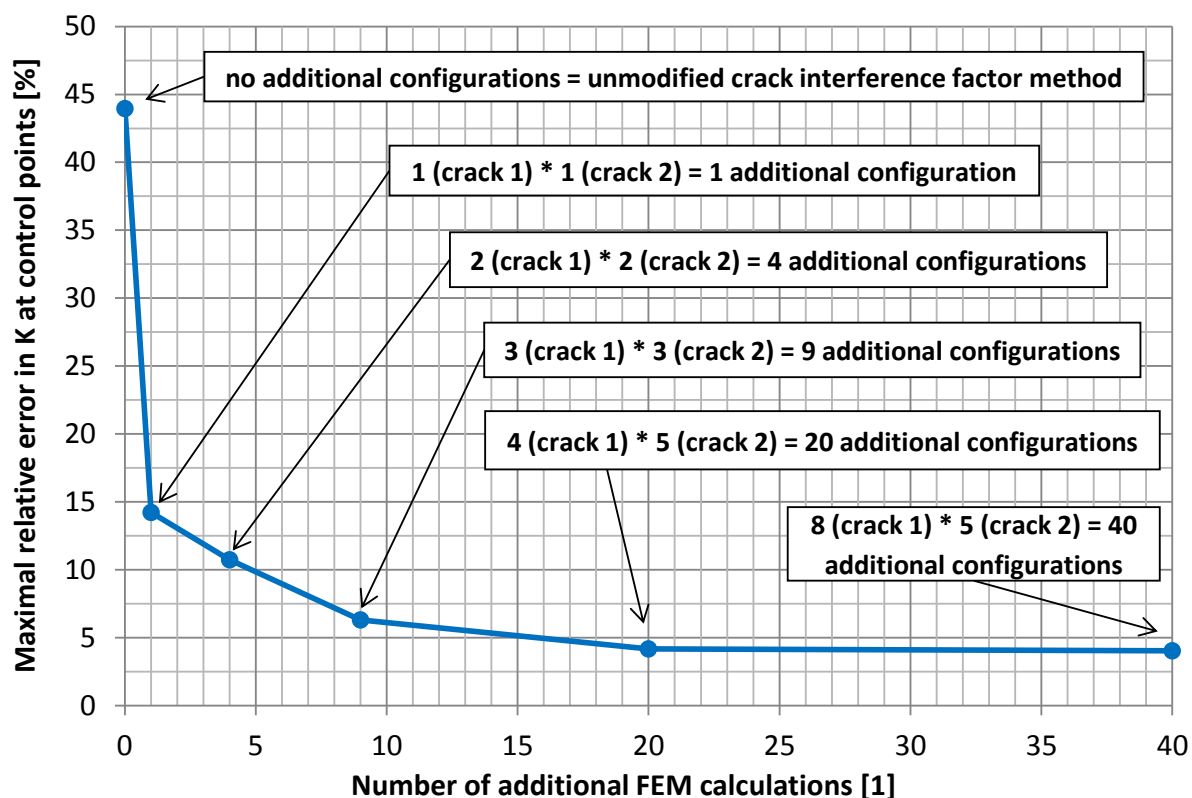
Figure 5.11 Comparison of the modified and unmodified crack interference factor method. 103 total stand-alone crack propagation data points (63 for crack 1, 40 for crack2).
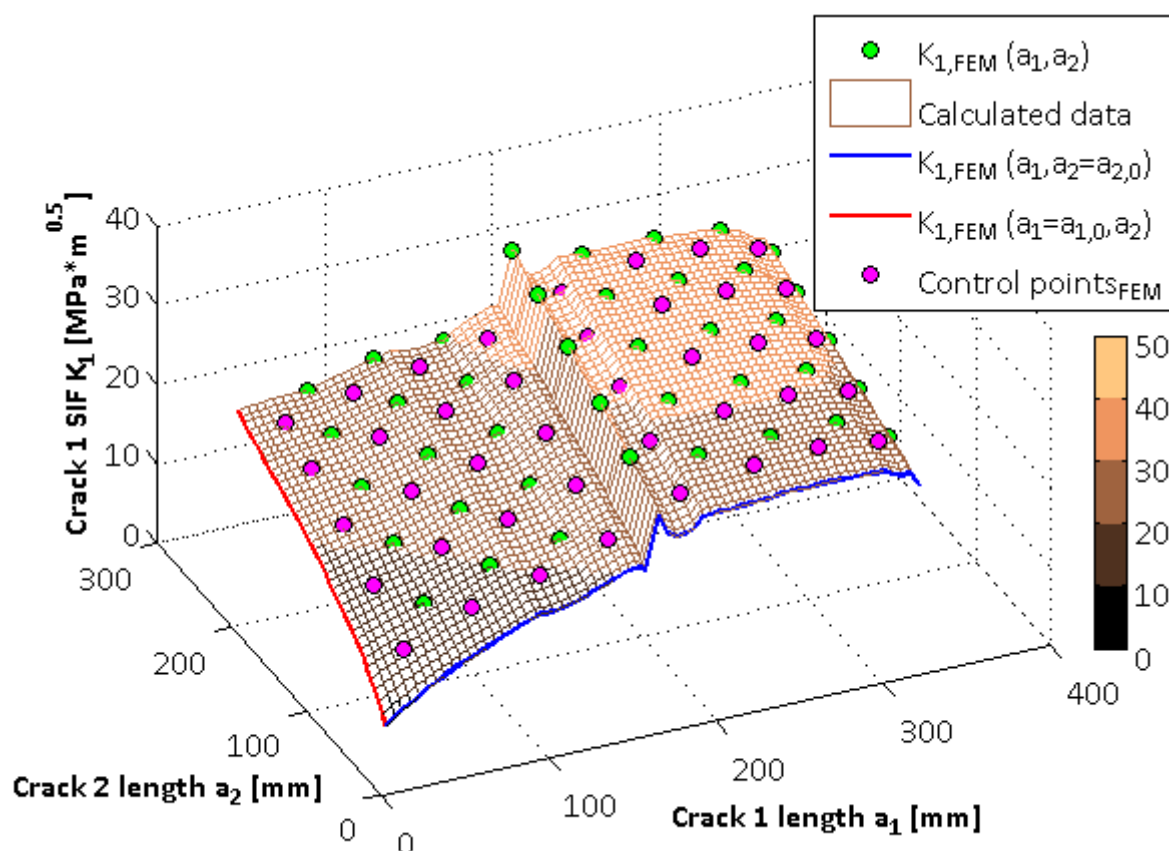

Figure 5.12 Control points for error evaluation. Scenario: propagation of a through crack in the wing bottom panel of the L 410 NG.

5.3 Fatigue crack growth prediction

The following two subcases are distinguished in fatigue crack growth prediction, analogical to the stress intensity factor calculation described in Subchapter 5.2:

- **Quasi-independent crack growth** – Standard procedure used so far in L 410 NG damage tolerance analysis with minor modifications applied in stages 1 and 2.
- **Dependent crack growth** – Employs a complex method of β-function update during the calculation to account for the growth of the other crack in stage 3.

5.3.1 Propagation of quasi-independent cracks

A **standard way** of calculating fatigue crack growth **in AFGROW** software is utilized in stages 1 and 2 of the analysis. An illustration of this procedure is in Figure 3.10 and more details can be found in [10].

Minor modifications are introduced in the form of **stress level increase** (step or gradual), in order to account for load redistribution in the structure, in accordance with Subchapter 5.2.1.

5.3.2 Propagation of dependent cracks

Crack interaction, which is assumed to have a crucial effect on the propagation in stage 3, was accounted for in the SIF calculation by creating a function for K with lengths of both cracks being its variables, as stipulated in Subchapter 5.2.2.

This subchapter deals with the ways of implementing these two-variable functions in the fatigue crack growth prediction procedure, since it is obvious, that the dependent multiple crack growth calculation cannot be performed separately for each of the flaws, as was the case of stages 1 and 2.

The prediction process must be further divided into **steps**, to include the effect of parallel growth of the other crack and **update the β-function** accordingly. The following two strategies of doing so were proposed:

- **Constant K in step**
- **Linear K in step**

Constant-K-in-step β-function update method

The crack propagation prediction in stage 3 is split into several steps, in which the β-function is recalculated, to account for simultaneous crack growth. These steps are defined by a given crack length increment Δa, which is being added to the faster growing crack. Following is a brief description of the procedure, which is also depicted in the form of a flowchart in Figure 5.14.

Firstly, the SIF function is used to obtain K for the initial configuration in a given step of the calculation. The same is performed for an estimated final configuration of the step (step initial length of each flaw increased by Δa), and the maximum of these two values defines a **constant K vs. a function in the given step** – see Figure 5.13. The maximum is taken so that the growth life is not over-predicted.
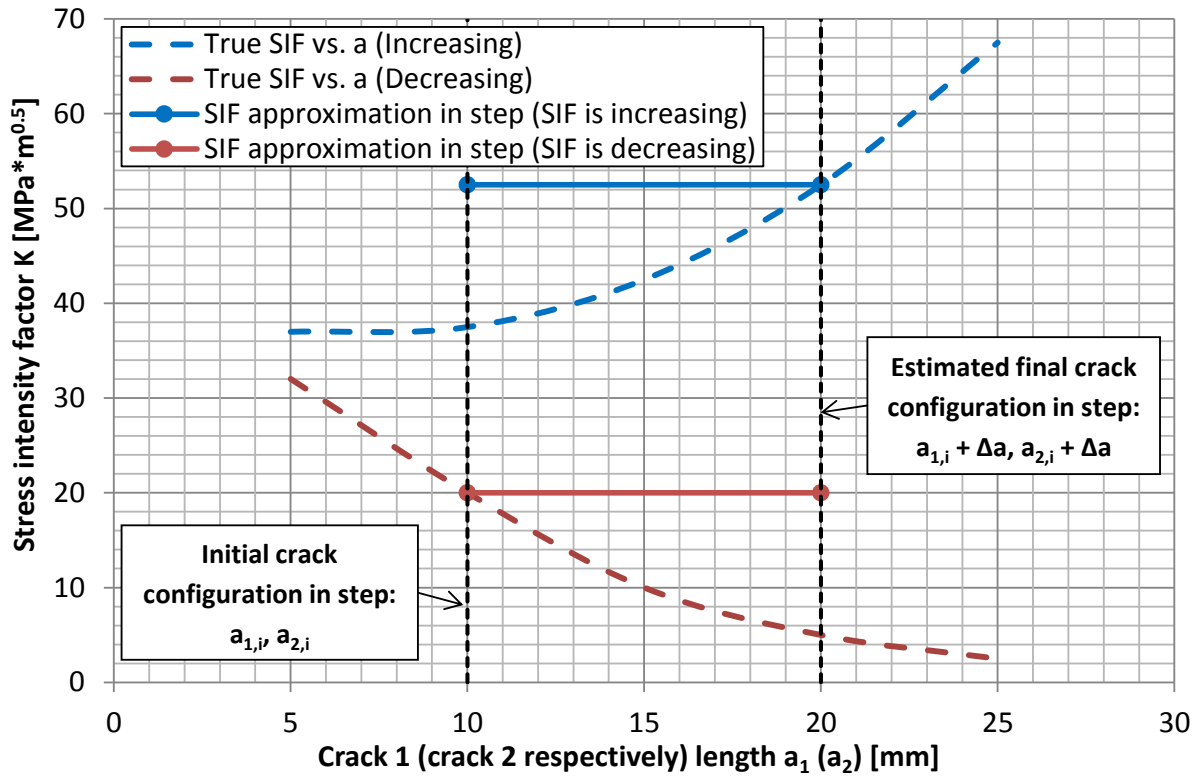
Figure 5.13 Constant stress intensity factor in a step. Conservatively defined as the maximum of K values for the step initial and estimated step final configuration. General example.

Next, a prediction in AFGROW is made for the faster growing crack, bounded by its step initial length $a_{faster,i}$ and step final length $a_{faster,f} = a_{faster,i} + \Delta a$. The resultant growth life in the step N is stored.

Subsequently, an AFGROW prediction is made for the slower growing crack, from its initial step length $a_{slower,i}$ until the previously determined step growth period N is reached. The final step length of the slower crack achieved in the step $a_{slower,f}$ is stored.

Finally, an evaluation of which crack was faster in the performed step is carried out and the procedure continues with the next step, until desired lengths of the flaws are exceeded.
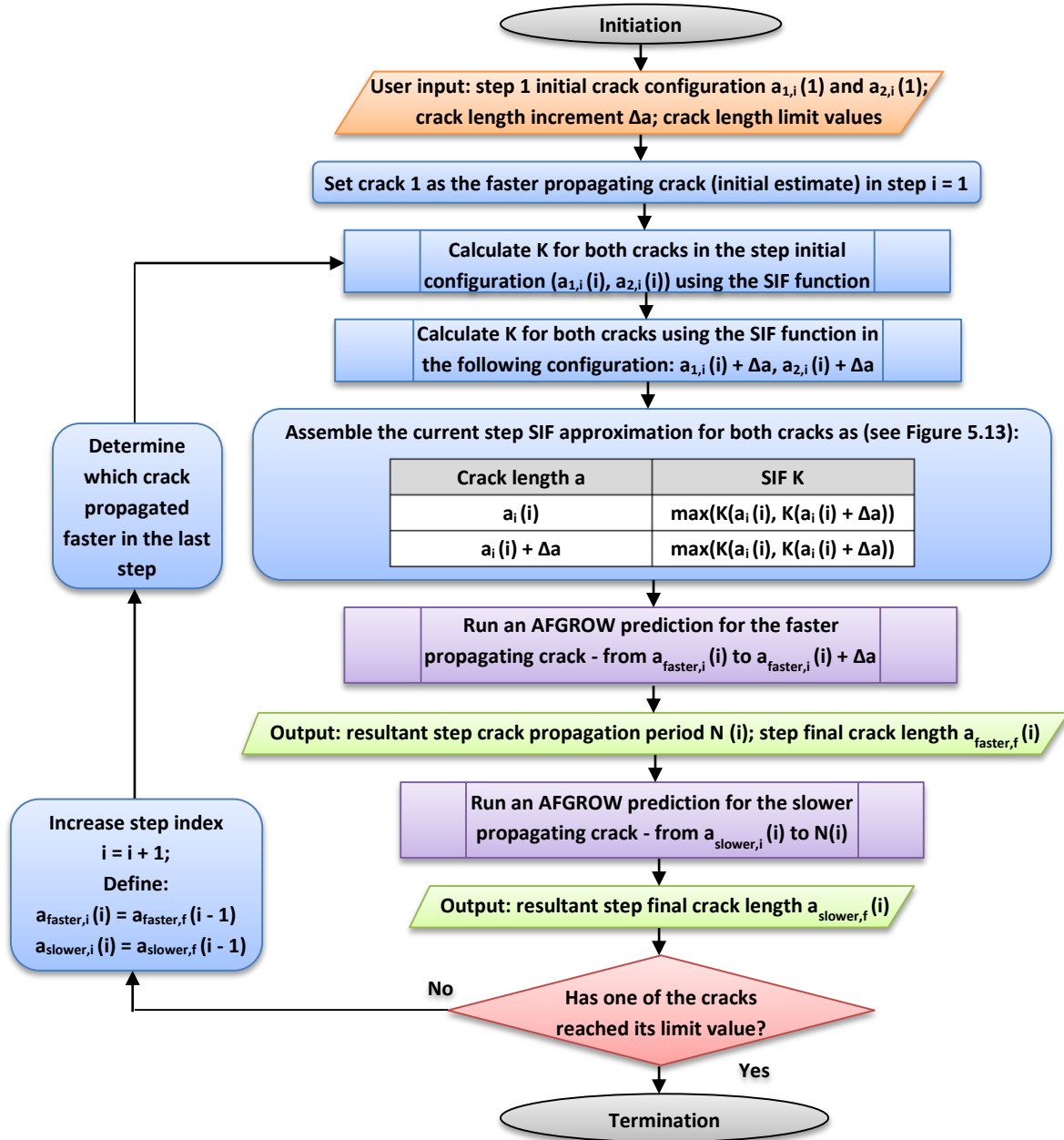
Figure 5.14 Flowchart of the crack growth prediction using constant-K-in-step method.

Linear-K-in-step β-function update method

The following alternative strategy of β-function update was developed as an attempt to achieve more accurate results.

At first, a step final configuration is estimated, based on the growth ratio of the cracks in the last step.

SIF is then calculated for both the step initial and final configurations. These values are used to define a **linear K vs. a curve for the given step** – see Figure 5.15.

Next, AFGROW predictions are run for both flaws, bounded by their initial and final lengths in the step and with their step propagation lives N_1 and N_2 stored as output.

An absolute error $\Delta N = N_1 - N_2$ and a relative error $\delta N = \Delta N / \min(N_1, N_2)$ are enumerated.
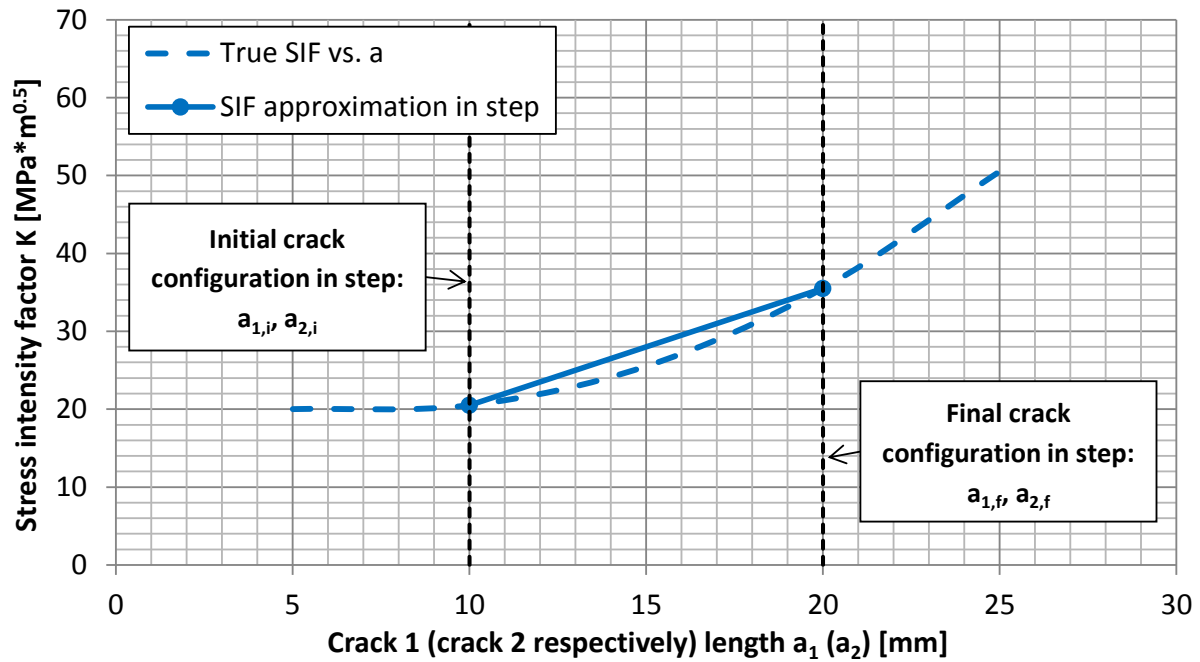
Figure 5.15 Linear stress intensity factor in a step. General example.

The final step length of the slower growing crack is a subject to further iterative adjustments conducted using the combination of the secant and regula falsi method, in order to minimalize the absolute and relative errors – see Figure 5.16.
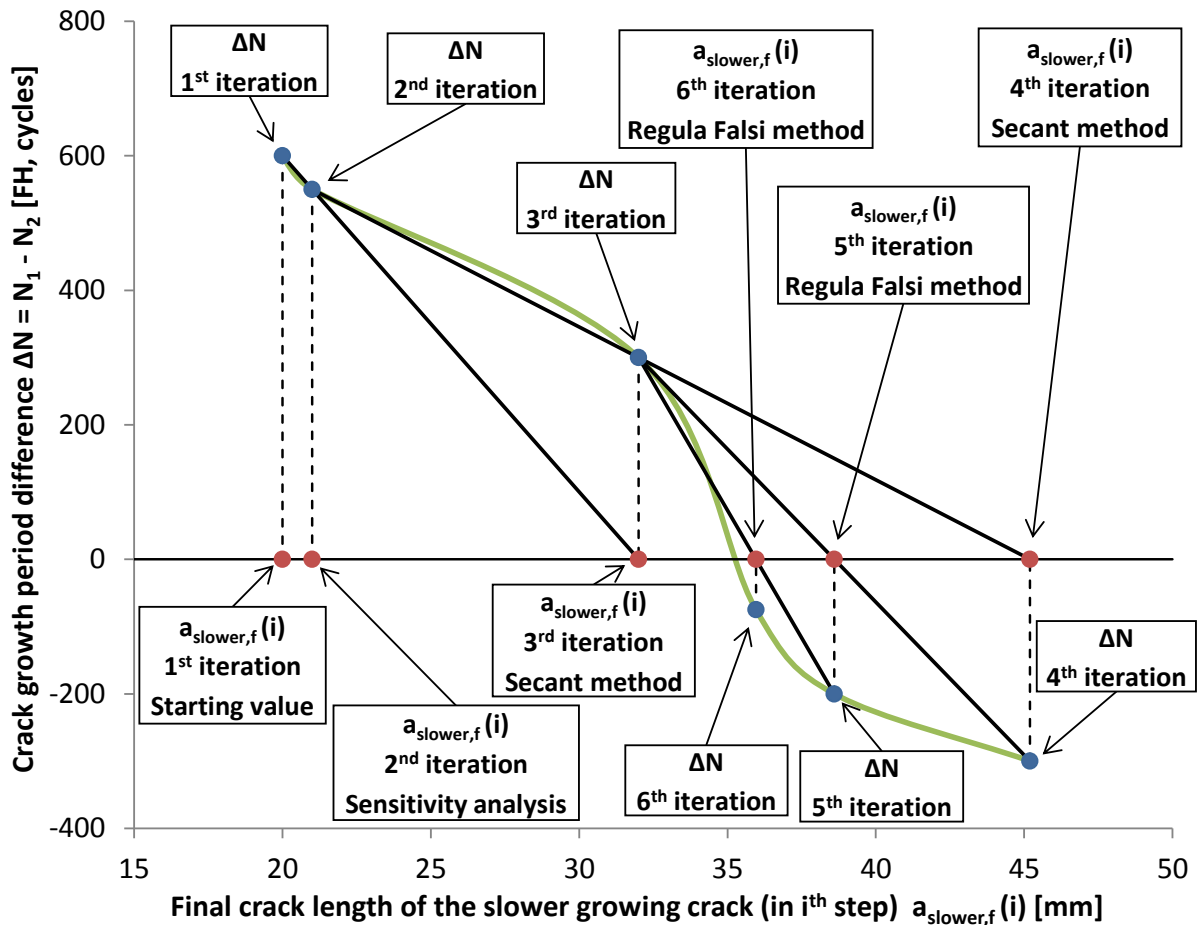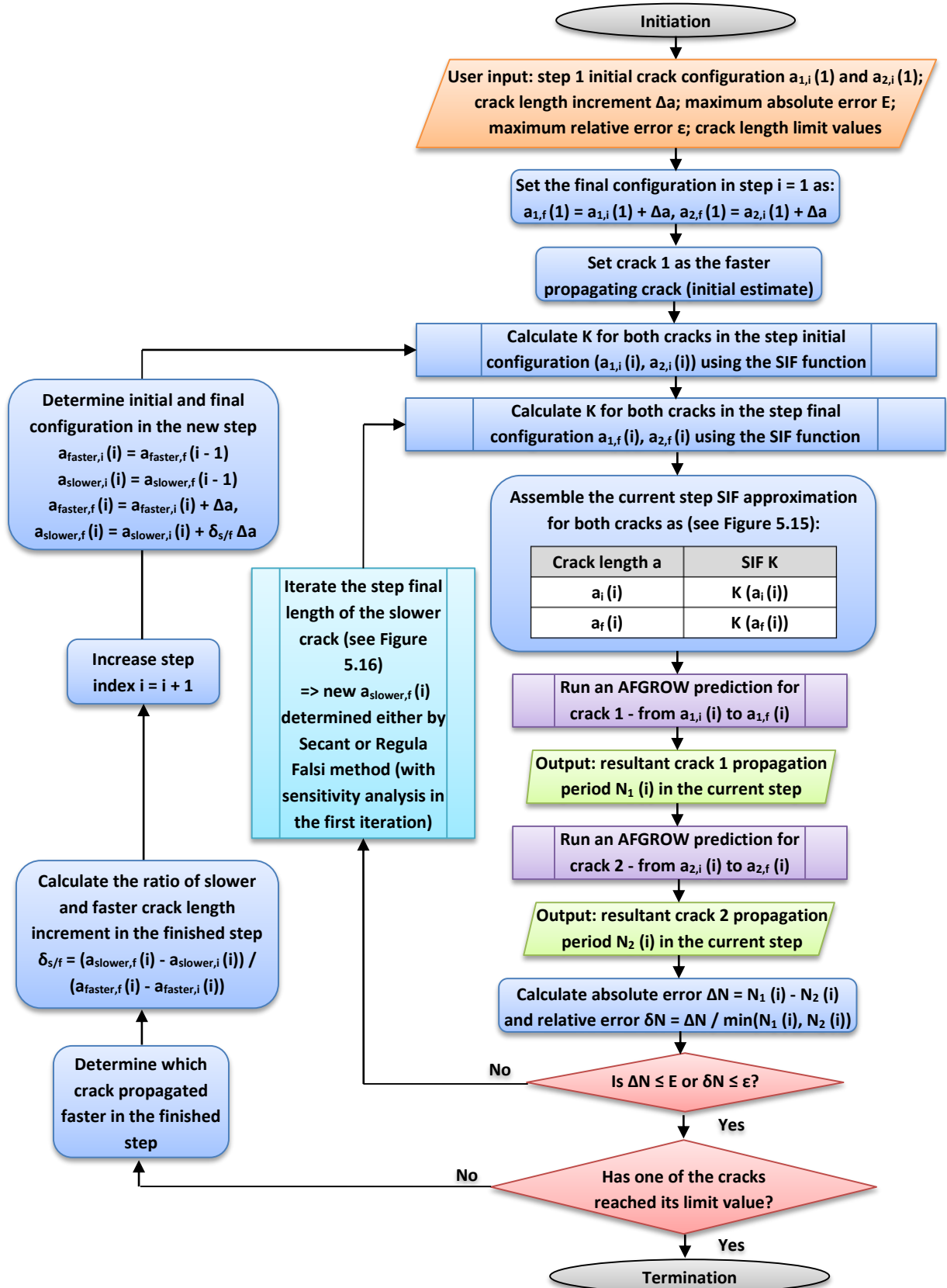

Figure 5.16 Iterative minimization of the crack growth life error. General example.

Initiation

User input: step 1 initial crack configuration $a_{1,i}(1)$ and $a_{2,i}(1)$; crack length increment Δa; maximum absolute error E; maximum relative error ε; crack length limit values

Set the final configuration in step $i = 1$ as:
$a_{1,f}(1) = a_{1,i}(1) + \Delta a$, $a_{2,f}(1) = a_{2,i}(1) + \Delta a$

Set crack 1 as the faster propagating crack (initial estimate)

Calculate K for both cracks in the step initial configuration $(a_{1,i}(i), a_{2,i}(i))$ using the SIF function

Calculate K for both cracks in the step final configuration $a_{1,f}(i)$, $a_{2,f}(i)$ using the SIF function

Determine initial and final configuration in the new step
$a_{faster,i}(i) = a_{faster,f}(i - 1)$
$a_{slower,i}(i) = a_{slower,f}(i - 1)$
$a_{faster,f}(i) = a_{faster,i}(i) + \Delta a$,
$a_{slower,f}(i) = a_{slower,i}(i) + \delta_{s/f} \Delta a$

Assemble the current step SIF approximation for both cracks as (see Figure 5.15):

Crack length a	SIF K
$a_i(i)$	$K(a_i(i))$
$a_f(i)$	$K(a_f(i))$

Iterate the step final length of the slower crack (see Figure 5.16)
=> new $a_{slower,f}(i)$ determined either by Secant or Regula Falsi method (with sensitivity analysis in the first iteration)

Increase step index $i = i + 1$

Run an AFGROW prediction for crack 1 - from $a_{1,i}(i)$ to $a_{1,f}(i)$

Output: resultant crack 1 propagation period $N_1(i)$ in the current step

Run an AFGROW prediction for crack 2 - from $a_{2,i}(i)$ to $a_{2,f}(i)$

Output: resultant crack 2 propagation period $N_2(i)$ in the current step

Calculate the ratio of slower and faster crack length increment in the finished step
$\delta_{s/f} = (a_{slower,f}(i) - a_{slower,i}(i)) / (a_{faster,f}(i) - a_{faster,i}(i))$

Calculate absolute error $\Delta N = N_1(i) - N_2(i)$ and relative error $\delta N = \Delta N / \min(N_1(i), N_2(i))$

Determine which crack propagated faster in the finished step

No — Is $\Delta N \leq E$ or $\delta N \leq \varepsilon$?

Yes

No — Has one of the cracks reached its limit value?

Yes

Termination

Figure 5.17 Flowchart of the crack growth prediction using linear-K-in-step method.

Once one of the precision criteria is met, the procedure continues with another step, until desired crack lengths are reached.

From the process flowchart, depicted in Figure 5.17, it is clear, that one loop is embedded in another, which increases the computational time, when compared to the constant-K-in-step method with a single loop (Figure 5.14). But thanks to the assumption of linear K vs. a in a step it is also expected to yield more accurate results.

The applicability of the two proposed dependent growth prediction strategies is therefore reviewed in the last paragraph of this subsection.

Comparison, Recommendations & Remarks

Figure 5.18 shows the confrontation of the two presented dependent crack growth calculation strategies applied on a scenario of bottom panel crack growth in section 102 R (see Figure 5.1).
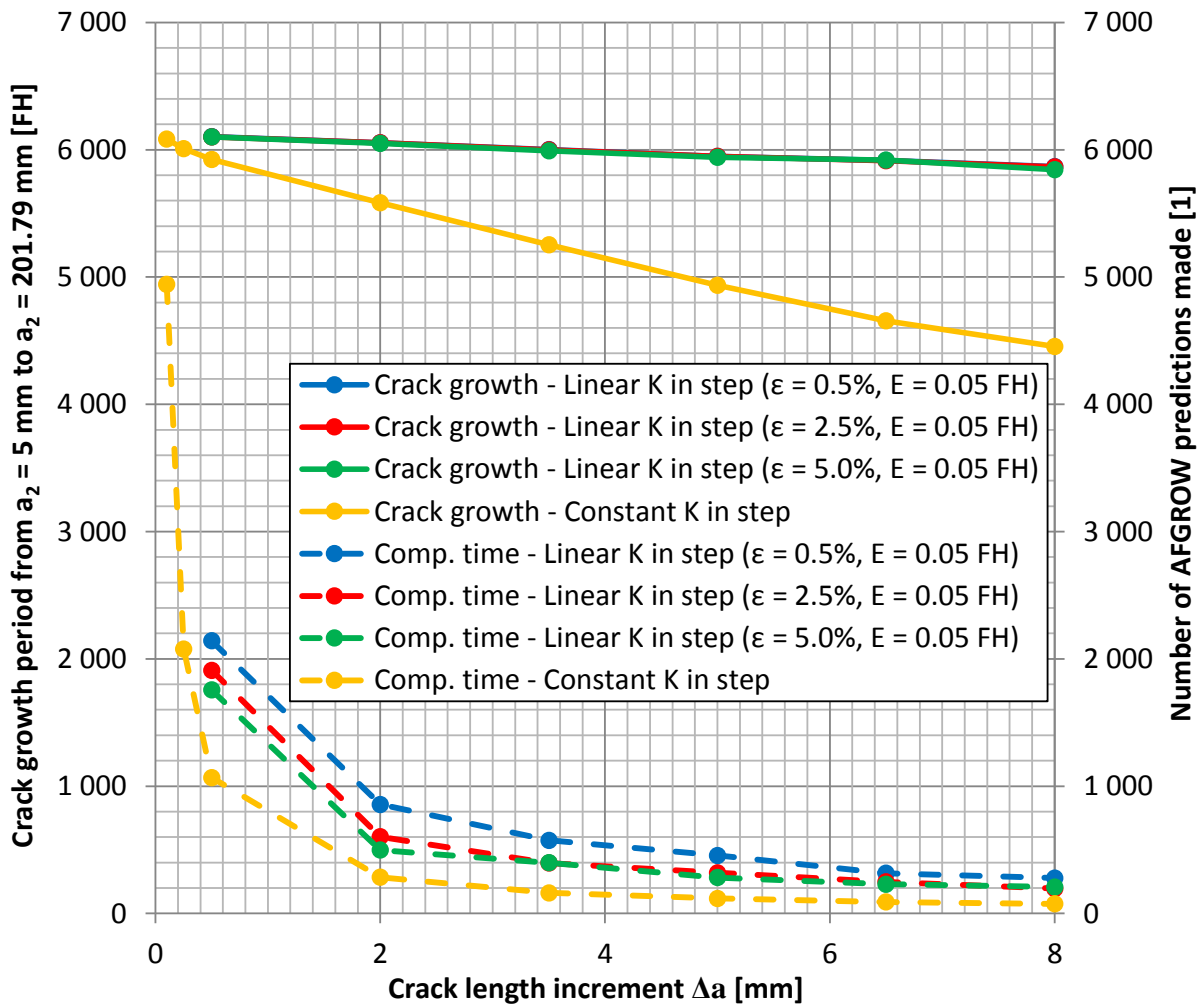
Figure 5.18 Comparison of the two multiple crack growth analysis methods. Scenario: wing bottom panel crack propagation.

It is clear, that the **linear-K-in-step method** is **more demanding from the computational time point of view**, while showing a significantly **lower drop in accuracy with increasing crack length increment**. It is therefore considered to be **more effective** and is **recommended** to be used in L 410 NG analyses with **parameters according to Table 5.1**.

Both methods are included in the appended SIMGROW macro for automated multiple crack growth analysis.

Table 5.1 Recommended solution setup. Valid for L 410 NG wing analysis.

Parameter	Recommended value
Solution type	Linear K in step
Crack length increment Δa	2.5 mm (50 % of the 5 mm step used in FEM stand-alone stress intensity factor calculation for both cracks)
Maximal absolute error E	30 cycles / 0.05 FH
Maximal relative error ε	2.5 %

It is important to note that these procedures were developed while **assuming that no retardation models are used**, which was valid for L 410 NG DT analyses performed at the time. However, if a retardation model would be included, then the results would become invalid, since **splitting AFGROW prediction causes the loss of plastic wake information**. The SIMGROW macro is therefore to be modified to **run only whole predictions** (including stages 1 and 2). A feature enabling the modification of the parameters of the running AFGROW prediction is to be included in the next version of AFGROW. Such a feature will make the modification of the SIMGROW macro much more practical.

5.4 Residual strength analysis

The standard methods of residual strength analysis used in L 410 NG damage tolerance analyses are applicable to full extent to the problem of multiple crack growth, which is the subject of investigation of this master's thesis. This subchapter therefore presents only an overview of procedures closely described in [10]. The following aspects of residual strength are dealt with:

- **Unstable tear**
- **Net section yield**
- **Fastener bearing capacity**
- **Surrounding structure strength**
- **Buckling**

All data required for the analysis of the aspects mentioned above are usually obtained by a single linear / non-linear finite element method calculation. Automation of the residual strength analysis is therefore deemed ineffective. The only exception is the unstable tear evaluation, with its specifics discussed in Subchapter 5.4.1.

Note: All limit states are evaluated at 100 % limit load.

5.4.1 Unstable tear

The theoretical principles of unstable tear evaluation were discussed in Subchapter 3.3. Special consideration must be given to the selection of appropriate R-curve, which should reflect the following properties of the evaluated structural members:

- **Thickness** – thickness of the specimen should be equal to or greater than the thickness of the real part.
- **Width** – specimen width should be equal to or less than the width of the real part.
- **Orientation** – L-T, T-L, etc.

Moreover, the K vs. a curve used for unstable tear analysis should be calculated for the most critical load case at 100 % limit load, while **taking all potential non-linear effects into consideration**, such as adjacent structure yielding, rivet yielding, etc.

The ability to evaluate the unstable tear dynamically during dependent crack growth prediction (stage 3) is provided by the developed SIMGROW macro. This saves some computational time, since it is possible to abort the multiple crack growth prediction after occurrence of the unstable tear was detected. For a demonstration of a practical application the reader is referred to the appendices of this master's thesis.

5.4.2 Net section yield

Net section yield is a simple criterion of the residual cross-section failure of the flawed element. This cross-section is assumed to fail when the **net stress** reaches the **yield strength** of the material – see Equation (5.16).

$$\sigma_{NET} = \frac{F_{NET}}{S_{NET}} = R_{p,0.2} \tag{5.16}$$

σ_{NET} is the net cross-section stress, F_{NET} is the total force acting on the residual cross section, S_{NET} is the area of the residual cross-section and $R_{p,0.2}$ is the material yield strength.

5.4.3 Fastener bearing capacity

The bearing capacity of joints (usually riveted joints) is often a limiting factor of the residual strength, since **fasteners adjacent to a crack are significantly overloaded**, when compared to the unflawed state. This is illustrated in Figure 5.19 below.
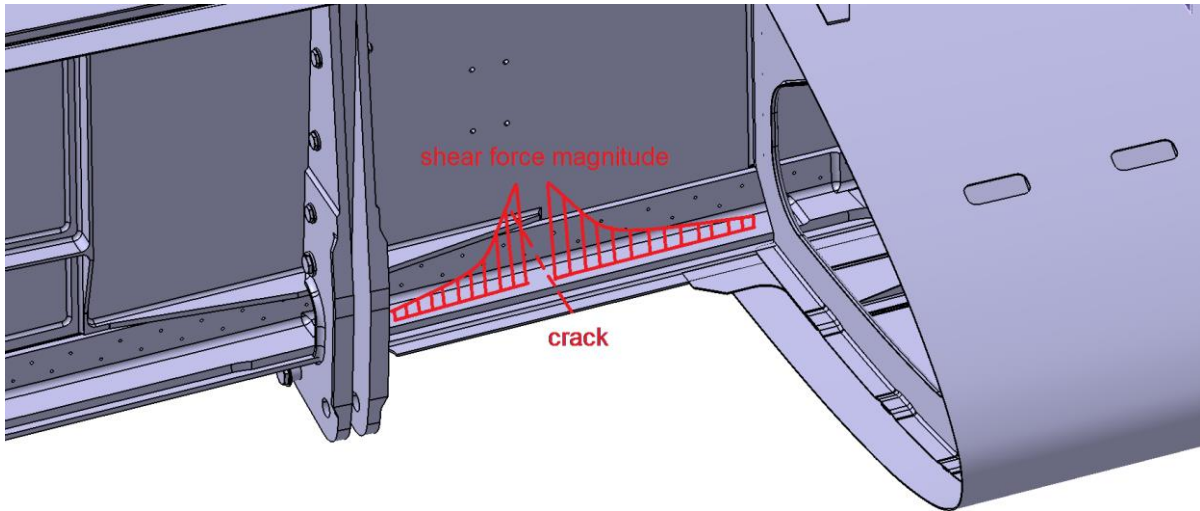
Figure 5.19 Shear force acting on the rivets in the vicinity of a crack [10].

The shear loading of the fasteners is obtained by means of finite element analysis. Two basic strategies of fastener bearing capacity analysis, differing in fastener stiffness modelling and applied fastener failure criteria, are described in the bullet points on the next page.

- **Linear analysis** – fastener stiffness is modelled analytically, e.g. using the Huth method [22] – Equation (5.18). Reserve factor is evaluated as per Equation (5.17), where F is the fastener shear load and F_{CRIT} is the maximum allowable fastener load, as defined in the pertaining standard (e.g. [32]).

$$RF = \frac{F_{CRIT}}{F} \tag{5.17}$$

$$K_{shear} = \frac{\kappa}{m} \left(\frac{t_1 + t_2}{2d}\right)^{\lambda} \left(\frac{1}{E_1 t_1} + \frac{1}{m E_2 t_2} + \frac{1}{2 E_F t_1} + \frac{1}{2 E_F t_2}\right) \tag{5.18}$$

In the equation above:

K_{shear} – Fastener stiffness in shear

κ, λ – Constants depending on the fastener type

m – Number of shear planes

$E_{1,2}$ – Young's modulus of the connected parts

$t_{1,2}$ – Thickness of the connected parts

E_F – Young's modulus of the fastener

d – Fastener diameter

- **Non-linear analysis** – elasto-plastic fastener behaviour is modelled according to experimental results, as depicted in Figure 5.20. Reserve factor is evaluated as per Equation (5.19), where δ is the rivet shear displacement and δ_{CRIT} is the maximum allowable shear displacement observed in the experimental results.
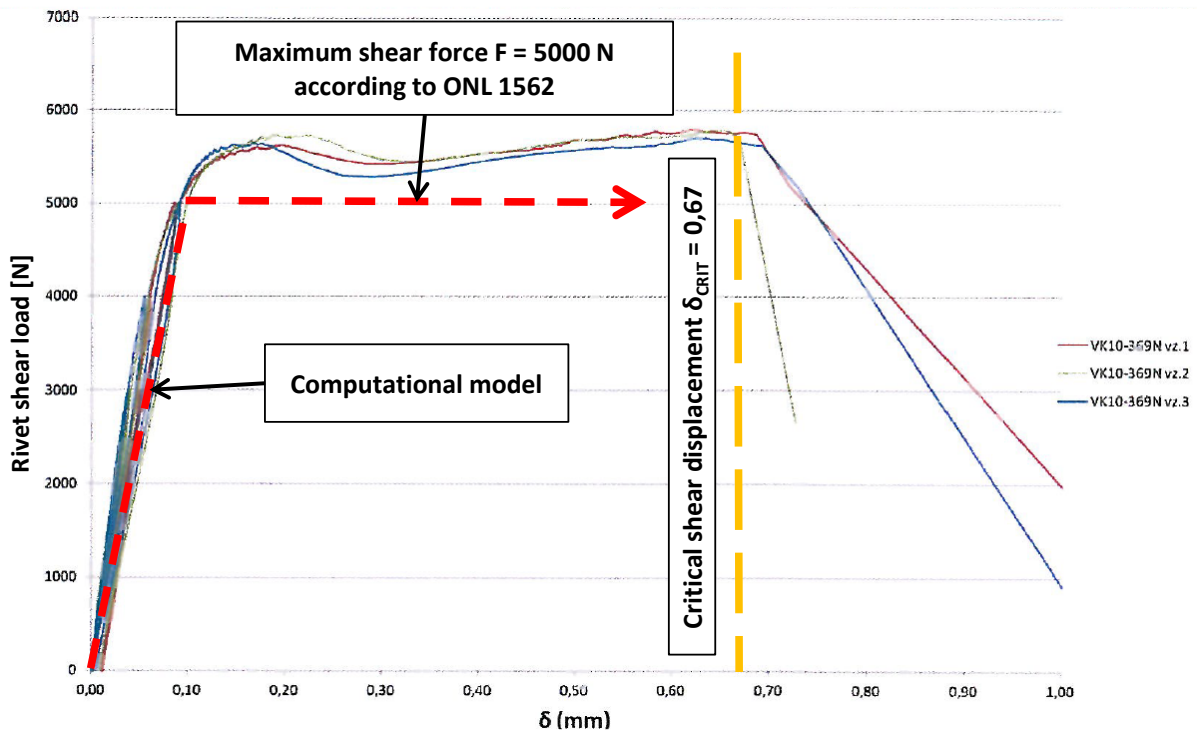
Figure 5.20 Rivet shear stiffness – experimental results and computational model [24].

62

$$RF = \frac{\delta_{CRIT}}{\delta} \tag{5.19}$$

Further possibilities of advanced fastener modelling techniques were previously examined by the author and are presented in [29]. These techniques allow for modelling fastener failure during the non-linear FE calculation. This enables the applicant to find the true limit state of the fastener bearing capacity, i.e. the chained failure of all fasteners of a given joint, rather than a single fastener failure, which necessarily does not induce a complete structural failure (the neighbouring fasteners are able to transfer the extra load).

5.4.4 Surrounding structure strength

The structural **elements adjacent to a crack** are also subjected to an **increased load**, when compared to the intact state (see Figure 5.21). Their stress level should be therefore checked as per Equation (5.20), where $\sigma_{VON\ MISES}$ is von Mises stress obtained by means of linear / non-linear FE analysis at 100 % limit load and R_m is the material strength.

$$RF = \frac{R_m}{\sigma_{VON\ MISES}} \tag{5.20}$$
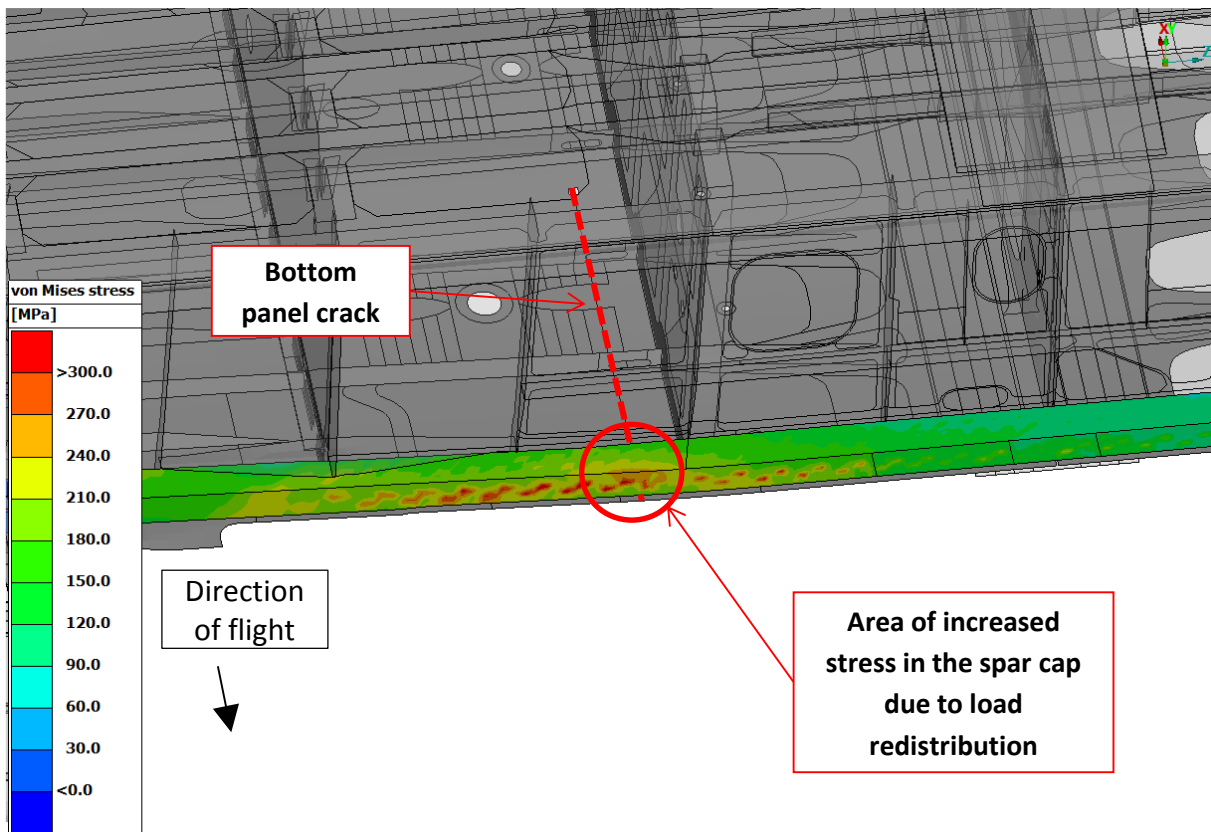
Figure 5.21 Increased load of unflawed adjacent structural members. Contour plot of von Mises stress at 100 % limit load on the spar cap.

5.4.5 Buckling

Stability of the structure should be analysed where applicable using one of the two following approaches:

- Confronting the minor **principal stress σ₃** in the structural member obtained by FE computation with a **critical buckling stress σCRIT** calculated according to a certain literature (e.g. [19]), while allowing a some extent of structure idealisation – Equation (5.21).

$$RF = \frac{\sigma_{CRIT}}{\sigma_3}$$

(5.21)

- Performing a **non-linear FE analysis** and utilizing **sub-modelling technique**. This approach was agreed to be suitable for complex parts (e.g. shear webs with irregular cut-outs and variable thickness) and flawed elements. Specific details of this approach are introduced in previous author's work [30]. Figure 5.22 depicts an example of such analysis.
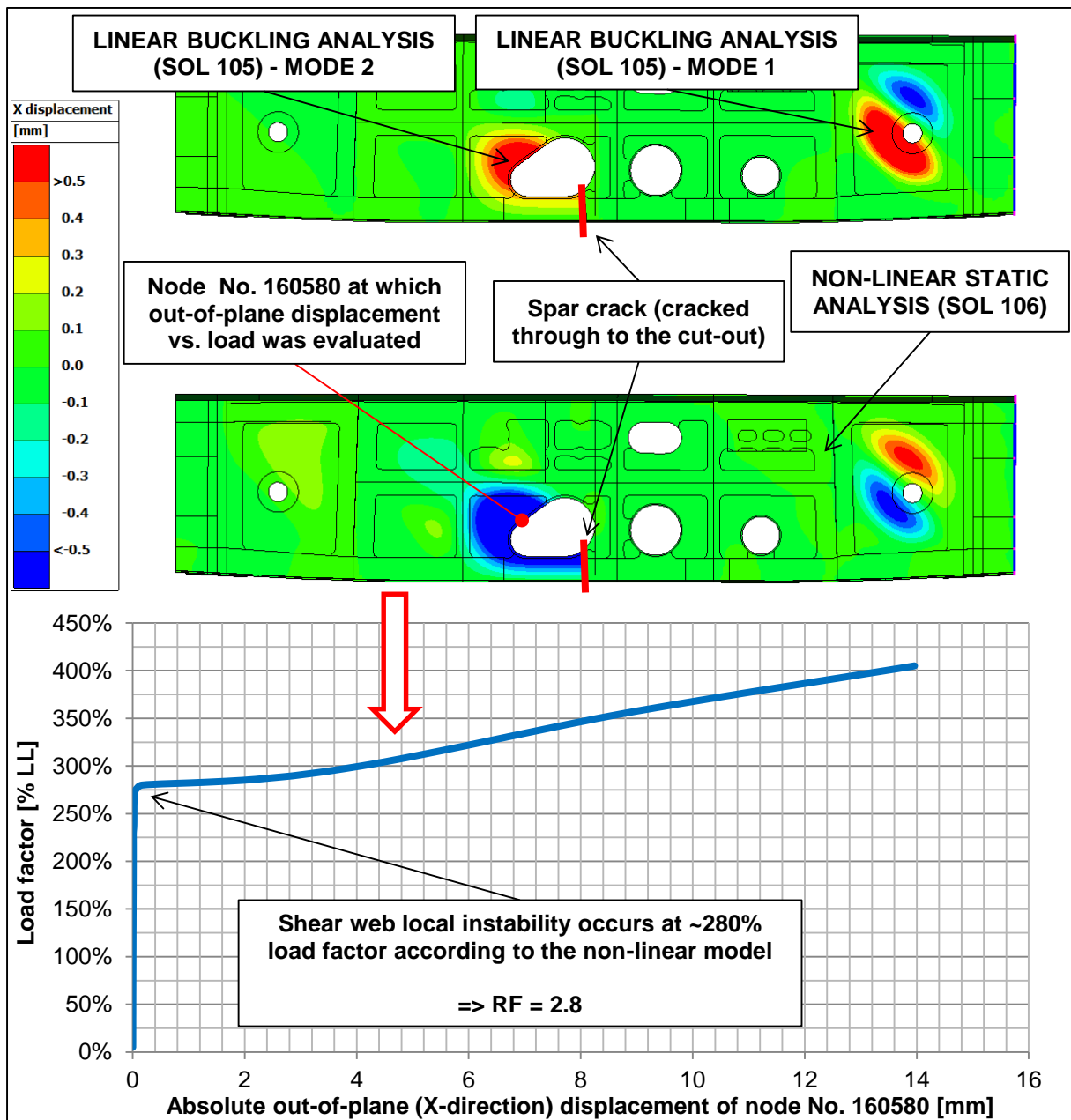
Figure 5.22 Example of buckling analysis of rear spar shear web by sub-modelling [30].

5.5 Final methodology overview

The proposed methodology of analysing dependent growth of multiple cracks is schematically summarized in Figure 5.23.
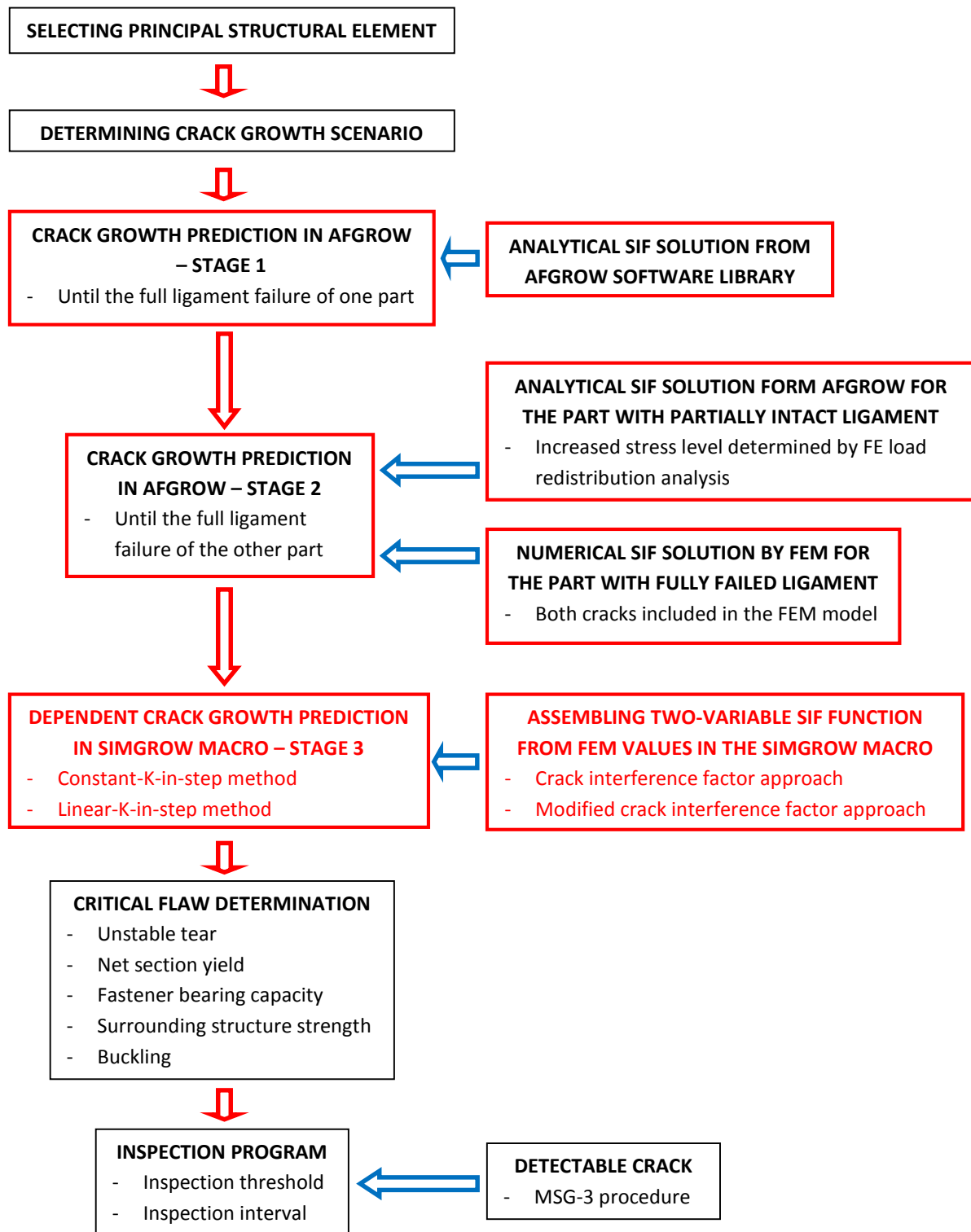
Figure 5.23 Flowchart of the dependent multiple crack growth analysis according to the proposed methodology.

6 PRACTICAL APPLICATION OF THE PROPOSED METHODOLOGY

This chapter presents the results of the practical application of the proposed methodology, as described in detail in Chapter 5.

The application was carried out in the following locations on the wing of the L 410 NG aeroplane:

- **Cut-outs in stringers of the integral bottom panel in section 102** – this case served for the development of the proposed methodology. The whole analysis procedure is presented.
- **Cut-outs in the integral rear spar in sections 0 and 102** – this case was used to further review the benefits of the proposed methodology compared to a simplified conservative solution (as discussed in Subchapter 2.2). Only a partial analysis was performed, while adopting multiple results from previously conducted DT analysis of the location by the author in report [28].

6.1 Cut-outs in stringers of the integral bottom panel of the L 410 NG wing

The analysis targeted the cut-outs in the stringers of the integral bottom panel in section 102, which were considered to be fatigue sensitive areas within the analysed location. The DT analysis was performed on the right wing, where slightly higher stress values were present (according to the FE model). A general identification of the location is illustrated in Figure 6.1.
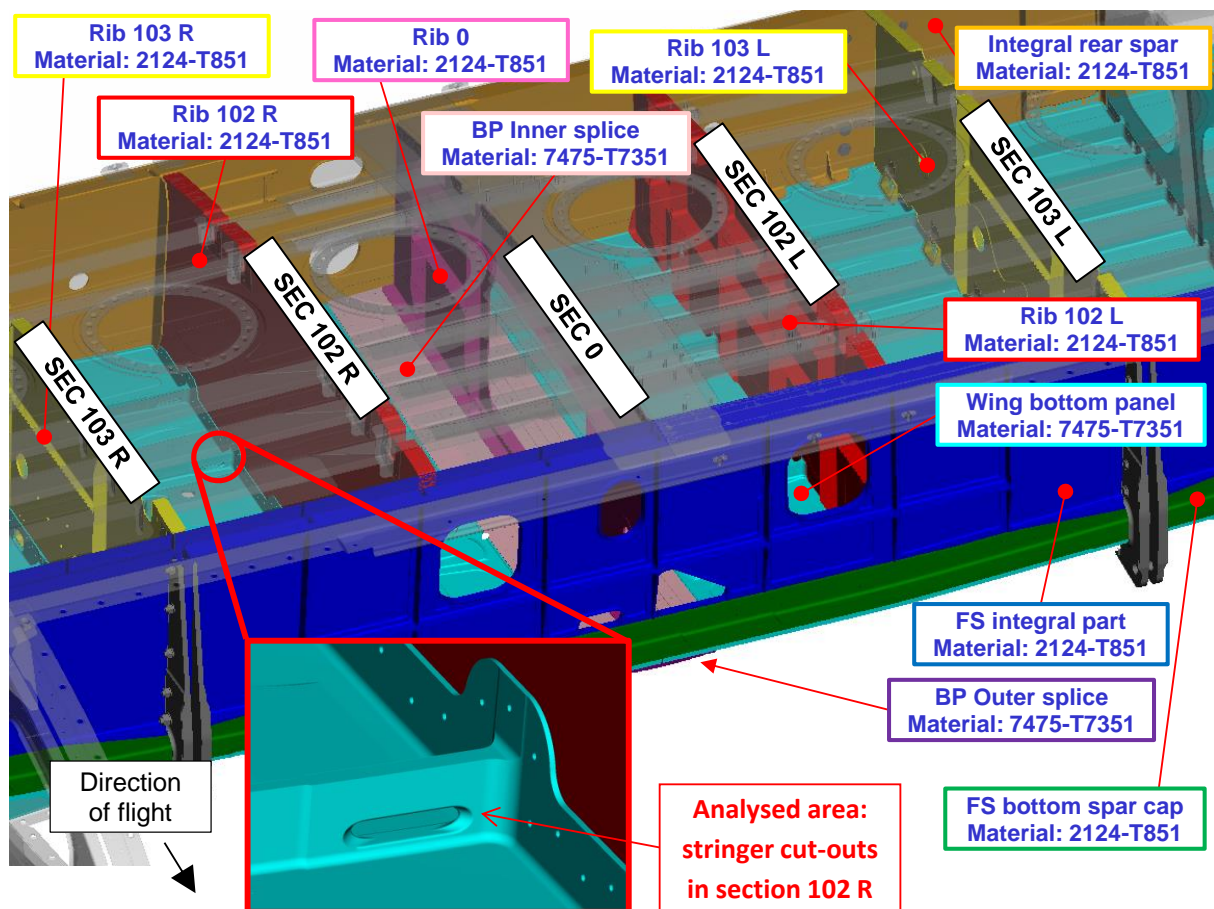
Figure 6.1 General view of the analysed location.

6.1.1 Initial flaw distribution

A FEM analysis of the area in the intact state was conducted in order to identify the most critical areas. The results are depicted in Figure 6.2.
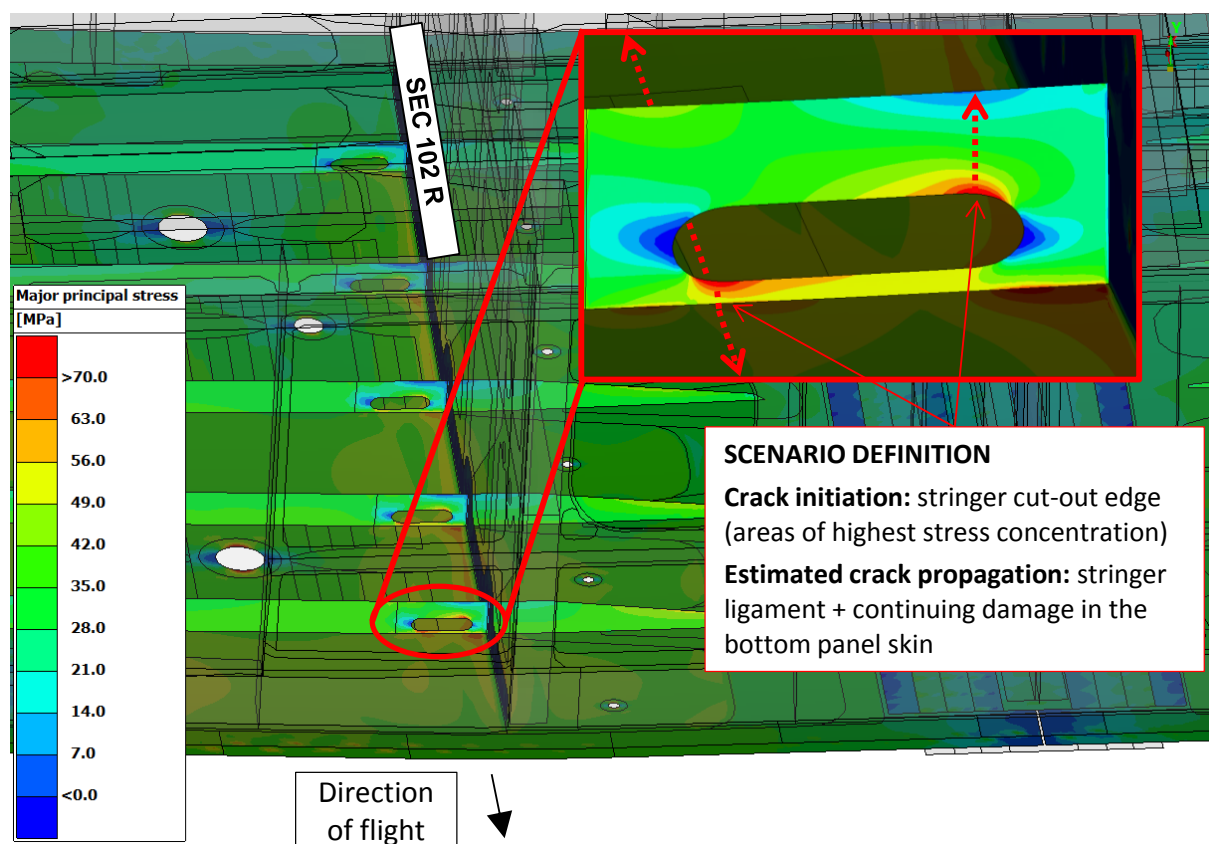
Figure 6.2 Identification of the most critical areas and crack growth scenario definition. Contour plot of major principal stress on the bottom panel in cruise flight (LC 111).

The stress analysis revealed that the most loaded stringer was the one closest to the front spar, with the anticipated stress concentration taking place around the corners of the cut-out.

Flaws were assumed to exist in the most unfavourable locations, in accordance with JSSG-2006 (see Subchapter 2.1.3), and the following crack growth scenario, shown also in Figure 6.3, was defined:

- **Primary (rogue) flaw** of quarter circular part-through shape (1.27 mm) located in the area of highest stress concentration, growing in the stringer ligament.
- **Secondary (quality) flaw** of quarter circular part-through shape (0.127 mm) located in the area of highest stress concentration, growing opposite the stringer ligament into the integral panel skin.

No further scenarios were needed for the analysed location, since the defined scenario was considered to be critical from all points of view.
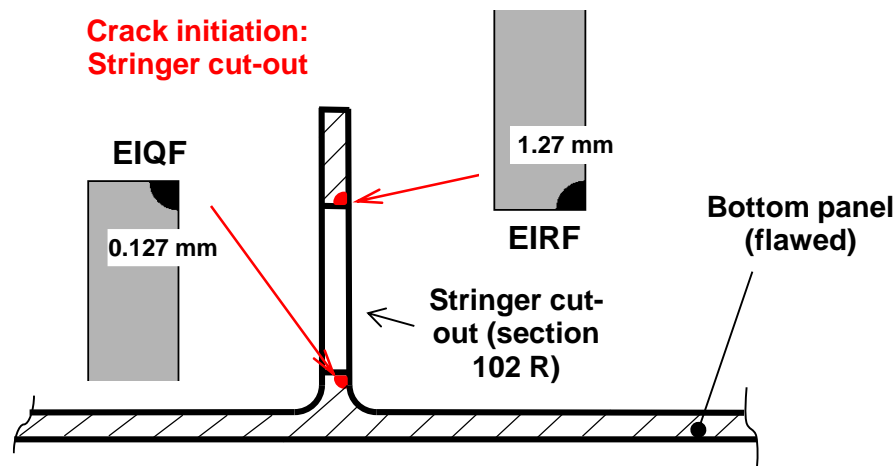
Figure 6.3 Initial flaw distribution in the stringer closest to the front spar.

6.1.2 Material data

Bottom panel is made of aluminium alloy 7475-T7351, while the majority of the surrounding structure is made of aluminium alloy 2124-T851 (see Figure 6.1). The following material data of the two mentioned materials are stated in the next paragraphs of this subchapter:

- **Basic mechanical properties** (e.g. ultimate strength, yield strength, etc.)
- **da/dN vs. ΔK curves**
- **R-curves**

7475-T7351 aluminium alloy

Basic mechanical properties of the 7475-T7351 alloy used in the calculations are stated in Table 6.1 below.

Table 6.1 Basic mechanical properties of the 7475-T7351 alloy, t = 76 mm, L-T [25].

Property	Value
Ultimate strength R_m [MPa]	486
Yield strength $R_{p,0.2}$ [MPa]	418.6
Young's modulus E [MPa]	69 260

The constant amplitude da/dN vs. ΔK curves of the 7475-T7351 alloy, which were used for fatigue crack growth predictions, are shown in Figure 6.4 on the next page. Furthermore, these data are extrapolated backwards from the Paris region, as discussed in Subchapter 3.2.1. No load interaction model was utilized.
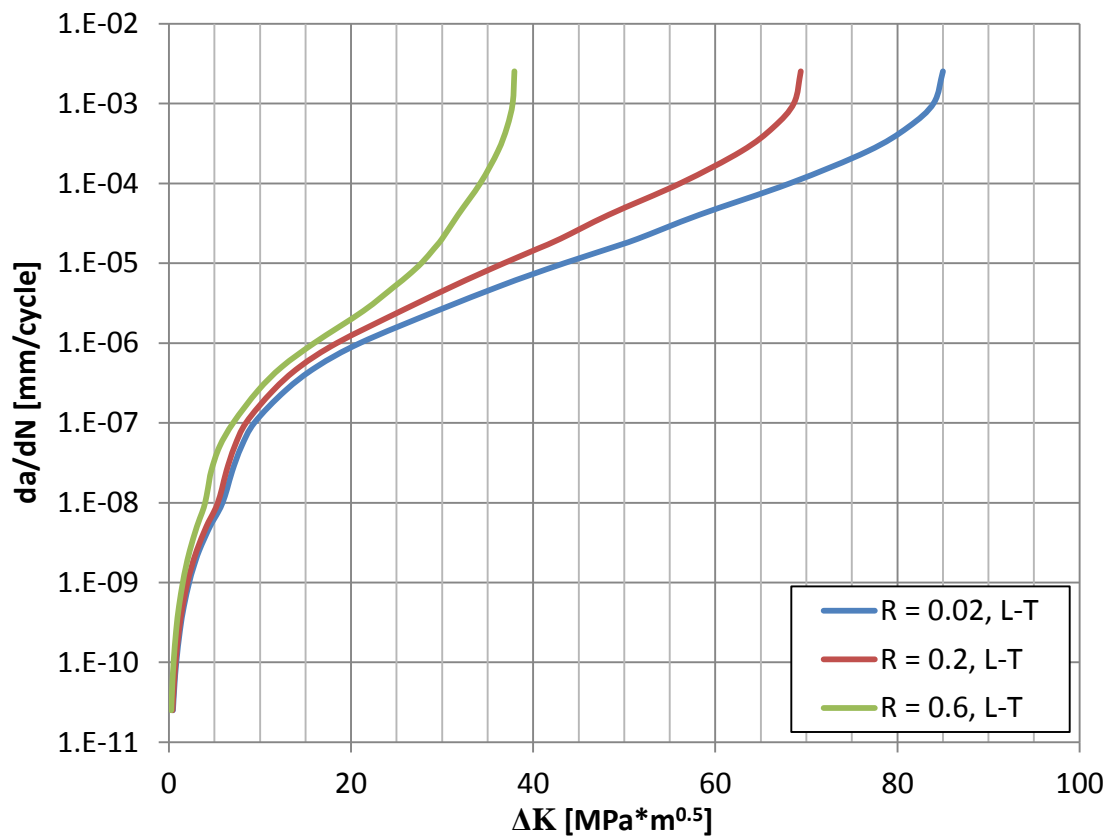
Figure 6.4 da/dN vs. ΔK curves of the 7475-T7351 alloy, t = 76 mm, L-T [25].

R-curve used for unstable tear analysis of parts made of 7475-T7351 alloy is depicted in Figure 6.5 below.
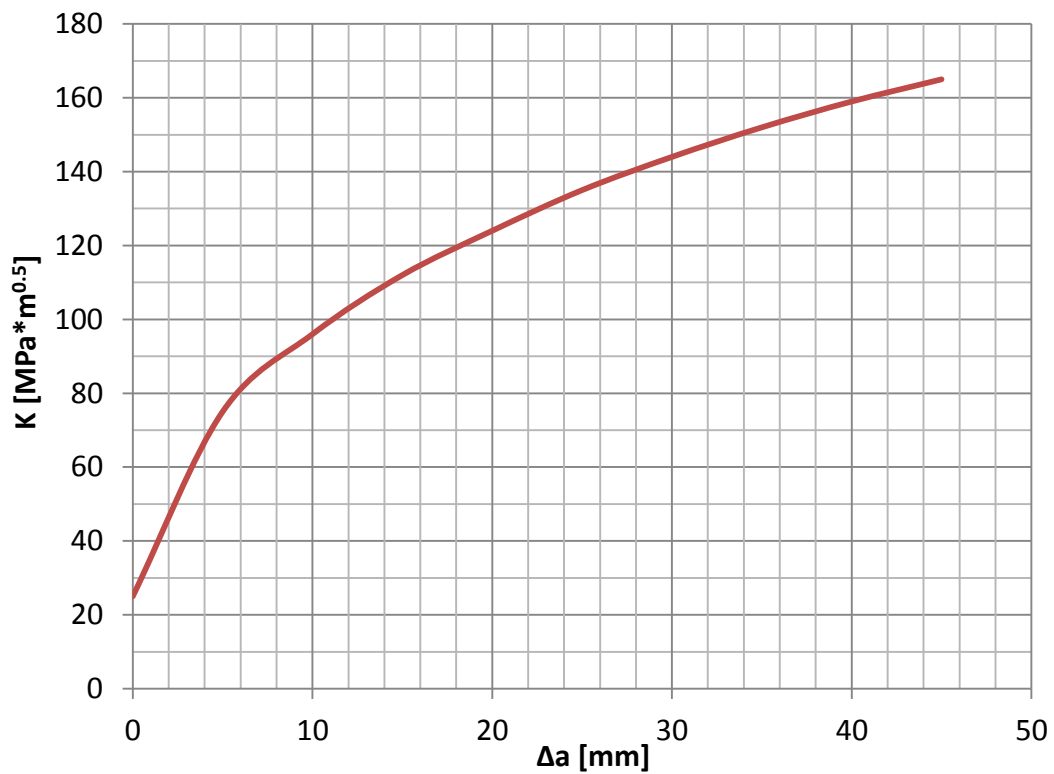
Figure 6.5 R-curve, 7475-T7351 alloy, t = 76 mm, L-T [25].

2124-T851 aluminium alloy

Basic mechanical properties of the 2124-T851 alloy used in the analysis are stated in Table 6.2 below.

Table 6.2 Basic mechanical properties of the 2124-T851 alloy, t = 50 mm, L-T [26].

Property	Value
Ultimate strength R_m [MPa]	488
Yield strength $R_{p,0.2}$ [MPa]	446.7
Young's modulus E [MPa]	70 000

The constant amplitude da/dN vs. ΔK curves of the 2124-T851 alloy, which were used for fatigue crack growth predictions, are shown in Figure 6.6 below. Furthermore, these data are extrapolated backwards from the Paris region, as discussed in Subchapter 3.2.1. No load interaction model was utilized.
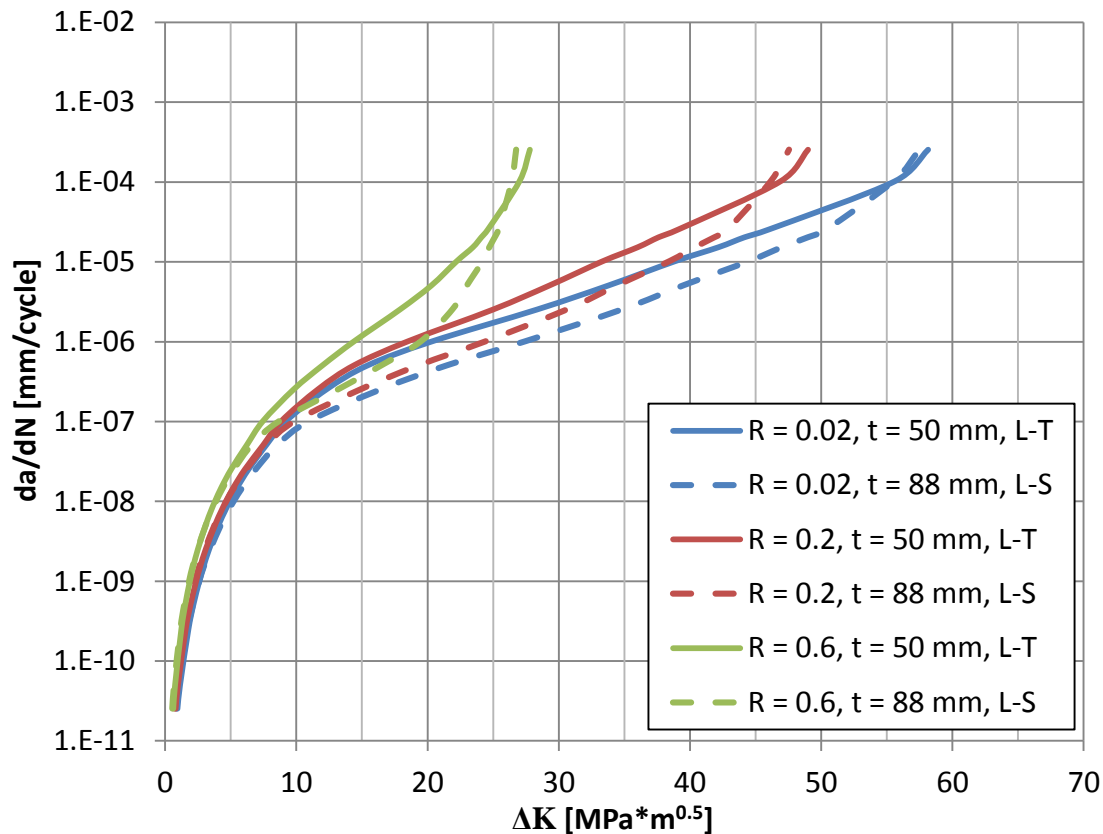
Figure 6.6 da/dN vs. ΔK curves of the 2124-T851 alloy [26].

R-curve used for unstable tear analysis of parts made of 2124-T851 alloy is depicted in Figure 6.7 on the next page.
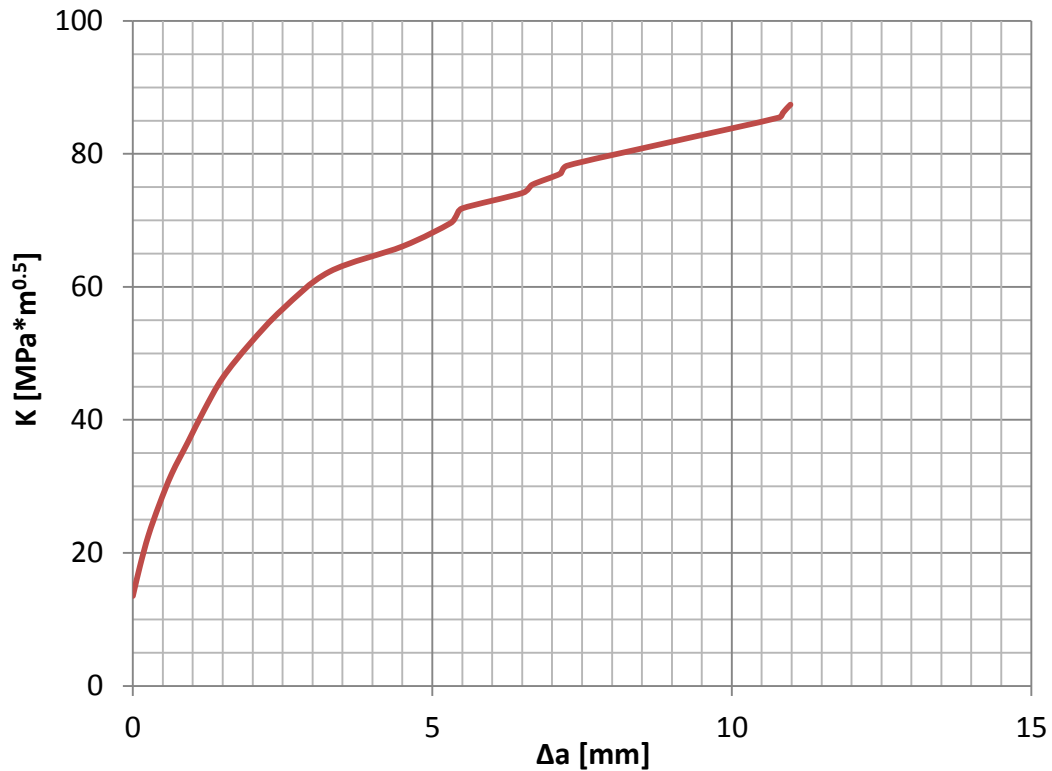
Figure 6.7 R-curve, 2124-T851 alloy, t = 50 mm, L-T [26].

6.1.3 Description of the calculation process, stress intensity factor solution

The fatigue crack growth calculation procedure was split into three stages (denoted 1 to 3), differing in the used crack growth model and the means of obtaining the β-function. This subchapter describes the assumptions made in all three stages in question.

Stage 1

Stage 1 includes the crack growth from the initial crack lengths until the full stringer ligament failure, as shown in Figure 6.8.
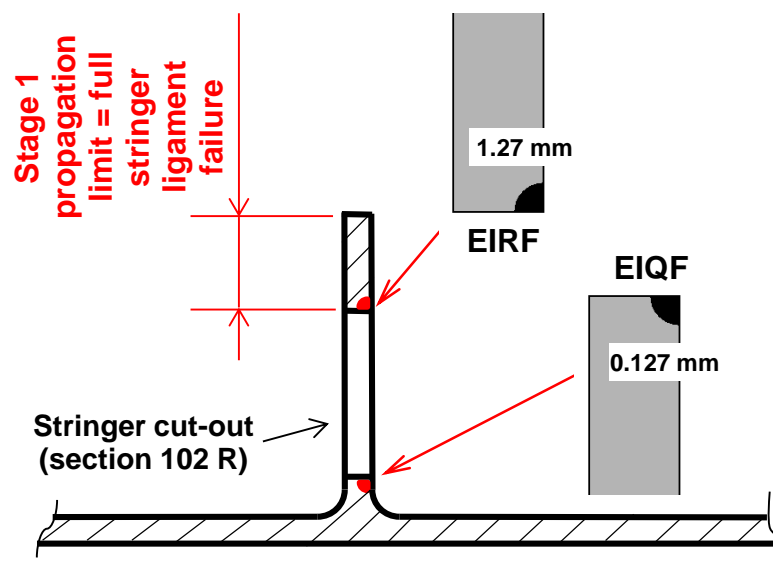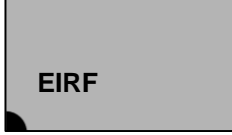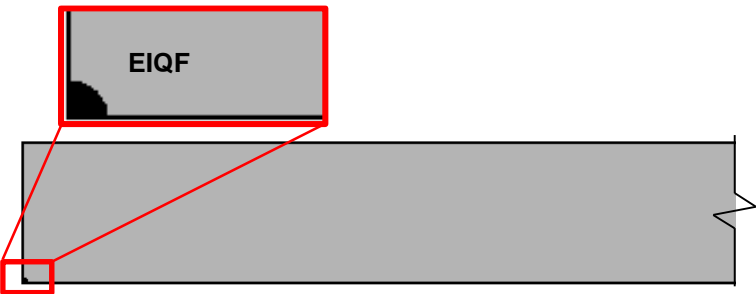
Figure 6.8 Crack propagation in stage 1. EIRF – Equivalent Initial Rogue (Primary) Flaw. EIQF – Equivalent Initial Quality (Secondary) Flaw.

Detailed description of stage 1 crack growth models and their parameters is in Table 6.3 below. All models use a loading sequence generated from stresses obtained by FEM analysis. More details concerning the loading sequence can be found in Subchapter 3.2.3.

Table 6.3 Description of methods used in stage 1. Remarks: 1) Multiple of the loading sequence reference stress (78.19 MPa in cruise flight – LC 111).

Stage	Flaw	AFGROW model description
1	Rogue (primary)	 Model type: Standard (edge corner crack) β-function: Analytical (AFGROW library) + β-correction Usage: Growth of the primary flaw from 1.27 mm (quarter circular) to 4.1 mm (width direction) Dimensions: Width = 13.5 mm, Thickness = 8 mm Stress level [1]: 1.0697 Model type: Standard (edge through crack) β-function: Obtained by FEM Usage: Growth of the primary flaw from 4.1 mm until it induces full stringer ligament failure Dimensions: Width = 13.5 mm, Thickness = 8 mm Stress level [1]: 1.0000
	Quality (secondary)	 Model type: Standard (edge corner crack) β-function: Analytical (AFGROW library) + β-correction Usage: Growth of the secondary flaw opposing the ligament from 0.127 mm (quarter circular) Dimensions: Width = 100 mm, Thickness = 8 mm Stress level [1]: 1.0503 – 1.1769 (increase during growth to account for redistribution caused by primary crack growth)

It is important to note, that the analytical SIF solutions provided by AFGROW library were corrected in order to account for the stress gradients in the corners of the stringer cut-out, which are clearly visible in Figure 6.2. This correction is done in AFGROW by entering the gradient normalized to the stress value at the crack root (see AFGROW manual [6] for

more details). The stress gradients were obtained by means of FEM analysis with a very fine mesh (element size ~ 0.5 mm) and are presented in Figure 6.9.
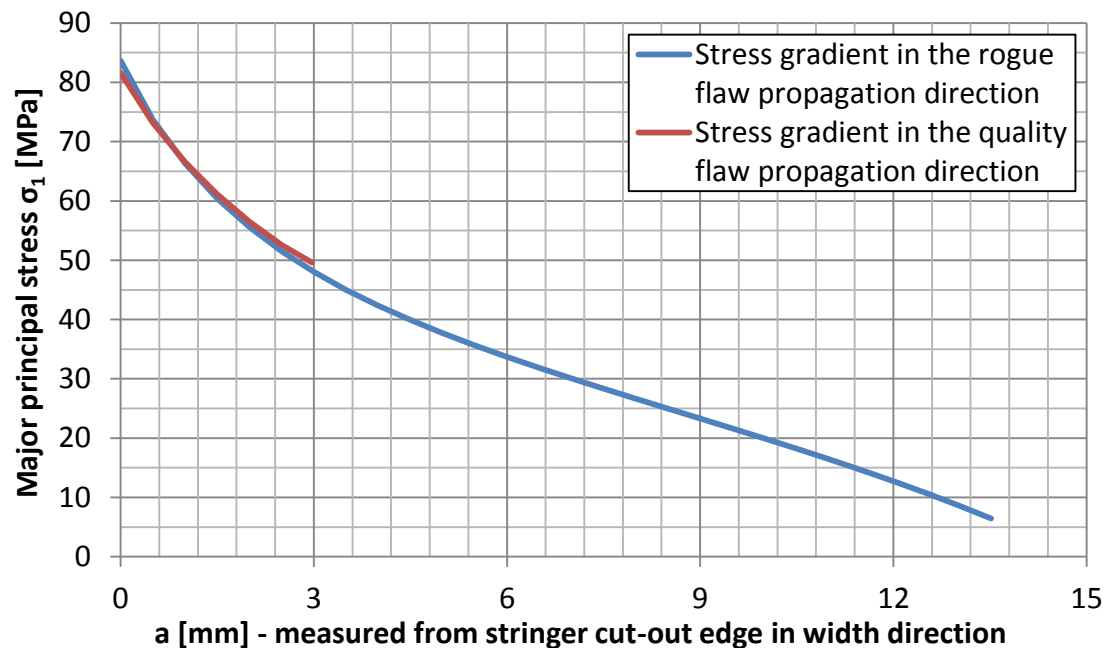

Figure 6.9 Stress gradients along the propagation paths, calculated by FEM analysis for cruise flight (LC 111).

Furthermore, the stress level of secondary crack model was increased several times during the fatigue crack growth prediction, in order to account for the propagation of the primary crack and the resulting load redistribution. This redistribution was evaluated by FEM and is presented in Figure 6.10. The growth of the secondary crack was considered to have a negligible effect on the load redistribution in the structure at this stage of the analysis.
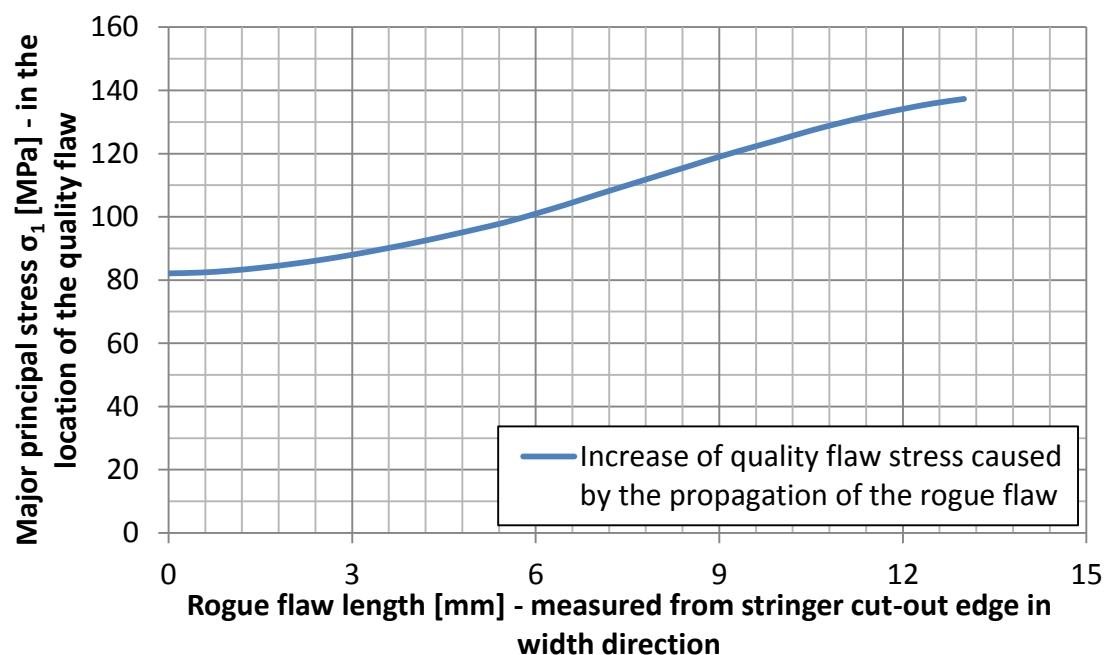
Figure 6.10 Load redistribution in the structure obtained by FEM in cruise flight (LC 111).

The resultant stage 1 β-function in the width direction for the primary (rogue) flaw is shown in Figure 6.11. From this figure it is clear, that analytical β-function model was replaced by FEM β-function model once it became more favourable for crack growth prediction (i.e. from the crack length it yielded lower β values). The reason for that is that the effect of a part-through crack, rather than a through crack in the FE model, was dominant for short crack lengths. On the other hand, load redistribution effect, which is accounted for in the FEM calculation, was crucial for longer crack lengths.
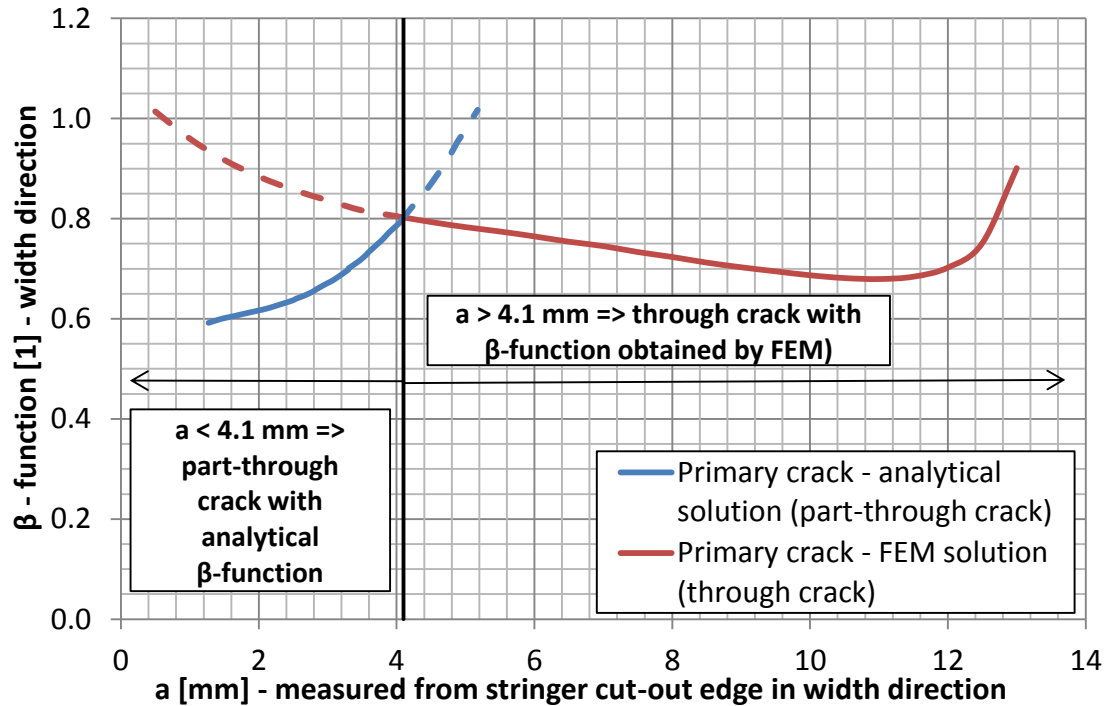
Figure 6.11 Stage 1 β-function in the width direction for the primary (rogue) flaw.

Stage 1 β-function in the width direction for the secondary (quality) flaw is in Figure 6.12. It accounts for the load redistribution caused by primary flaw growth (Figure 6.10).
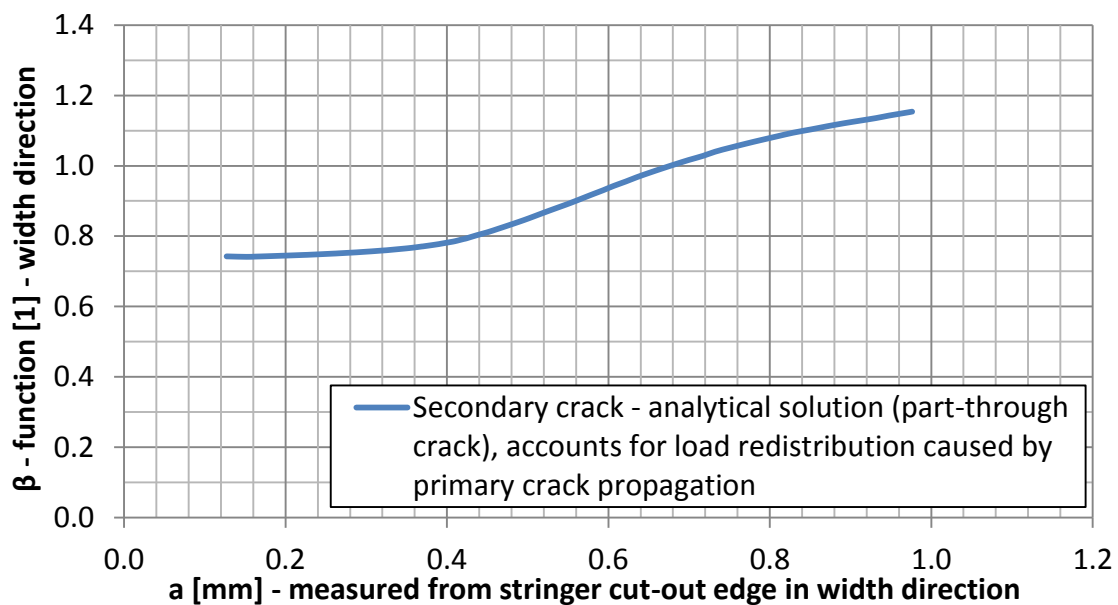

Figure 6.12 Stage 1 β-function in the width direction for the secondary (quality) flaw.

74

β-functions in the through-the-thickness direction in stage 1 are presented in Figure 6.13 for both cracks.
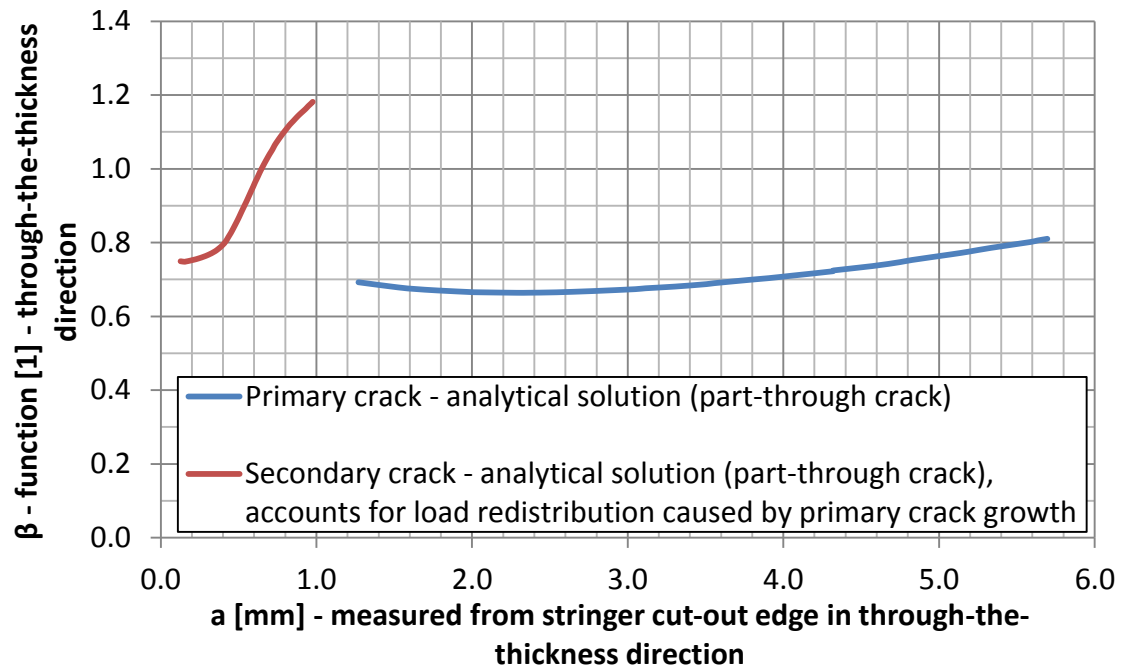

Figure 6.13 Stage 1 β-function in the through-the-thickness direction for both flaws.

Stage 2

Stage 2 includes the continuing damage growth (represented by the secondary crack) from the crack length at the end of stage 1 until the flaw reaches a length of 2 mm, as illustrated in Figure 6.14. This propagation limit was imposed to preclude the propagation of the secondary crack into the stringer-skin transition area.
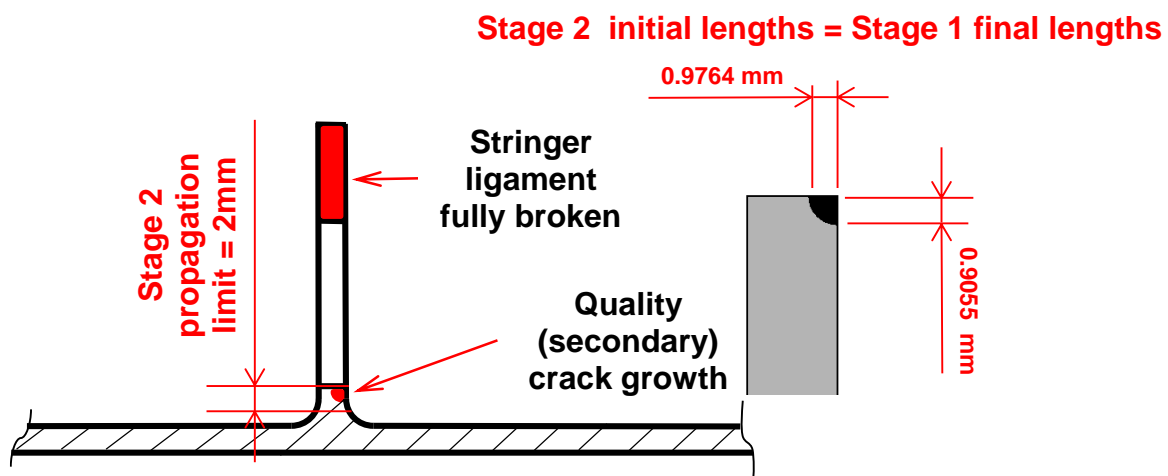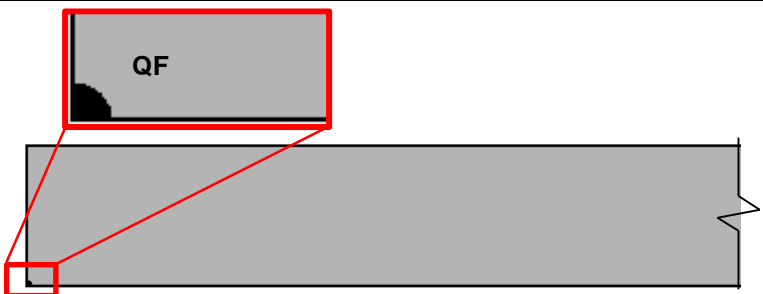

Figure 6.14 Crack propagation in stage 2.

Detailed description of stage 2 crack growth model and its parameters is in Table 6.4 on the next page.

Table 6.4 Description of the method used in stage 2. Remarks: 1) Multiple of the loading sequence reference stress (78.19 MPa in cruise flight – LC 111).

Stage	Flaw	AFGROW model description
2	Quality (secondary)	**Model type:** Standard (edge corner crack) **β-function:** Analytical (AFGROW library) + β-correction **Usage:** Growth of the continuing damage opposing the ligament from 0.9055 mm (width direction) and 0.9764 mm (through-the-thickness direction) until the secondary (quality) flaw reaches the length of 2 mm in the width direction **Dimensions:** Width = 100 mm, Thickness = 8 mm **Stress level [1]:** 2.5425 (accounts for redistribution after full stringer ligament failure)

The analytical solution for the quality (secondary) crack in stage 2 was corrected for stress gradient in the same manner as in stage 1 (see Figure 6.9). Secondary crack stress level for stage 2 was obtained by recalculating the FEM model with a fully failed stringer ligament. The resultant stage 2 β-functions of the secondary (quality) flaw are depicted in Figure 6.15.
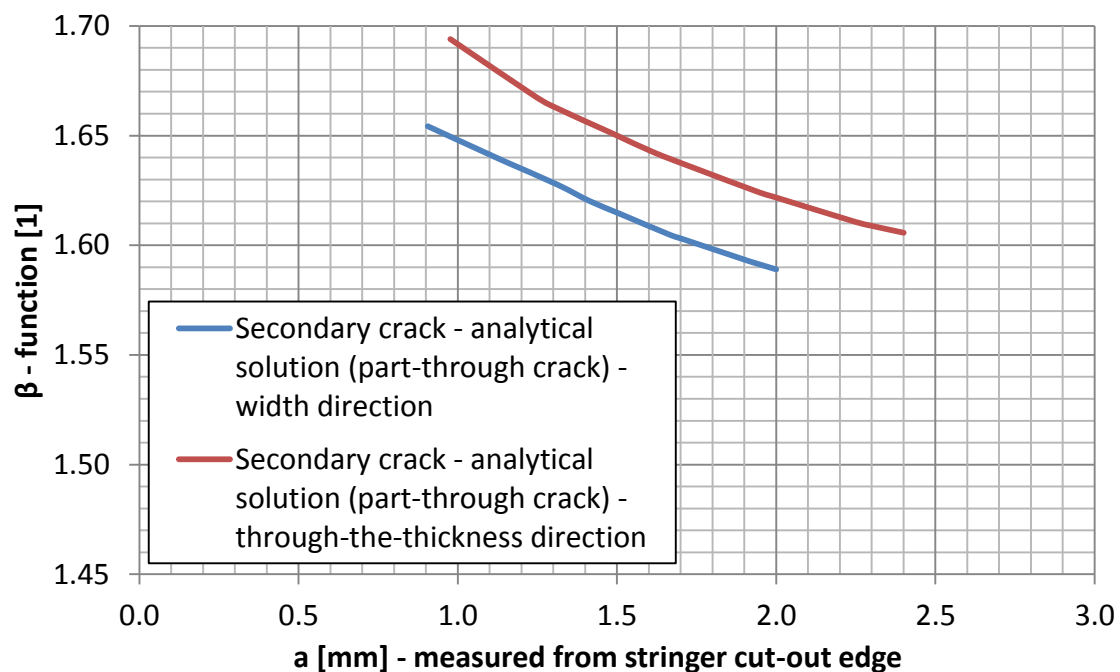

Figure 6.15 Stage 2 β-functions for the secondary (quality) flaw.

Stage 3

Stage 3 represents the growth of the secondary crack after it propagated to the skin of the integral panel (illustrated in Figure 6.16). Stage 3 ends when the crack reaches the end of the panel at the location of the front spar. The crack growth period between stage 2 and stage 3, during which the continuing damage grows in the stringer-skin transition area, was conservatively disregarded, since no suitable SIF solutions for such geometrical conditions were available.
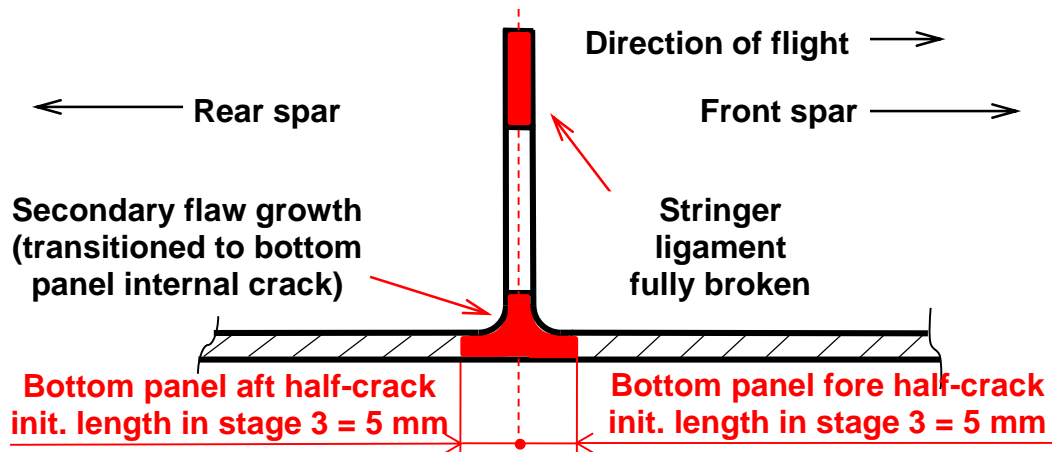

Figure 6.16 Crack propagation in stage 3.

The **unsymmetrical growth of the internal through crack** in the skin of the integral panel **was treated as the simultaneous propagation of two half-cracks**, hereinafter also denoted as "Fore crack" and "Aft crack". The SIF calculation and the growth prediction of **each half-crack were calculated separately**, while the mutual **interaction of the half-cracks was accounted for** by means proposed in Subchapters 5.2.2 and 5.3.2.

Practical application of the proposed methods on the calculation of two interfering cracks (half-cracks in this case) and comparison of the results with a simplified procedure used in L 410 NG analyses so far was one of the main objectives of this master's thesis.

Table 6.5 states the description of AFGROW model used for stage 3 fatigue crack growth calculation.

Table 6.5 Description of the method used in stage 3. Remarks: 1) Multiple of the loading sequence reference stress (78.19 MPa in cruise flight – LC 111).

Stage	Flaw		AFGROW model description
3	Quality (secondary)	Fore crack	**Half-crack of the secondary flaw in the panel**
		Aft crack	Model type: Standard (edge through crack)
			β-function: Obtained by FEM (accounts for the simultaneous growth of both half-cracks)
			Usage: Growth of the half-cracks from their initial lengths of 5 mm until half-crack 2 terminates at the panel edge under the front spar
			Dimensions: Width = 400 mm, Thickness = 4.45 mm
			Stress level [1]: 1.000

Two **variable stress intensity factor functions** (i.e. K vs. fore crack and aft crack lengths) were created **from FEM data** using the **modified crack interference factor method**, which was proposed in Subchapter 5.2.2. The FEM data consisted of 63 calculations with increasing aft crack length by an increment of 5 mm while fore crack remained its stage 3 initial length of 5 mm, 40 calculations with increasing fore crack length by the same increment while aft crack remained its stage 3 initial length and 40 calculations for various combinations of fore and aft crack lengths. The resulting SIF functions are presented in the form of a surface graph in Figure 6.17 and Figure 6.18.
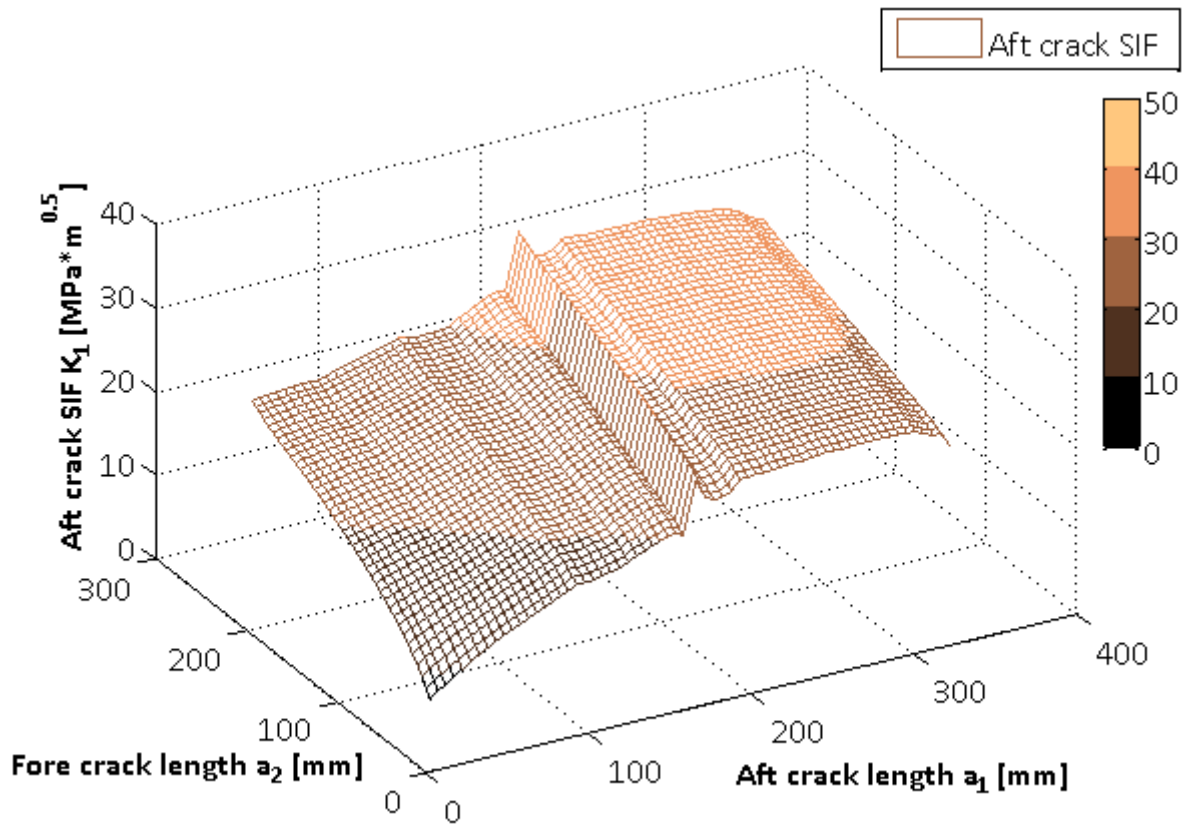

Figure 6.17 Stress intensity factor function for aft crack obtained from FEM data by modified crack interference factor method for cruise flight (LC 111).
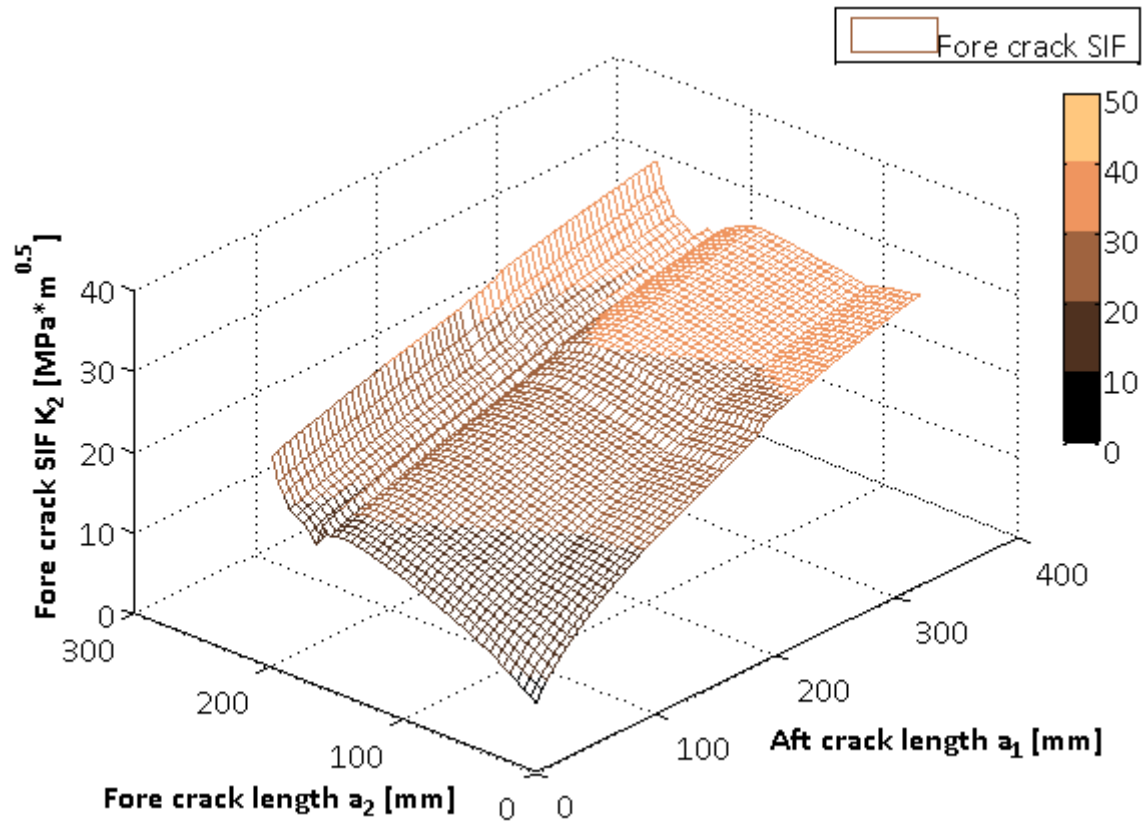
Figure 6.18 Stress intensity factor function for fore crack obtained from FEM data by modified crack interference factor method for cruise flight (LC 111).

The resultant stress intensity factor vs. crack length curves are presented in Figure 6.19 and Figure 6.20. These curves were **generated from the two-variable functions** depicted in figures above **by a step-by-step crack growth prediction procedure**, which is closely described in Subchapter 6.1.4. A simplified solution (1:1 propagation) is also presented.
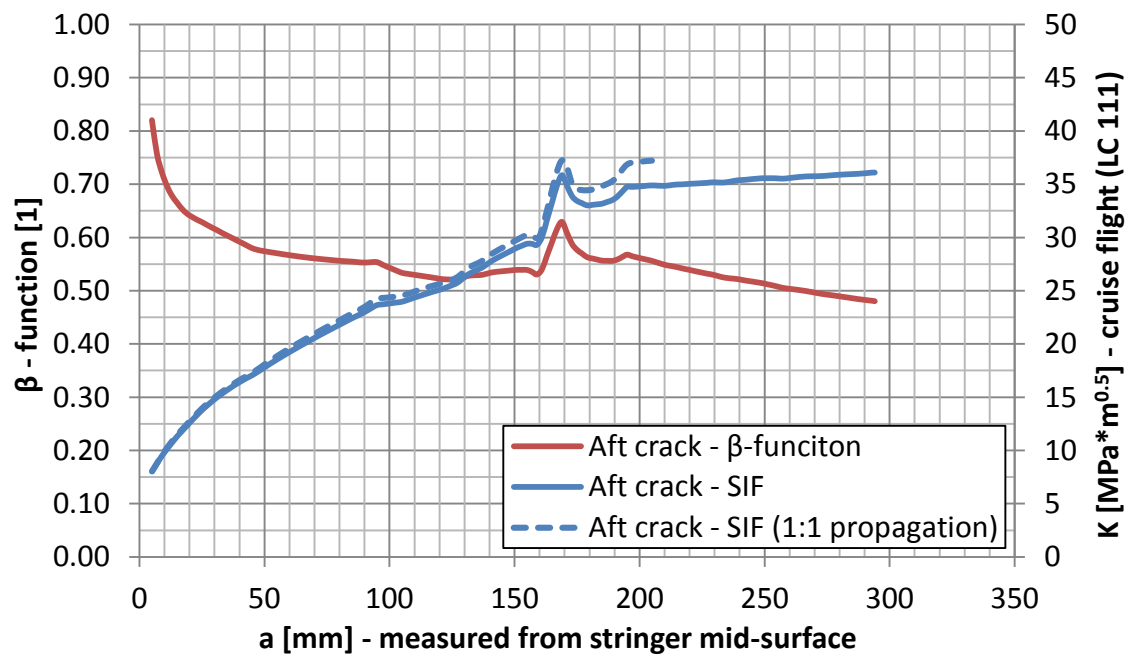

Figure 6.19 Stage 3 β-function for aft crack. Accounts for the simultaneous propagation of fore crack.
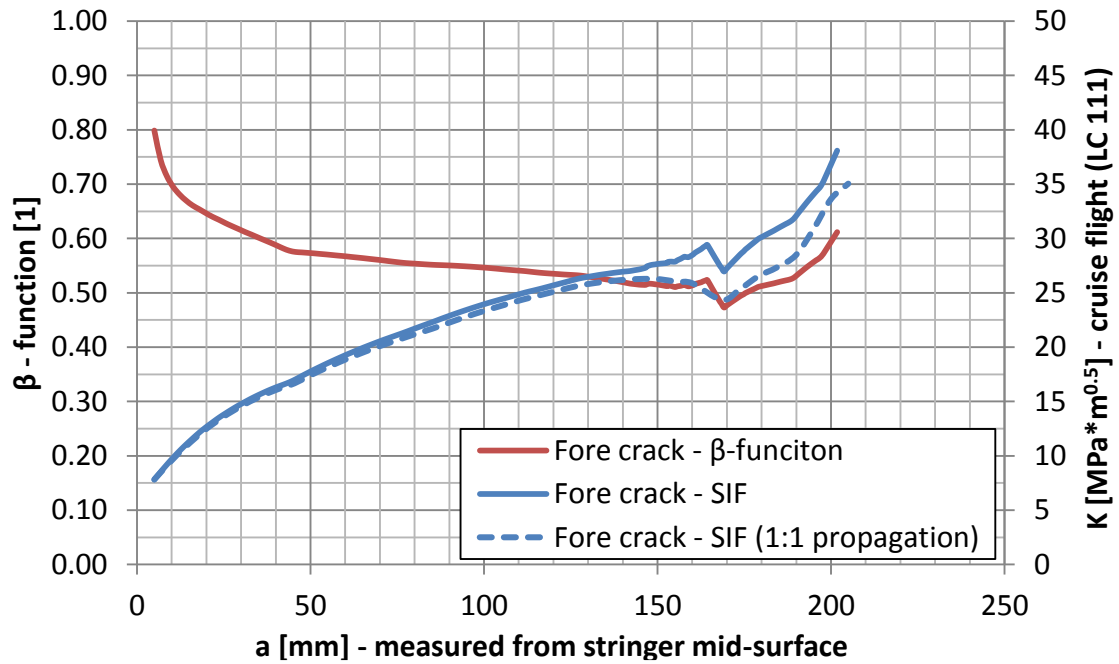
Figure 6.20 Stage 3 β-function for fore crack. Accounts for the simultaneous propagation of aft crack.

6.1.4 Fatigue crack growth prediction

Fatigue crack growth predictions were carried out in AFGROW software with settings described in the previous subchapter.

The developed **SIMGROW macro** was utilized in calculation of the **dependent crack growth** in stage 3. The linear-K-in-step solution (see Subchapter 5.3.2) was opted for with maximum absolute error of 0.05 flight hours, maximum relative error of 0.5 % and a crack length increment in step of 2 mm.

The resultant crack growth curves are shown in Figure 6.21 and Figure 6.22.
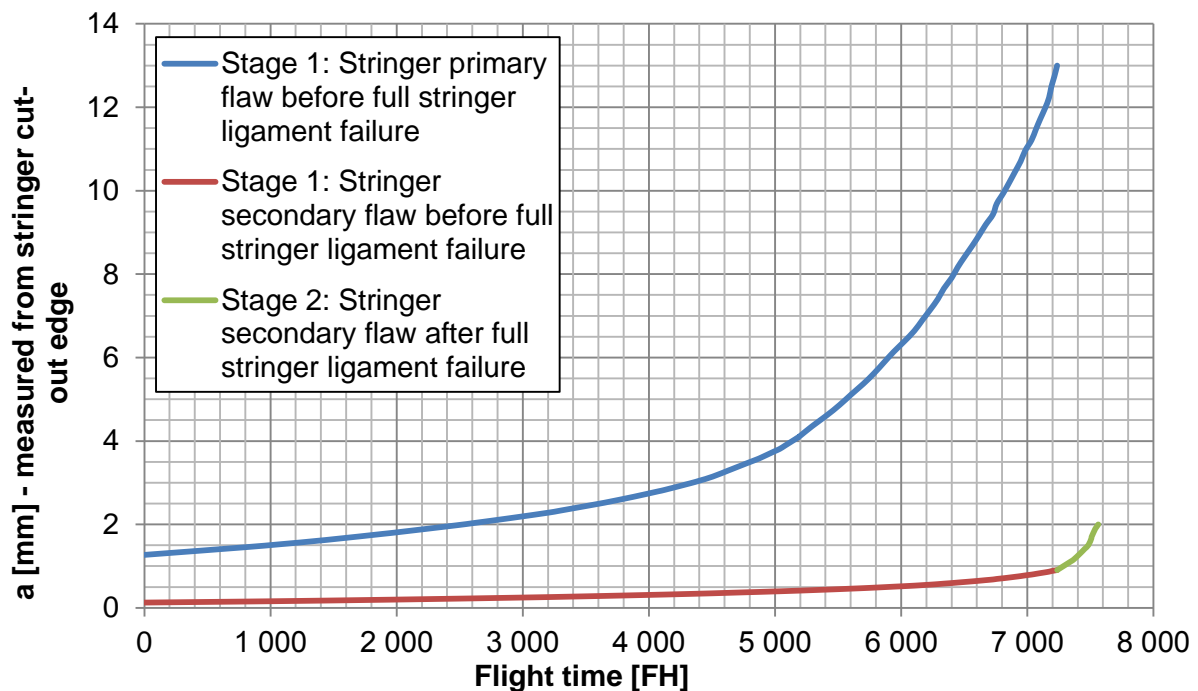

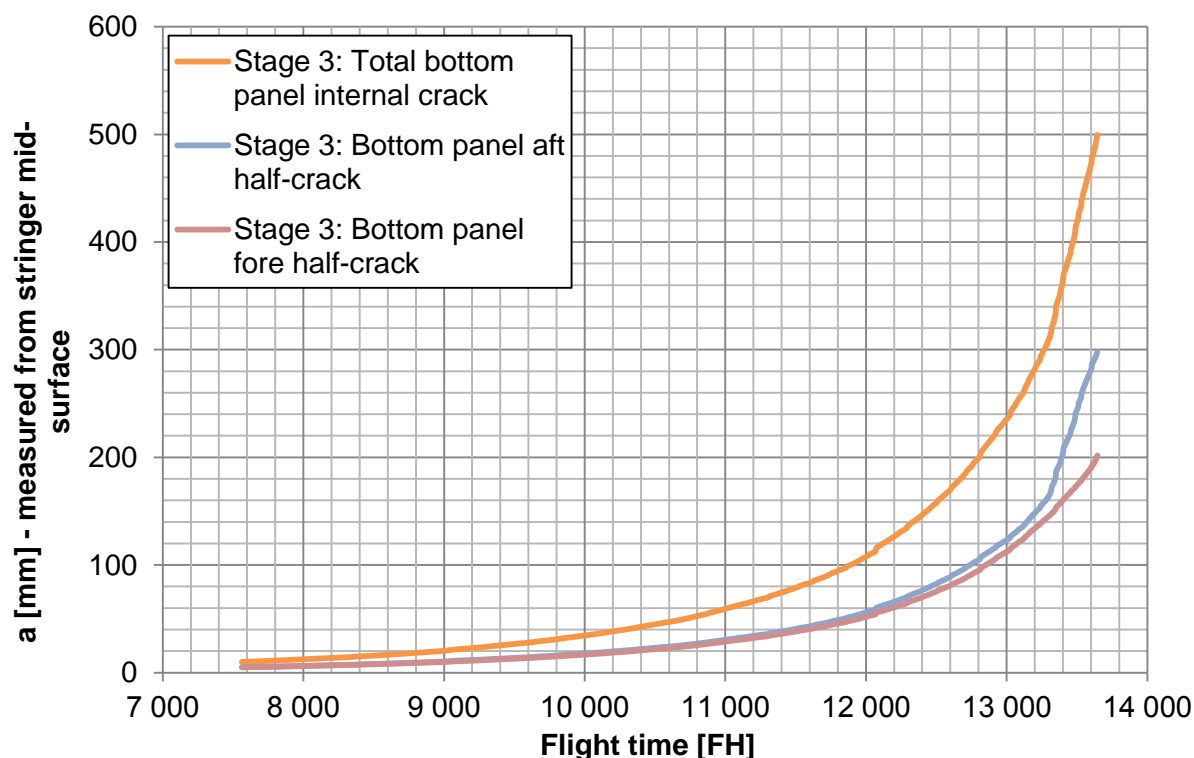**Figure 6.21 Calculated crack propagation in stages 1 and 2.**

Figure 6.22 Calculated simultaneous crack propagation in stage 3 using SIMGROW macro.

6.1.5 Residual strength analysis

All aspects of the residual strength stated in Subchapter 5.4 were investigated in **stage 3** (growth in the bottom panel skin) for **100 % limit load**. **Fastener yield effect** was included in **all residual strength FE calculations**. The limit load cases selected for critical length determination are in Table 6.6.

Table 6.6 Limit Load cases for residual strength analysis.

Load case (LC)	Description	Reasoning	Acc. to
MOSTA3KN-0424-064	Vertical gust on wing	Maximal bending moment upwards	[23]
MOSTA3KN-0429-084		Maximal bending moment downwards	

Unstable tear

Stress intensity factors for unstable tear analysis were obtained for the limit load case in the same manner as for cruise flight (see Subchapter 5.2.2 and 6.1.3). The FE analyses of the limit load case included fastener yielding. The unstable tear evaluation (see Subchapter 5.4.1) is presented in Figure 6.23 and Figure 6.24 on the next page and summarized in Table 6.7 below.

Table 6.7 Unstable tear analysis results. LC MOSTA3KN-0424-064.

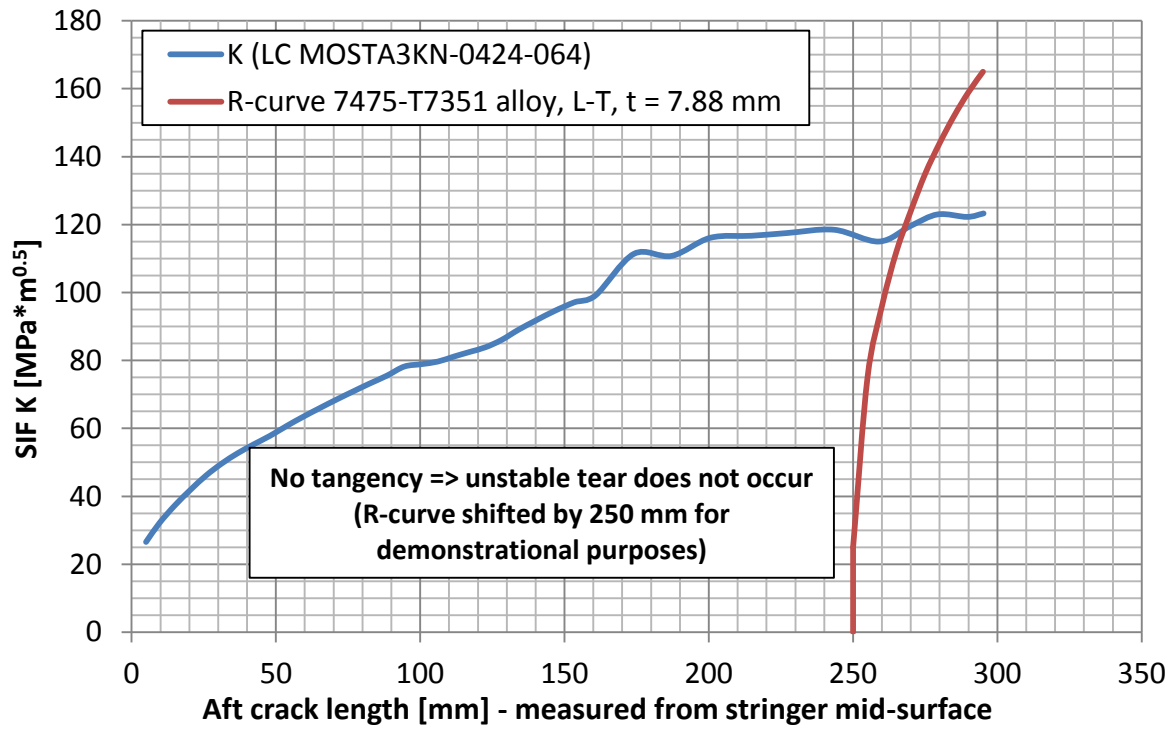| Aft crack length a_1 [mm]	Fore crack length a_2 [mm]	Total panel crack a [mm]	Limit state	RF [1]
243.5	174	417.5	Fore crack unstable tear	1.00

81

Figure 6.23 Unstable tear analysis of the aft crack.
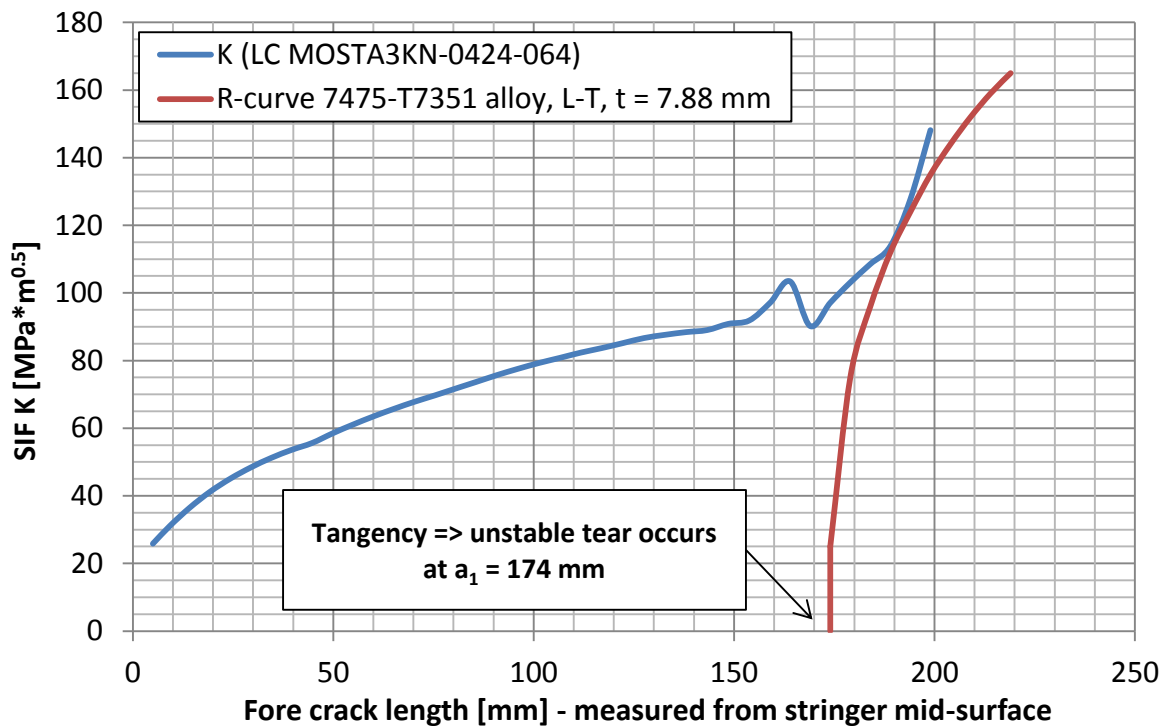

Figure 6.24 Unstable tear analysis of the fore crack.

Net section yield

The net section yield summary is presented in Table 6.8 on the next page. Forces for net stress calculation were obtained by FE calculation with non-linear fasteners. The reader is referred to Subchapter 5.4.2 for more details.

Table 6.8 Net section yield. Bottom panel - material: 7475-T7351. LC MOSTA3KN-0424-064.

Half-crack	Crack length a_1, a_2 [mm]	Total panel crack a [mm]	F_{NET} [N]	S_{NET} [mm^2]	σ_{NET} [MPa]	$R_{p,0.2}$ [MPa]	RF [1]
Aft	270	454	398 234	2028.3	196.3	418.6	2.13
Fore	184		41 364.6	126.3	327.5		1.28

Fastener bearing capacity

A non-linear FE analysis with fastener yielding was carried out in order to check the rivet bearing capacity in the vicinity of the bottom panel crack. The numbering system of the front spar bottom cap – bottom panel joint is depicted in Figure 6.25.
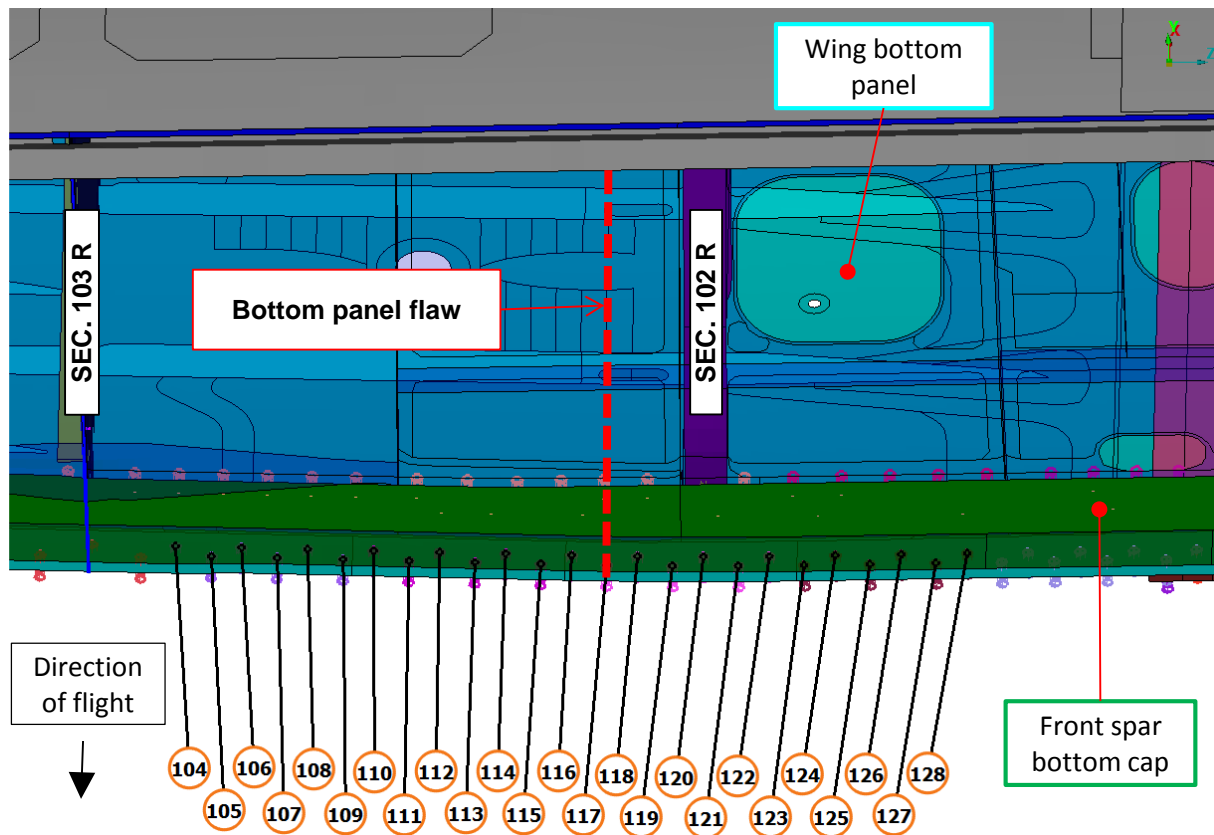

Figure 6.25 Rivet numbering system of the front spar bottom cap – bottom panel joint.

Rivet stiffness was modelled according to experimental results presented in [24] – see Figure 5.20. The evaluation of the rivet bearing capacity was done in accordance with Subchapter 5.4.3.

The summary of the rivet strength check is presented in Table 6.9 below and in Figure 6.26 on the next page.

Table 6.9 Rivet strength check summary. LC MOSTA3KN-0424-064. Critical rivet No. 110.

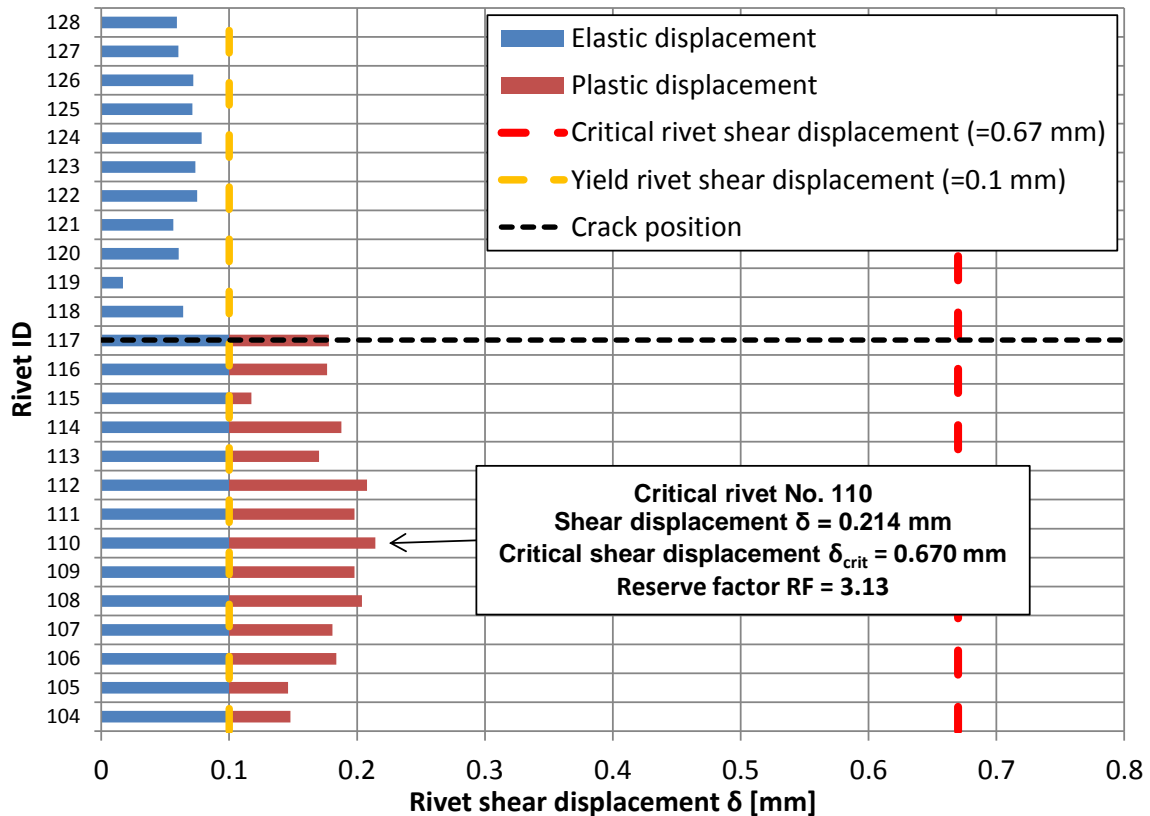| Aft crack length a_1 [mm]	Fore crack length a_2 [mm]	Total panel crack a [mm]	δ [mm]	δ_{CRIT} [mm]	RF [1]
270	184	454	0.214	0.67	3.13

Figure 6.26 Result of the non-linear FE analysis of rivet bearing capacity. LC MOSTA3KN-0424-064. Front spar bottom cap – bottom panel joint.

Surrounding structure strength

The increased load of the front spar bottom cap was the subject of the surrounding structure strength check – see Figure 6.27.
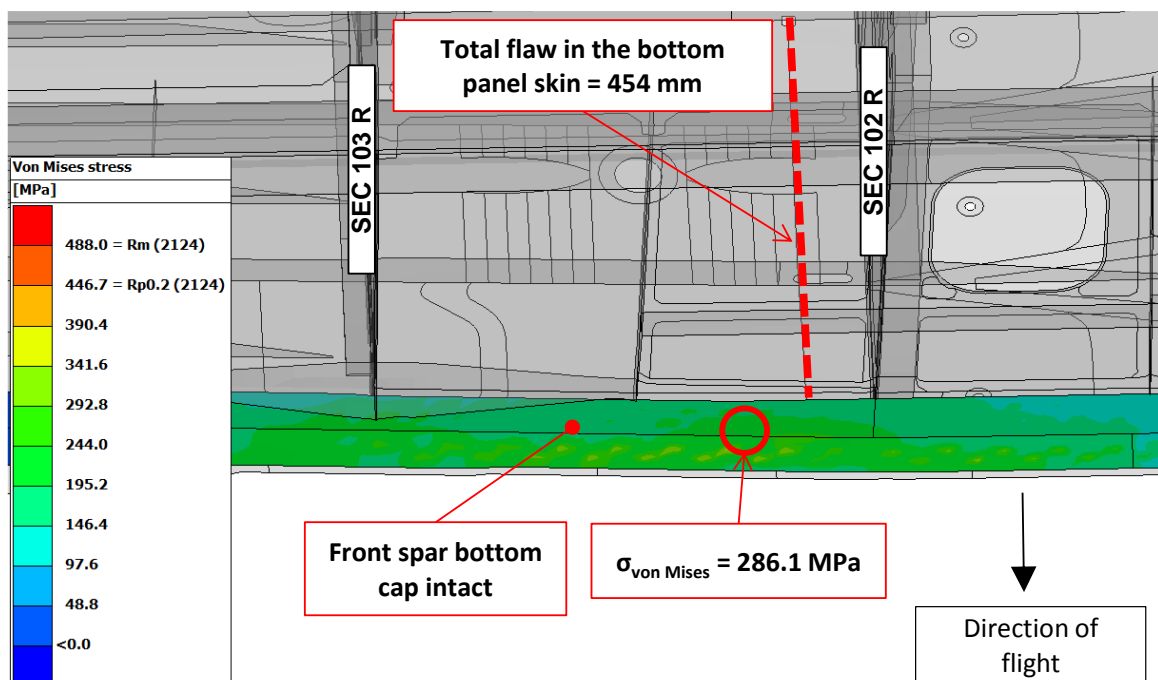

Figure 6.27 Front spar bottom cap stress check. Contour plot of von Mises stress on the front spar bottom cap in LC MOSTA3KN-0424-064. Non-linear rivets.

The evaluation of the front spar bottom cap strength is summed up in Table 6.10 below.

Table 6.10 Bottom cap strength check. Material: 2124-T851. LC MOSTA3KN-0424-064.

Aft crack length a_1 [mm]	Fore crack length a_2 [mm]	Total panel crack a [mm]	$\sigma_{von\ Mises}$ [MPa]	R_m [MPa]	RF [1]
270	184	454	286.1	486	1.70

Buckling

The most critical location from the structure stability point of view was found to be the intact bay of the integral bottom panel neighbouring with the flawed panel bay – see Figure 6.28.
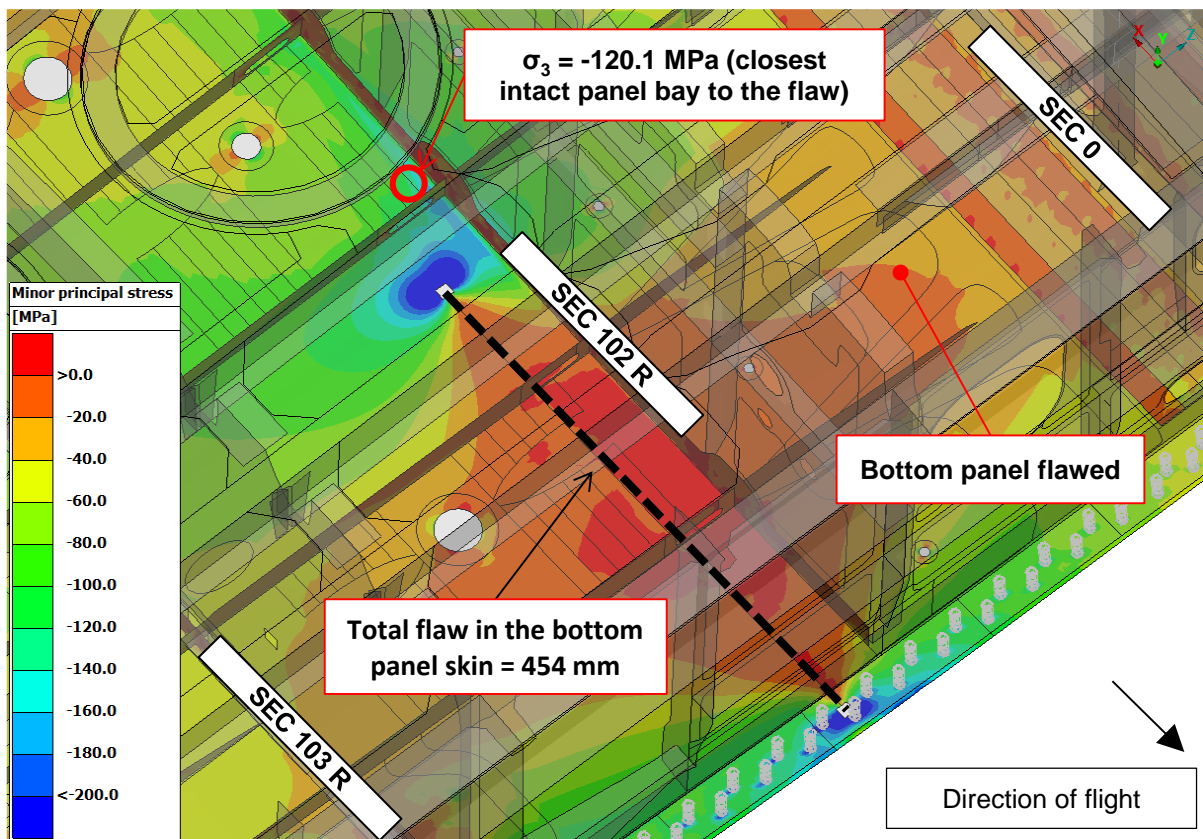

Figure 6.28 Buckling evaluation of the bottom panel. Contour plot of minor principal stress on the bottom panel in LC MOSTA3KN-0429-084. Non-linear rivets.

Critical stress of the intact panel bay was calculated according to Niu [19]. First of all, some extent of structure idealisation was performed. The intact bay skin and stringers were considered to be of uniform thickness and without any cut-outs – see Figure 6.29. The thicknesses used for calculation were conservatively set as the minimal thicknesses found in the bay in question. Compression coefficient was subsequently determined according to Figure 6.30 and the critical buckling stress was calculated as per Equation (6.1) [19].

The calculated critical buckling stress was then confronted with the peak value of minor principal stress on the intact panel bay (identified in Figure 6.28). The reserve factor is enumerated in Table 6.11.
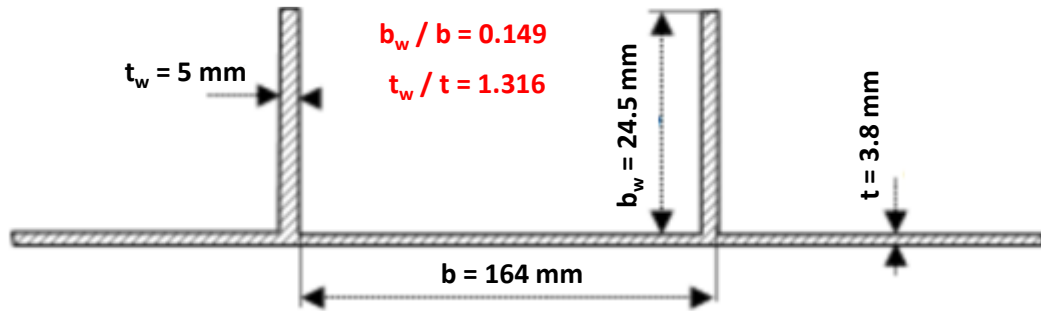
Figure 6.29 Idealized integral panel dimensions.
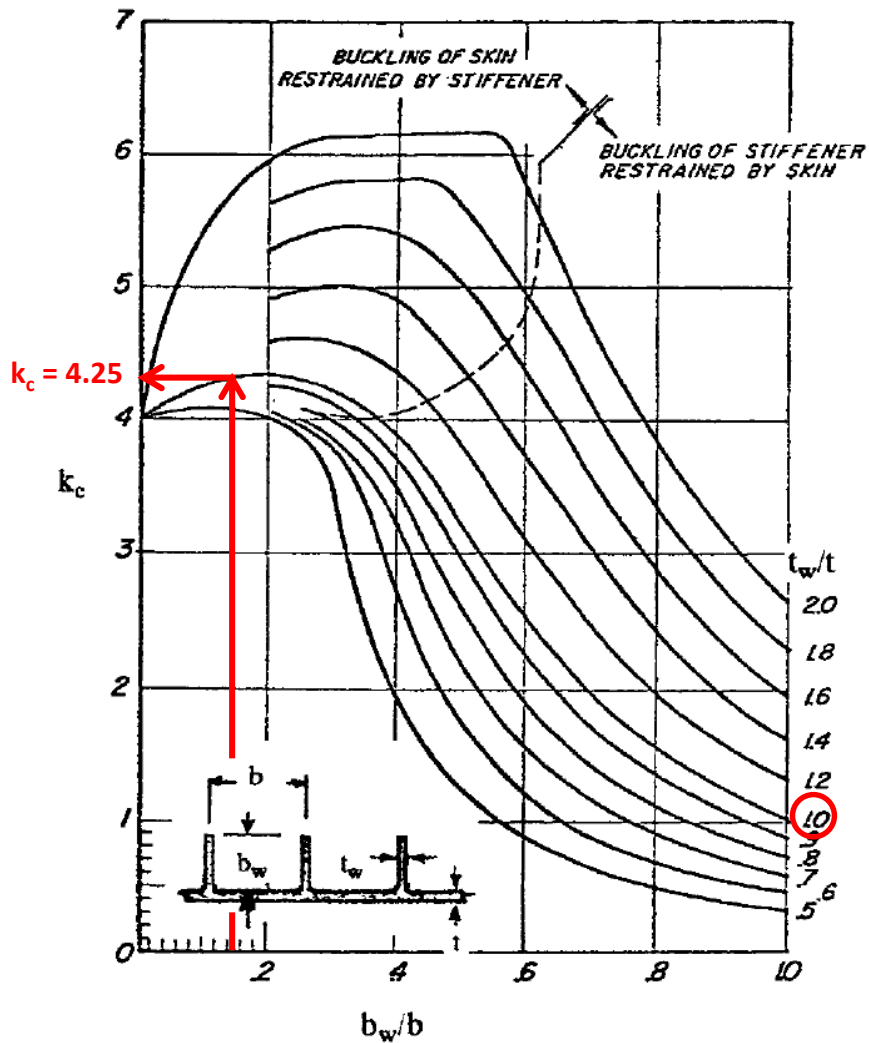
Figure 6.30 Compression coefficient k_c for infinitely wide idealized stiffened panel [19].

$$\sigma_{CRIT} = \frac{k_c \pi^2 E}{12(1-\mu)} \left(\frac{t}{b}\right)^2 = \frac{4.25 \, \pi^2 \, 70\,000}{12(1-0.3)} \left(\frac{3.8}{164}\right)^2 = 187.7 \, MPa \qquad (6.1)$$

In the equation above, σ_{CRIT} is the critical buckling stress, k_c is the panel compression coefficient, E is the Young's modulus of elasticity, μ is the Poisson's ratio, t is the panel thickness and b is the stringer spacing (pitch).

Table 6.11 Bottom panel buckling check. Material: 7475-T7351. LC MOSTA3KN-0429-084.

Aft crack length a_1 [mm]	Fore crack length a_2 [mm]	Total panel crack a [mm]	$|\sigma_3|$ [MPa]	$|\sigma_{CRIT}|$ [MPa]	RF [1]
270	184	454	120.1	187.7	1.56

Critical length determination summary

According to Table 6.12 the **total flaw in the bottom panel skin of 417.5 mm** was considered to be the **critical flaw length**. **Unstable tear of bottom panel fore half-crack** was the limiting factor of the residual strength.

Table 6.12 Critical crack length summary.

Aft crack length a_1 [mm]	Fore crack length a_2 [mm]	Total panel crack a [mm]	Limit state	RF [1]
243.5	174	417.5	Unstable tear of the fore crack	1.00
270	184	454	Net section yield	1.28
			Fastener bearing capacity	3.13
			Surrounding structure strength	1.70
			Buckling	1.56

6.1.6 Detectability

Detectability was evaluated using MSG-3 procedure [5] – see Figure 6.31 below.

Figure 6.31 Determining detectable crack length according to MSG-3 methodology.

The resultant value was **13.75 mm**, which can be considered to correspond with the moment of **full stringer ligament failure** (i.e. the end of stage 1). The location is assumed to be **inspected through the integral fuel tank**, while **detailed visual inspection (DET)** was considered. For more details see Figure 2.3 and Subchapter 2.1.4.

6.1.7 Summary of the results

The results of the damage tolerance analysis of the cut-outs in stringers of the bottom integral panel in section 102 are summarized in Figure 6.32 and Table 6.13.
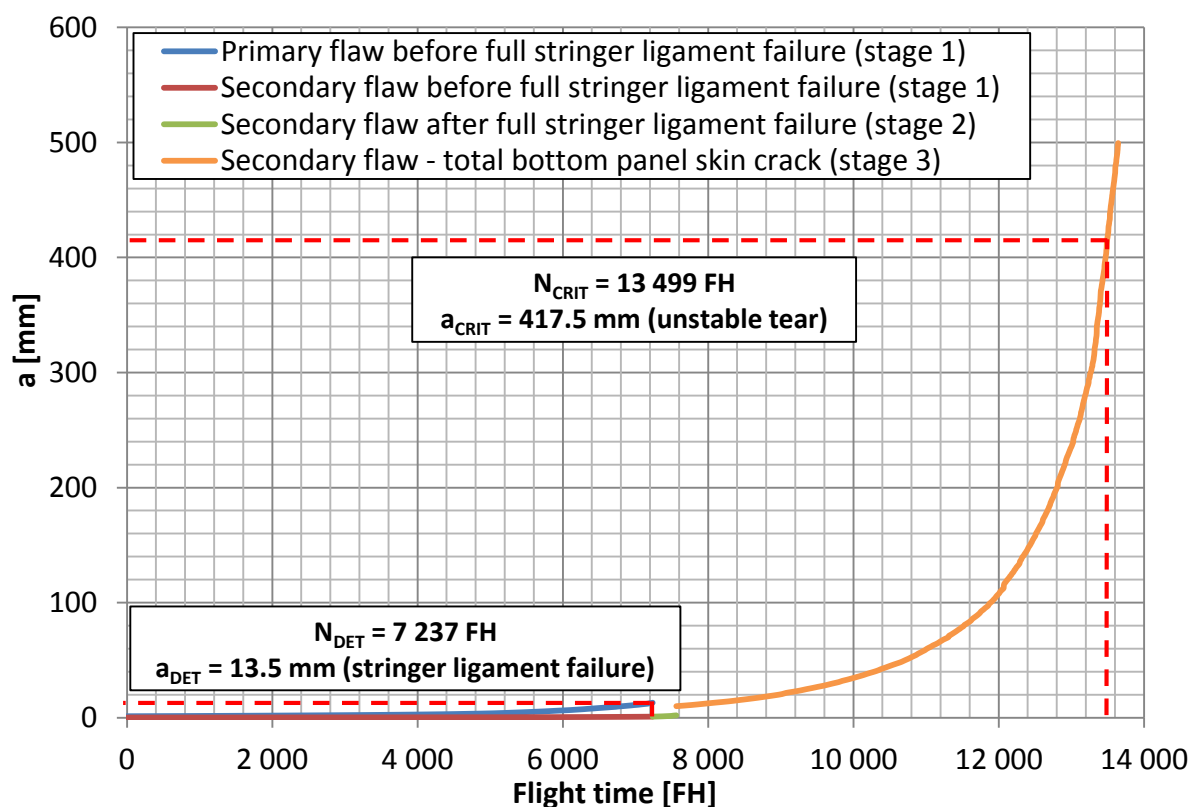
Figure 6.32 Graphical summary of the bottom panel DT analysis – crack growth.

Table 6.13 Resultant inspection task of the integral bottom panel in section 102.

Result	Value	Remark
a_{CRIT} [mm]	417.5	Total bottom panel internal crack
N_{CRIT} [FH]	13 499	
Limit state	Unstable tear	Fore half-crack (under front spar)
a_{DET} [mm]	13.5	Stringer primary crack
N_{DET} [FH]	7 237	
Detectable state	Full stringer ligament failure	
N_{CRIT} - N_{DET} [FH]	6 262	Interval of reliable detection
SF for threshold	2.5	[9]
Inspection threshold [FH]	5 400	N_{CRIT} / SF
SF for Interval	3	[9]
Inspection interval [FH]	2 087	(N_{CRIT} - N_{DET}) / SF

Critical length of the total internal crack in the bottom panel is reached after N_{CRIT} = **13 499 flight hours**. Unstable tear of fore half-crack (growing towards front spar) occurring at this crack length turned out to be critical for the entire structure. **Detectable state** (full stringer ligament failure) is reached after N_{DET} = **7 237 flight hours**. This gives the **interval of reliable detection** of $N_{CRIT} - N_{DET}$ = **6 262 flight hours**. The resulting values of **inspection threshold** and **inspection interval**, obtained by dividing N_{CRIT} and $N_{CRIT} - N_{DET}$ by appropriate scatter factors, are **5 400** and **2 087 flight hours**.

In order to pass judgement on the efficiency of the proposed methodology, the results have been compared with a simplified approach of dealing with simultaneous crack growth used in L 410 DT analyses at the time.

This approach, discussed in Subchapter 2.2, assumes 1:1 propagation ratio of the half-cracks in stress intensity factor calculations using FEM. The resultant growth curve is then based on the growth curve of the faster growing half-crack.

Stage 3 of the fatigue crack growth prediction was the subject of the comparison. The critical fore half-crack length of 174 mm was adopted for the simplified solution from the unstable tear analysis performed in Subchapter 6.1.5. This yields the critical total crack length of 2 * 174 = 348 mm for the simplified approach. The comparison is presented in Figure 6.33 and Table 6.14.
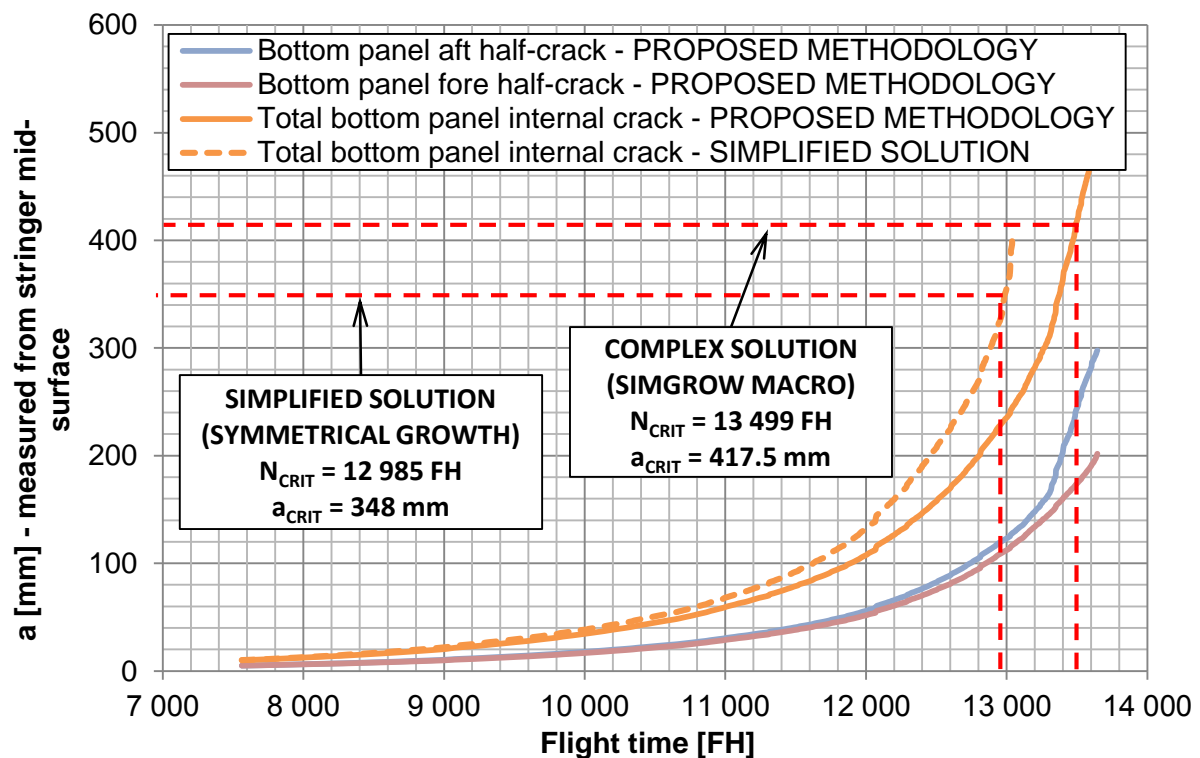
Figure 6.33 Comparison of the crack growth curves in stage 3 obtained by complex analysis of simultaneous crack growth and a simplified solution assuming symmetrical growth.

In this particular case, there was **only a small gain** in the results (**4 % in threshold, 8.9 % in interval**, see Table 6.14), with respect to the **increase in the number of performed FEM** analyses needed to obtain the stress intensity factor solution.

This is caused by the fact, that the simultaneous growth of the two half-cracks calculated by the complex approach is **nearly symmetrical** (see Figure 6.33), with some asymmetry occurring at large crack lengths with high growth rate. The effect of this asymmetry on the results is therefore very limited.

Table 6.14 Comparison of the proposed methodology with a simplified solution.

Result	Simplified solution (symmetrical growth)	Proposed methodology (SIMGROW macro)
a_{CRIT} [mm]	348	417.5
N_{CRIT} [FH]	12 985	13 499
N_{DET} [FH]	7 237	
N_{CRIT} - N_{DET} [FH]	5 748	6 262
Inspection threshold [FH]	5 194	5 400
Threshold increase [FH]	N/A	206
Relative threshold increase [%]	N/A	4
Inspection interval [FH]	1 916	2 087
Interval increase [FH]	N/A	171
Relative interval increase [%]	N/A	8.9
No. of FE analysis for SIF solution [1]	40	123

DT analysis of additional location, introduced in Subchapter 6.2, where significantly asymmetrical crack growth was expected, was conducted in order to further investigate the possible benefits of the proposed methodology.

6.2 Cut-outs in the integral rear spar of the L 410 NG wing

This subchapter presents a DT analysis of an additional location, in order to further examine the possible gains of the proposed methodology when compared to the simplified solutions used at the time in L 410 NG DT analyses.

The scenario of crack initiation in the commonly drilled hole of the riveted joint of the integral rear spar and the integral bottom panel was selected – see Figure 6.34. This scenario was selected due to the strongly unsymmetrical crack growth, which was reported in the analysis of the location previously performed by the author at Aircraft Industries summed up in [28]. The problem of strongly asymmetrical crack propagation was expected to fully reveal the capabilities of the proposed methodology.

Multiple results, such as critical crack length, detectable crack length and growth curves in stages 1 and 2, are adopted for the purpose of this analysis from the report [28].
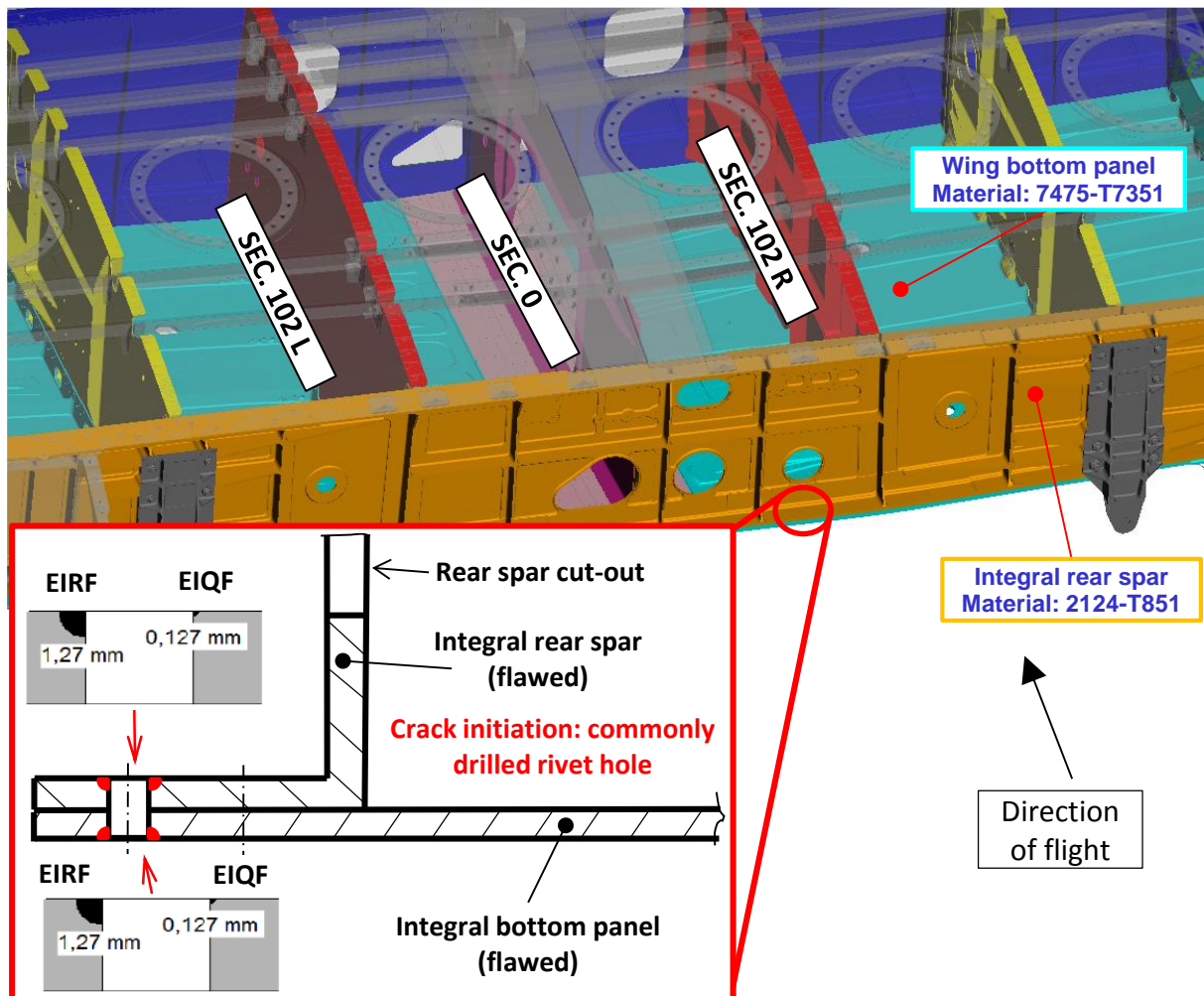
Figure 6.34 General view of the analysed location and initial flaw distribution.

6.2.1 Material data

Material data used were identical to those stated in Subchapter 6.1.2.

6.2.2 Description of the calculation process, stress intensity factor solution

The calculation was split into three stages. Results presented in report [28] were adopted for stages 1 and 2, while stage 3 (crack growth after full ligament failure occurred on both parts) was the subject of a detailed analysis - see Figure 6.35.

Figure 6.35 Crack growth in stage 3.

Table 6.15 states AFGROW model settings for crack growth analysis in stage 3.

Table 6.15 Description of the method used in stage 3. Remarks: 1) Multiple of the loading sequence reference stress (20.78 MPa in cruise flight – LC 111).

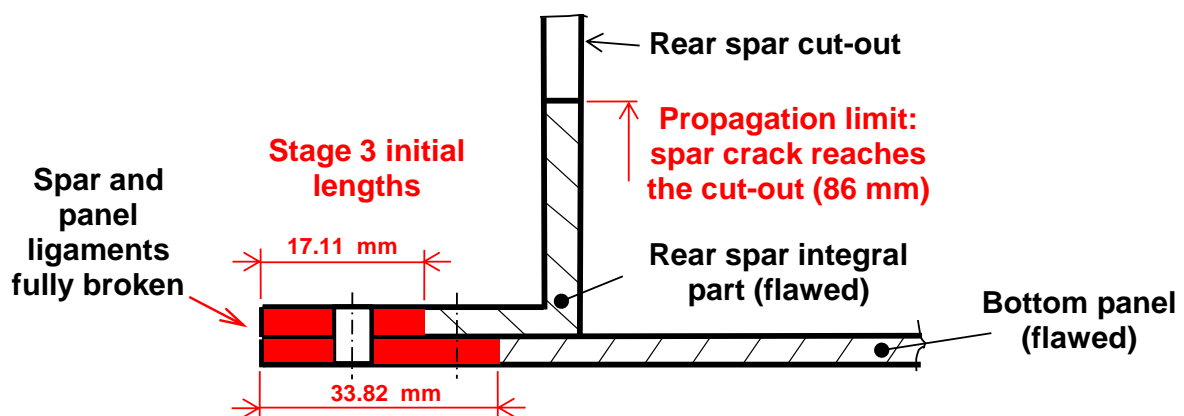| Stage	Flaw		AFGROW model description
3	Quality (secondary)	Spar	Secondary flaw in the rear spar (bottom panel)
		Panel	Model type: Standard (edge through crack) β-function: Obtained by FEM (accounts for the simultaneous growth of both half-cracks) Usage: Growth of the half-cracks from their initial lengths (17.11 mm total crack in the spar, 33.82 mm total crack in the panel) until the spar crack reaches the cut-out (total spar crack of 86 mm) Dimensions: Width = 400 mm, Thickness = 4.1 mm Stress level [1]: 1.000

Modified crack interference factor approach (as per Subchapter 5.2.2) was utilized to calculate the two-variable SIF functions from FEM data. 15 FE calculations were performed for enlarging spar crack only, 31 calculations for enlarging panel crack only and 8 for various combinations of spar and panel crack lengths. The obtained SIF functions are depicted in the form of a surface plot in Figure 6.36 and Figure 6.37.
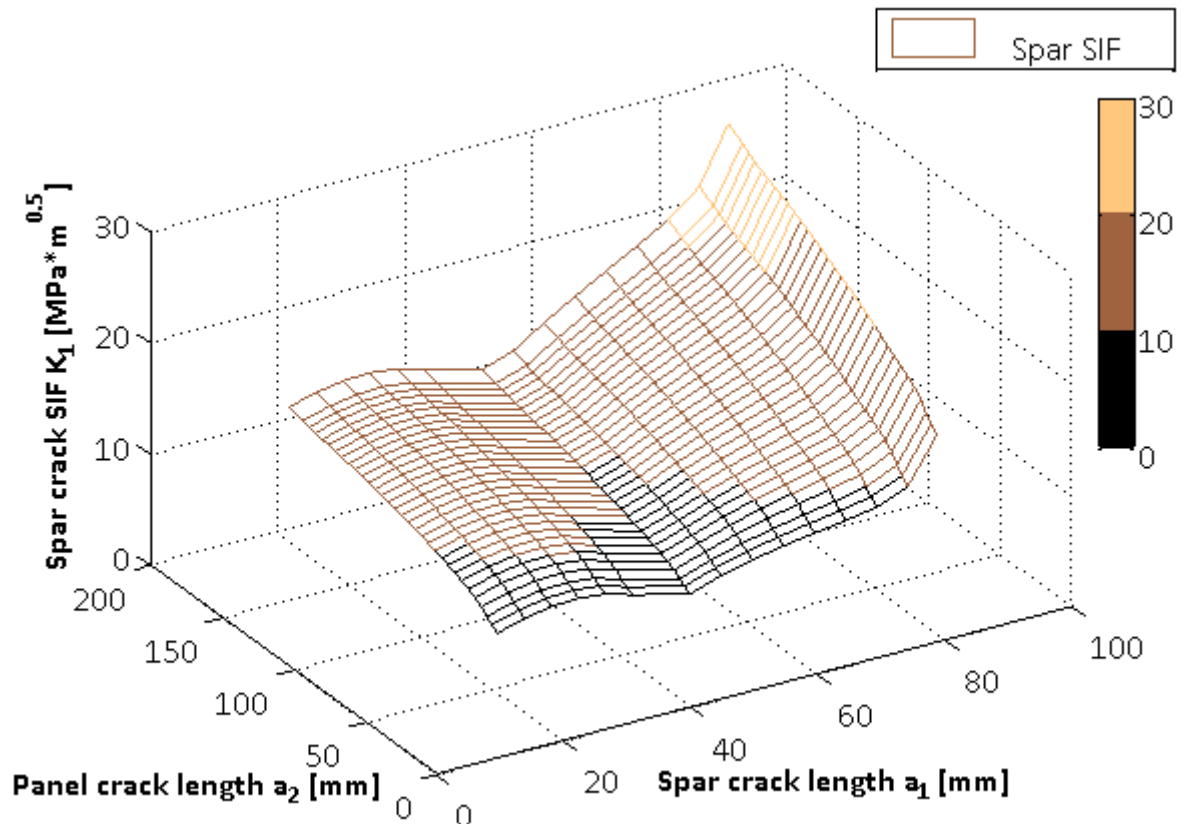
Figure 6.36 Stress intensity factor function for spar crack obtained from FEM data by modified crack interference factor method for cruise flight (LC 111).
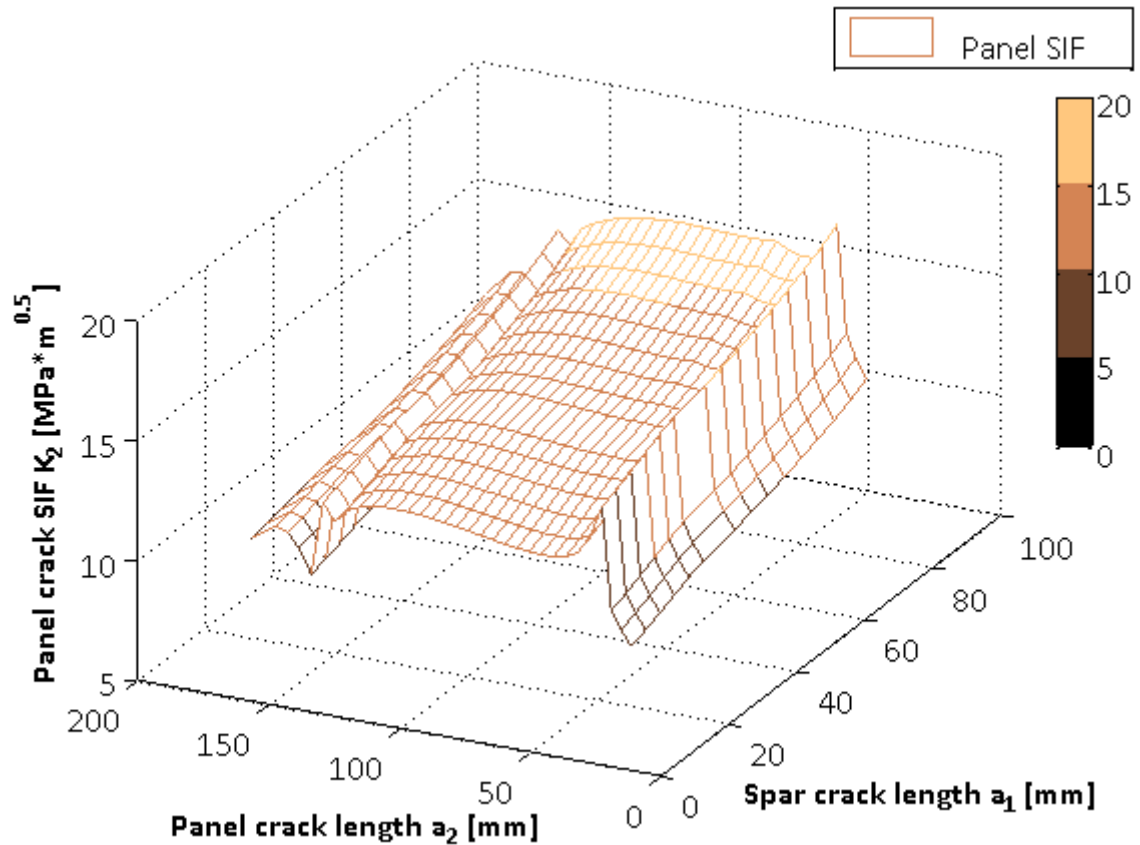
Figure 6.37 Stress intensity factor function for panel crack obtained from FEM data by modified crack interference factor method for cruise flight (LC 111).

The resultant stress intensity factor vs. crack length curves, generated from the two-variable functions depicted in figures above by a step-by-step crack growth prediction procedure, which is closely described in Subchapter 6.1.4, are presented in Figure 6.38 and Figure 6.39. The curve representing a simplified solution (1:1 propagation) is also presented.
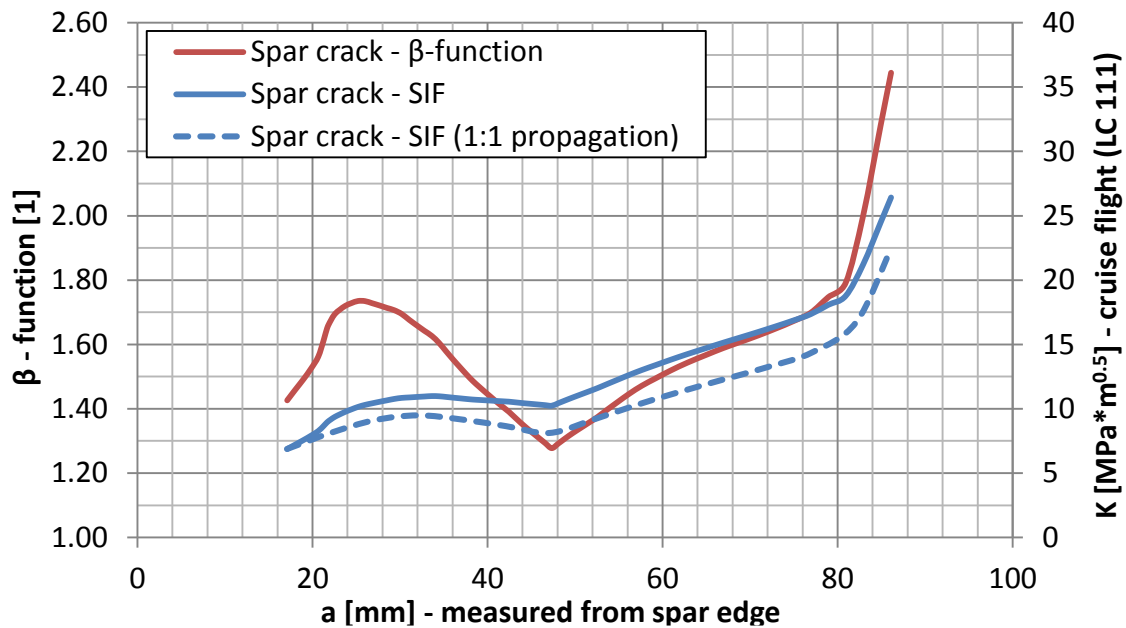
Figure 6.38 Stage 3 β-function for spar crack. Accounts for the simultaneous propagation of panel crack.
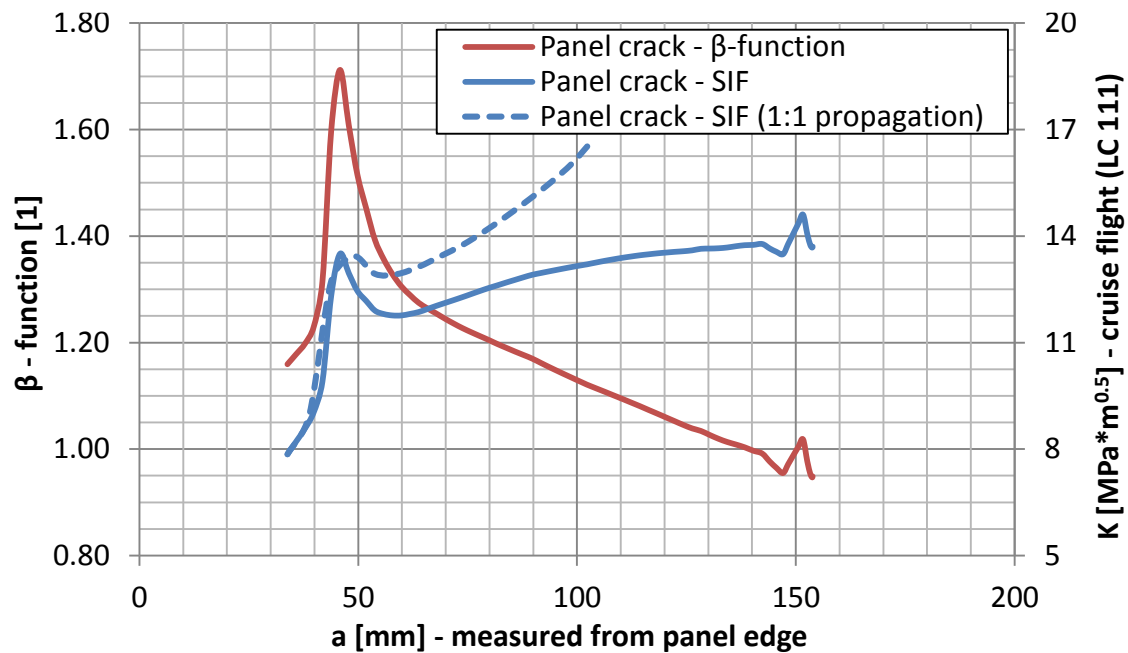
Figure 6.39 Stage 3 β-function for panel crack. Accounts for the simultaneous propagation of spar crack.

6.2.3 Fatigue crack growth prediction

Results in report [28] were used to define the crack growth life spent in stage 1 and 2. Crack propagation in stage 3 was calculated by the linear-K-in-step approach (as defined in Subchapter 5.3.2) in the prepared SIMGROW macro with maximum absolute step error of 0.05 FH, maximum relative step error of 2.5 % and step crack length increment of 2 mm. A simplified solution using β-function obtained from FEM data while assuming 1:1 propagation ratio was then performed and the results are confronted in Subchapter 6.2.6.

6.2.4 Residual strength analysis

Report [28] states that no limit state occurs for the configuration of **spar crack propagated to the cut-out and panel crack of 155 mm**. This configuration was conservatively taken as critical for the purpose of this analysis.

6.2.5 Detectability

The integral rear spar is assumed to be inspected by a detailed visual inspection after the removal of the wing – fuselage fairing. The detectable flaw was determined by MSG-3 methodology with the same assumed parameters as in Figure 6.31, except for the gauge factor of 1.00 (thickness < 5 mm) and the hidden crack length of 10 mm (rivet head). The resultant value of the **detectable spar flaw length was 21 mm**.

6.2.6 Summary of the results

The results of the DT analysis are presented in Figure 6.40 and Table 6.16. Note again that only the crack growth after the full ligament failure of both parts is dealt with. Report [28] defines the crack growth life spent in stage 1 and 2.
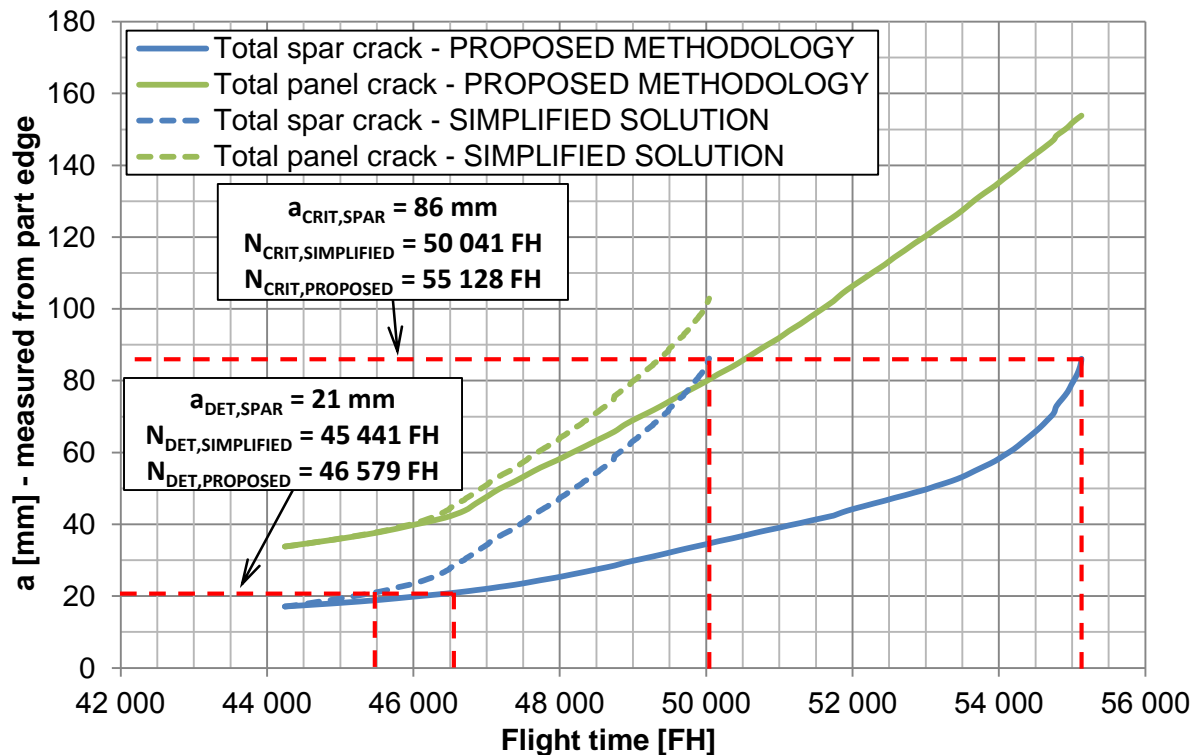
Figure 6.40 DT analysis of the rear spar – bottom panel joint in section 102. Stage 3 only.

It is clear that the crack growth in the two parts is **strongly asymmetrical**. This asymmetry is considered to be the cause of the **vast gains in the results** when compared to the simplified solution, which assumes 1:1 propagation (**10.2 % in inspection threshold** and **85.9 % in inspection interval**), as opposed to the scenario in Subchapter 6.1, where the growth was nearly symmetrical and the gains small (4 % in threshold and 8.9 % in interval).

The increase in the number of FE calculations needed for SIF solution (15 vs. 54) is deemed as acceptable, since the computations are performed on a cluster and are independent of the crack propagation prediction, i.e. can be conducted all at once.

Table 6.16 Comparison of the proposed methodology with a simplified solution.

Result	Simplified solution (1:1 growth)	Proposed methodology (SIMGROW macro)
a_{CRIT} [mm]	86 (total spar flaw)	
N_{CRIT} [FH]	50 041	55 128
a_{DET} [mm]	21 (total spar flaw)	
N_{DET} [FH]	45 441	46 579
N_{CRIT} - N_{DET} [FH]	4 600	8 549
Inspection threshold [FH]	20 016	22 051
Threshold increase [FH]	N/A	2 035
Relative threshold increase [%]	N/A	10.2
Inspection interval [FH]	1 533	2 850
Interval increase [FH]	N/A	1 317
Relative interval increase [%]	N/A	85.9
No. of FE analysis for SIF solution [1]	15	54

7   CONCLUSION

This master's thesis presents a proposal for methodology of damage tolerance analysis of an aircraft structure utilizing AFGROW software, with a special consideration for the simultaneous growth of multiple cracks. The crack propagation prediction was split into stages differing in the way of accounting for the parallel crack growth.

The key part of the thesis consisted of establishing a procedure of calculating the dependent growth of long cracks, for which the simultaneous propagation phenomenon, and the load redistribution associated with it, play a vital role. The most suitable approach, with respect to the technical backing available at Aircraft Industries, was selected and automated in the form of the SIMGROW macro, which is appended to this thesis.

The proposed calculation with the developed macro was practically applied on two cracking scenarios of the wing structure of the L 410 NG aeroplane, and the results were confronted with a simplified conservative approach of dealing with simultaneous crack propagation used in L 410 NG damage tolerance analyses at the time. This comparison revealed a possible increase up to 10 % in inspection threshold and 85 % in inspection interval for scenarios with strongly asymmetrical flaw propagation. The increase in computational costs, namely the number of FE calculations performed to obtain the β-function, is considered as acceptable, when considering the technical backing at Aircraft Industries (computational cluster) and also the possibility of conducting the required analysis all at once, independently of the fatigue crack growth prediction.

Based on the findings of this thesis it is possible to conclude that the proposed methodology is viable for L 410 NG damage tolerance analyses. It is especially well suited for scenarios with expected significantly unsymmetrical crack growth, due to the flawed parts being made of different materials, geometrical arrangements, loading conditions, etc. The calculation according to the proposed methodology can be also applied when the preliminary simplified analyses leads to impractical inspection tasks.

The possibilities of further development of the proposed methodology include:

- Modification of the macro to allow fatigue crack growth prediction with retardation models in AFGROW.
- Automation of FE calculations.
- Development of a complex software, capable of predicting simultaneous growth of multiple cracks from their initial lengths up to the limit state, implicitly utilizing both AFGROW software and FE code.

REFERENCES

[1]   FEDERAL AVIATION ADMINISTRATION (FAA). *Federal Aviation Regulation (FAR): Part 23.* Washington.

[2]   FEDERAL AVIATION ADMINISTRATION (FAA). *Advisory Circular AC 23-13A.* Washington: 2005.

[3]   FEDERAL AVIATION ADMINISTRATION (FAA). *Advisory Circular AC 25.571-1D.* Washington: 2011.

[4]   DEFENCE QUALITY AND STANDARDISATION OFFICE. *Joint Service Specification Guide 2006 (JSSG-2006).* Falls Church: 1998.

[5]   MSG-3. *Operator/Manufacturer Scheduled Maintenance Development.* Washington: Air Transport Association of America, 2007.

[6]   HARTER, James A. *AFGROW Users Guide and Technical Manual.* Version 5.02.01.18. Dayton: LexTech Inc., 2014. 321 p.

[7]   HARTER, James A. and Alex LITVINOV. *AFGROW Component Object Model (COM) Server Interface Manual.* Release 15. Dayton: Air Force Research Laboratory, 2008. 112 p.

[8]   ROZSÁR, Peter, et al. *Supplemental Inspection Document Development Program for the aircraft L 410 NG.* Initial release. Kunovice: Aircraft Industries, 2012. MOSTA.0439.A.U.MD.

[9]   VLČEK, Dalibor. *L 410 NG Fatigue & Damage Tolerance Compliance Guidelines*. Initial release. Kunovice: Aircraft Industries, 2015. MOSTA.0463.A.U.MD.

[10]   VLČEK, Dalibor. *Methodology of Crack Growth and Residual Strength Analyses.* Initial release. Kunovice: Aircraft Industries, 2014. MOSTA.0464.A.U.MD.

[11]   VLČEK, Dalibor. *Randomized loading sequence generator for F&DT analyses and testing.* Initial release. Kunovice: Aircraft Industries, 2014. MOSTA.0472.A.U.MD.

[12]   KUNZ, Jiří. *Základy lomové mechaniky.* 3rd ed. Praha: Vydavatelství ČVUT, 1991. ISBN 80-01-02248-X.

[13]   SCHIJVE, Jaap. *Fatigue of Structures and Materials.* 2nd ed. Delft: Springer, 2008. ISBN 978-1-4020-6807-2.

[14]   BROEK, David. *The Practical Use of Fracture Mechanics.* 3rd ed. Dordrecht: Kluwer Academic Publishers, 1991. ISBN 978-0-7923-0223-0.

[15]   KLESNIL, Mirko and Petr LUKÁŠ. *Únava kovových materiálů při mechanickém namáhání.* 2nd ed. Prague: Nakladatelství Academia, 1975.

[16]   GALLAGHER, Joseph P. *USAF Damage Tolerant Design Handbook: Guidelines for the analysis of damage tolerant aircraft structures.* Revision B. Dayton: University of Dayton Research Institute, 1984.

[17]   BENT, Les J. *Practical Airframe Fatigue and Damage Tolerance.* Coyton: Sigma K Ltd., 2010.

[18]   TADA, Hiroshi. *The stress analysis of cracks handbook*. 2nd ed. St. Louis: Paris Productions Incorporated, 1985.

[19] NIU, Michael C. Y. *Airframe Stress Analysis and Sizing*. 2nd ed. Hong Kong: Hong Kong Conmilit Press Ltd., 1999. 795 p. ISBN 962-7128-08-2.

[20] SCHMIDT, Hans-Jürgen and Bianka SCHMIDT-BRANDECKER. *Fatigue & Damage Tolerance Course for Metal Structure.* 6th issue. Buxtehude: AeroStruc, 2013.

[21] ERDOGAN, F. and G. C. SIH. On the crack extension in plates under plane loading and transverse shear. *Journal of Basic Engineering.* 1963, Series D.

[22] SCHWARMANN, Lüder. *Handbuch Strukturberechnung*. Revision C. Ottobrunn: LTH Koordinierungsausschuss, 1999.

[23] BUCHTA, Vít. *Critical load cases determination for the L 410 NG airplane wing.* Revision A. Kunovice: Aircraft Industries, 2015. MOSTA.0213.A.S.PD.

[24] KADLEC, Martin and Pavel KUCHARSKÝ. *Výsledky zkoušení tuhosti jednostřižných nýtových spojů letounu L-410 NG*. Initial Release. Praha: Výzkumní a zkušební letecký ústav, 2013. MOSTA.0437.V.U.PD.

[25] BVOC, M., J. MIČIC and D. VLČEK. *7475-T7351 aluminium alloy APPENDIX A103*. Initial Release. Kunovice: Aircraft Industries, 2014. MOSTA.0466.A.U.PD.

[26] BVOC, M., J. MIČIC and D. VLČEK. *2124-T851 aluminium alloy APPENDIX A101*. Initial Release. Kunovice: Aircraft Industries, 2014. MOSTA.0466.A.U.PD.

[27] ROZSÁR, Peter. *Vliv velikosti konečných prvků na přesnost výpočtu faktoru intenzity napětí.* Initial release. Kunovice: Aircraft Industries, 2012. DI_AI_027.

[28] RAKOVSKÝ, Kristián. *L 410 NG F&DT analysis of rear spar shear web cut-outs in section 0-102*. Initial release. Kunovice: Aircraft Industries, 2015. 97 p. SIGMA.4000.19.A.M.TR.

[29] RAKOVSKÝ, Kristián. *Výpočet nelineárního chování nýtů v řešiči MSC. NASTRAN*. Revision A. Kunovice: Aircraft Industries, 2014. 15 p. DI_AI_173.

[30] RAKOVSKÝ, Kristián. *Buckling analysis of wing spar shear webs in MSC. NASTRAN FE code*. Initial Release. Kunovice: Aircraft Industries, 2015. 17 p. DI_AI_173.

[31] MSC SOFTWARE. *MSC Nastran 2012.2 Quick Reference Guide.* Revision 0. Santa Ana: MSC.Software Corporation, 2012.

[32] ONL 1562. *Smykové pevnosti nýtových spojů*. Praha: Výzkumný a zkušební letecký ústav, 2000. 6 p.

DEFINITIONS AND ABBREVIATIONS

Value Abbreviation	Units	Description
β	[1]	Shape function
Δa	[m]	Crack length increment
ΔK	[MPa*m$^{0.5}$]	Stress intensity factor range; Crack interference factor
ΔK_{eff}	[MPa*m$^{0.5}$]	Effective stress intensity factor range
ΔK_{th}	[MPa*m$^{0.5}$]	Threshold stress intensity factor range
ΔN	[cycles, FH]	Absolute propagation life error
$\Delta\sigma$	[MPa]	Stress range
δ	[m]	Rivet shear displacement
δN	[1]	Relative propagation life error
E	[cycles, FH]	Maximal allowed absolute propagation life error
ε	[1]	Maximal allowed relative propagation life error
μ	[1]	Poisson's ratio
σ	[MPa]	Normal stress
σ_1	[MPa]	Major principal stress
σ_3	[MPa]	Minor principal stress
τ	[MPa]	Shear stress
a	[m]	Crack length
C	[1]	Modification factor
E	[MPa]	Young's modulus of elasticity
F	[N]	Force
K	[MPa*m$^{0.5}$]	Stress intensity factor
K_{IC}	[MPa*m$^{0.5}$]	Mode I fracture toughness
K_{op}	[MPa*m$^{0.5}$]	Crack opening stress intensity factor
N	[cycles, FH]	Crack propagation life
R	[1]	Cycle stress ratio
RF	[1]	Reserve factor
R_m	[MPa]	Material ultimate strength
$R_{p,0.2}$	[MPa]	Material yield strength
r_p	[m]	Plastic zone radius
S	[m^2]	Cross-sectional area
SF	[1]	Scatter factor
SIF	[MPa*m$^{0.5}$]	Stress intensity factor
TAS	[km/h]	True air speed
u	[m]	Displacement in the x-direction
v	[m]	Displacement in the y-direction
w	[m]	Displacement in the z-direction

Value Abbreviation	Units	Description
AC		Advisory Circular
ATA		Air Transport Association of America
COM		Component Object Model
DET		Detailed visual inspection
DSG		Design service goal
DT		Damage tolerance
EIQF		Equivalent initial quality flaw
EIRF		Equivalent initial rogue flaw
FE		Finite element
FEM		Finite element method
FH		Flight hours
GVI		General visual inspection
ISA		International Standard Atmosphere
LC		Load case
L-S		Longitudinal load direction – short transverse fracture direction
L-T		Longitudinal load direction – long transverse fracture direction
LEFM		Linear elastic fracture mechanics
LOV		Limit of validity
MED		Multiple element damage
MSD		Multiple site damage
MSG-3		Maintenance Steering Group 3
PSE		Primary structural element
QF		Quality (secondary) flaw
RF		Rogue (primary) flaw
T-L		Long transverse load direction – longitudinal fracture direction
VBA		Visual Basic for Applications
WFD		Widespread fatigue damage

LIST OF APPENDICES

Appendix 1 – SIMGROW macro for calculation of simultaneous growth of two long cracks
developed for the purposes of this master's thesis
(present in electronic form on the enclosed CD as Excel workbook
SIMGROW_v_1_0.xlsm)

Appendix 2 – SIMGROW macro technical manual and user's guide
(present in electronic form on the enclosed CD as PDF document
SIMGROW_Technical_Manual_Users_Guide_v_1_0.pdf)